Paired Electrolysis of Glycerol with CO_2 Electroreduction to CO in Zero-Gap Electrolyzers

CH3901: Master Thesis Project

Neziha Deniz Erkan

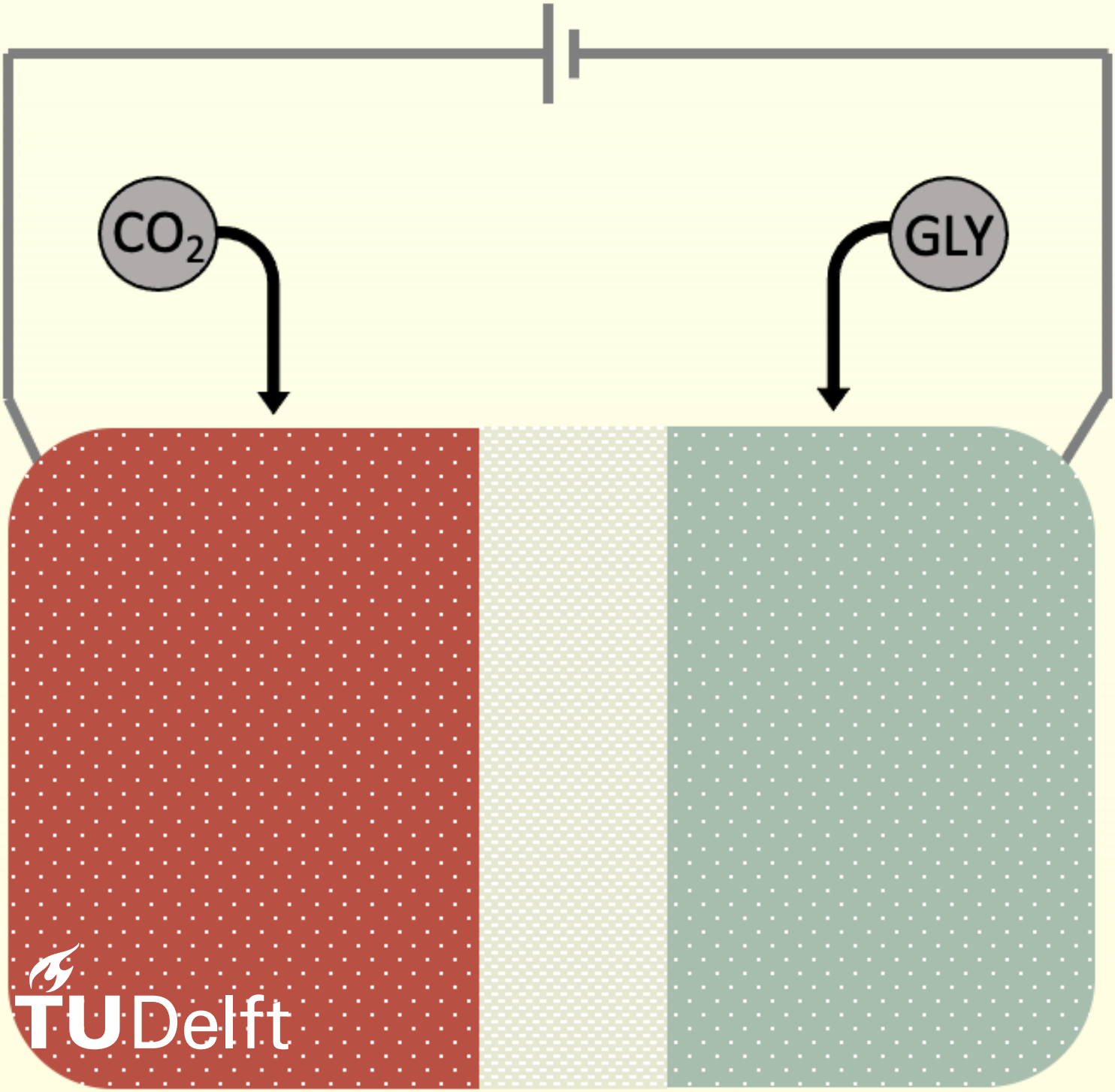

TU Delft

Paired Electrolysis of Glycerol with CO_2 Electroreduction to CO in Zero-Gap Electrolyzers

by

Neziha Deniz Erkan

Student Name	Student Number
Neziha Deniz Erkan	5599938

Instructor:	Dr. Thomas Burdyny
Daily Supervisor:	Siddhartha Subramanian
Committee Members:	Dr. Thomas Burdyny, Dr.ir. David A. Vermaas, Dr. Ludovic Jourdin
Project Duration:	January, 2023 - August, 2023
Faculty:	Faculty of Chemical Engineering, Delft

TU Delft

Acknowledgements

This thesis marks the end of my time as a master's student at TU Delft. It has truly been a period of immense growth in so many different ways, and like many other experiences would not have been possible without the support and help from the people around me.

First, I would like to thank my boyfriend Anders for his unshakable support during this time. Thank you for being the second pair of eyes on my report and helping me with all kinds of things when I have been a walking stress ball this past month. Your positivity, energy, and support have made this period so much easier, and I am incredibly lucky to have you by my side.

I would also like to thank Siddhartha Subramanian for his immense support and help during this thesis. From showing me the ins and outs of the lab to frequently checking on me when I was performing experiments and spending long hours discussing the project's progress with me, you have been an incredible daily supervisor. Thank you.

Moreover, I would like to express my gratitude towards Professor Burdyny for the time and effort he put into making this thesis a reality. Our weekly one-on-one meetings at the start were extremely helpful for my introduction to CO_2 electrolysis. I am grateful for our chats and your supervision.

Additionally, I would like to acknowledge the MECS group for interesting weekly discussions and for assisting me in the lab. A special thanks go to Herman, who helped me out with sputtering many times. I also would like to thank Dr. Ir. David A. Vermaas and Dr. Ludovic Jourdin for taking the time to read this report and agreeing to be part of my assessment committee.

And finally, I want to thank my parents for their constant support throughout the years. Even though I have been away from home for many years, you never let me feel alone and helped me countless times. I am incredibly lucky to be your daughter.

Neziha Deniz Erkan
Delft, August 2023

Abstract

As part of the efforts to mitigate climate change, the electrochemical reduction of CO_2 into valuable chemicals and fuels has been identified as a pivotal technology due to its potential for CO_2 utilization and ability to store excess electricity as chemical energy. While significant progress has been made in optimizing various aspects of the electrochemical CO_2 reduction system, an unexplored area pertains to the improvement of the anodic reaction. The conventional anodic reaction, namely the oxygen evolution reaction (OER), is constrained by kinetic and thermodynamic unfavorability, reliance on precious metal catalysts, and the need for costly downstream gas separation.

To address these limitations, a novel approach has gained traction within the research community: the paired electrolysis of CO_2 reduction reaction (CO_2RR) and glycerol oxidation reaction (GOR). However, these studies mostly employ expensive platinum group metal (PGM) catalysts in flow cells, failing to address cost dependency or scalability for future industrial applications due to inefficient energy use in this electrolyzer configuration. Therefore, this study intends to understand and optimize the paired electrolysis of CO_2RR with GOR in zero-gap electrolyzers while comparing the performances of Pt (a relatively rare PGM catalyst) and Ni (an abundant non-PGM catalyst). The effects of applied cell potential, glycerol concentration, active surface area, and ion exchange membrane type on GOR product selectivity and the system's energy demand are evaluated through potential and current controlled experiments. Gas chromatography (GC) and proton nuclear magnetic resonance spectroscopy (H-NMR) are used for product analysis.

This thesis demonstrates the viability of paired electrolysis in zero-gap electrolyzers, yielding major products like formate and lactate alongside minor byproducts such as acetate, glycerate, and dihydroxyacetone. The results reveal Ni's superior performance over Pt at current densities below 200 mA/cm² in zero-gap electrolyzers. The negative influence of increasing applied potentials on faradaic efficiencies (FEs) is presented, particularly in Ni, likely due to side reactions like OER or formate oxidation. The study also illustrates that increased glycerol concentrations decrease FEs and system activities due to heightened viscosity-related diffusivity issues. Moreover, the tests conducted using the Ni anode in zero-gap electrolyzers utilizing bipolar membranes (BPM) show a minor reduction in product selectivity likely caused by the increased amounts of OH^- ions near the anode coming from the water dissociation reaction (WDR).

The study also uncovers that the anticipated significant reduction in the cell's energy demand with the replacement of OER with GOR is not observed in zero-gap electrolyzers. No conclusive improvements are observed for either catalyst when anion exchange membranes (AEM) are employed, and only marginal improvements in the cell's energy demand are achieved when bipolar membranes are used with Ni. Although this behavior is speculated to be a consequence of the absence of a flowing electrolyte near the anode, further investigations are needed to identify the cause of this unexpected lack of improvement in the energy demand.

Contents

List of Abbreviations

Abbreviation	Definition
AA	Acetic Acid
AEM	Anion Exchange Membrane
AEMEA	Anion Exchange Membrane Electrode Assembly
BPM	Bipolar Membrane
BPMEA	Bipolar Membrane Electrode Assembly
CE	Counter Electrode
CEM	Cation Exchange Membrane
CO_2RR	CO_2 Reduction Reaction
CV	Cyclic Voltammetry
DEMS	Differential Electrochemical Mass Spectrometry
DHA	Dihydroxyacetone
EDX	Energy Dispersive X-ray Spectroscopy
FA	Formic acid
FE	Faradaic Efficiency
GA	Glyceric Acid
GC	Gas Chromatography
GDE	Gas Diffusion Electrode
GDL	Gas Diffusion Layer
GHG	Green House Gasses
GLAD	Glyceraldehyde
GLOX	Glyoxylic Acid
GLY	Glycerol
GOR	Glycerol Oxidation Reaction
H-NMR	Proton Nuclear Magnetic Resonance
HER	H_2 Evolution Reaction
HPLC	High-Performance Liquid Chromatography
LA	Lactic Acid
MA	Mesoxalic Acid
MEA	Membrane Electrode Assembly
MFC	Mass Flow Controller
NMR	Nuclear Magnetic Resonance
OA	Oxalic Acid
OER	O_2 Evolution Reaction
PGM	Platinum Group Metals
RE	Reference Electrode
RHE	Reversible Hydrogen Electrode
RHE	Reversible Hydrogen Electrode
SEM	Scanning Electrode Microscopy
TA	Tartronic Acid
WDR	Water Dissociation Reaction
WE	Working Electrode

List of Figures

List of Tables

1

Introduction

The industrial revolution, while undoubtedly bringing about numerous benefits and advancements since the 18th century, has been accompanied by a relentless surge in energy consumption and extensive reliance on fossil fuels. In fact, the global consumption of fossil fuel-based energy has increased around eight-fold since 1950, doubled since 1980, and reached over 135,000 TWh as of 2021 [1]. These are extraordinary numbers, constituting about 80% of the world's energy supply [2]. When fossil fuels are burned, large amounts of greenhouse gasses (GHG), especially CO_2, are released into the atmosphere. Each year human activities cause more CO_2 emissions than natural processes can remove, resulting in an accumulation of carbon dioxide. This increase can be seen in Fig. 1.1 where the atmospheric CO_2 levels and the CO_2 emissions since the start of the Industrial Revolution in 1750 are shown. The figure indicates a 50% increase in the atmosphere's carbon dioxide content in less than 200 years.

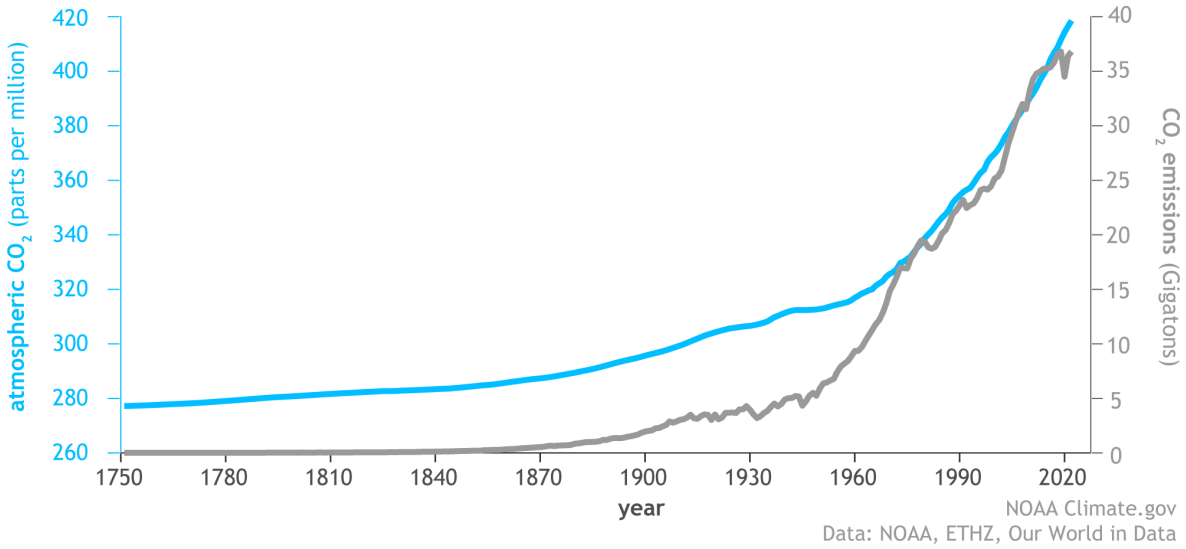

Figure 1.1: Global carbon dioxide concentration in the atmosphere (blue line) and global carbon dioxide emissions (gray line) since 1750. Sourced from [3]

The accumulation of CO_2 and other GHG as a result of human activities has been identified by the Intergovernmental Panel on Climate Change (IPCC) as the primary driver of climate change [4]. Looking at the average global temperatures across years reveals the unprecedented effects of anthropogenic CO_2 emissions in terms of global temperature rise. In fact, the latest decade (2010-2020) was determined to be warmer than any multi-century period in the past 125,000 years [4]. Already reaching an approximately 1.1°C higher average than the temperature baseline in the pre-industrial period,

the consequences of global warming are and will continue to affect every region on Earth in the form of extreme climate events [4]. As ambitious as it is, decreasing carbon dioxide emissions globally is thus obligatory to mitigate disastrous global temperature increases. If current policy and technology trends continue, global energy demand is expected to increase by 50% by 2050 from 2020 values due to economic and population growth. This makes developing and implementing renewable energy technologies even more essential for limiting warming to 1.5 °C above pre-industrial temperatures as decided under the Paris Agreement [4–6].

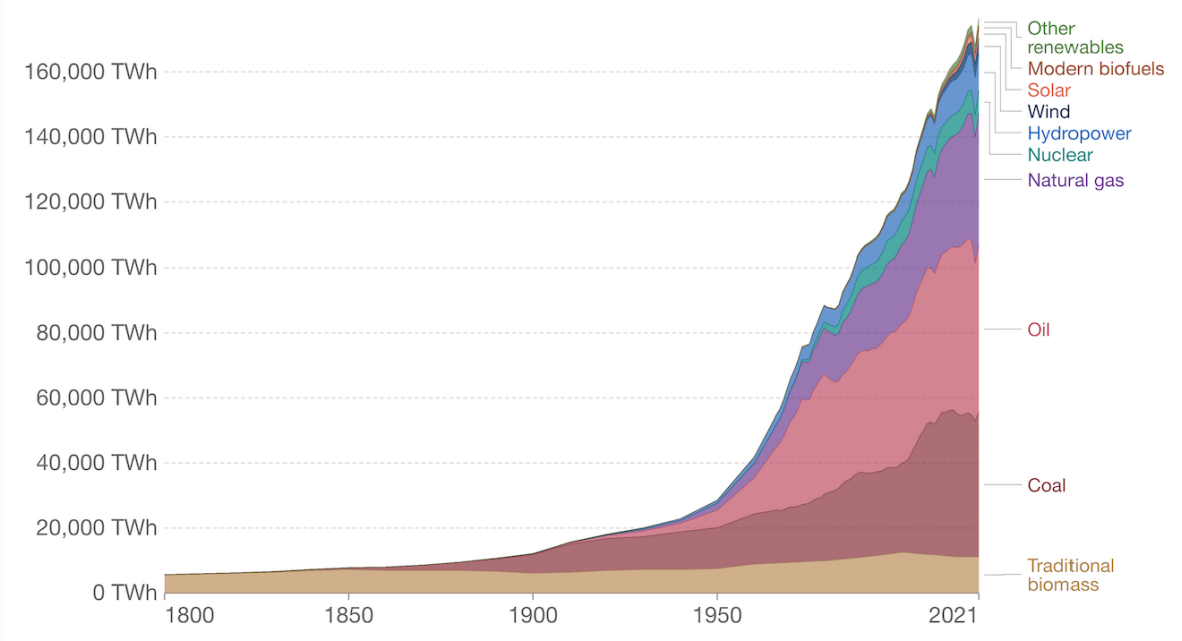

Figure 1.2: Global primary energy consumption by source since 1800. Sourced from [7–9]

The current global primary energy consumption trend, as seen in Fig. 1.2 above, reveals that as of 2021, only about 16% of our energy comes from low-carbon sources [7]. Considering the current and upcoming ramifications of global warming, it is clear that substantial and sustained reductions of CO_2 through a rapid energy transition are crucial. However, such restructuring of the energy landscape is a complex and multifaceted challenge that will require efforts from a wide range of people and improvements in many green technologies.

Despite being the market's two most established and fastest-growing renewable technologies, solar and wind energy still face many challenges. One of the most critical limitations of both is the mutual intermittency issue. Due to their dependency on natural phenomena, utilization of wind and solar energy as the primary energy source would bring expected and unexpected disruptions to the energy supply, creating a mismatch between the supply and demand [10]. Not only can this issue result in electricity shortages, but also interruptions in electricity supply are not conducive to the current power grid infrastructure available in many regions of the world [11]. Therefore, extensive research is being conducted to address the energy storage needs associated with their use and make the energy captured easily transportable and available for on-demand use.

Electrochemical reduction of CO_2 into value-added chemicals and fuels is one of the most promising technologies to address both the CO_2 emissions and the energy storage issues described above. This technology would allow captured CO_2 to be utilized as a feedstock for valuable products such as carbon monoxide (CO), formic acid, methanol, and ethylene, through an electrochemical approach [12]. Moreover, the ability to not only store but utilize CO_2 would allow us to simultaneously reduce our greenhouse gas emissions and realize the storage of electrical energy in the form of chemicals [13].

Value-added chemicals listed above are currently being manufactured via carbon-intensive methods using fossil fuels under high-pressure and/or high-temperature environments, and our demand

for them will continue for many years into the future [12]. Thus, implementing electrochemical CO_2 conversion technologies would also help decarbonize the manufacturing of these chemicals and allow for milder operational conditions. Capturing and utilizing the CO_2 emitted from the use of these hydrocarbons can also be implemented to close the carbon cycle and reduce the net emissions of the system to zero. Another benefit of this technology is that due to our longstanding dependency on fossil fuels, there is an established global infrastructure for storing and transporting hydrocarbons. Therefore, implementing CO_2 electrolysis to make valuable chemicals would allow us to utilize the current infrastructure, preventing extra costs [5].

Unfortunately, electrochemical reduction of CO_2 still has challenges to compete commercially with the cheaper and more energy-efficient fossil-fuel-based alternatives. Significant progress must be made to make the process energy efficient, selective, stable, and economically feasible while operating at commercially relevant reaction rates [14].

Significant research has already been dedicated to extensively exploring the various factors involved in the electrochemical reduction of CO_2 to optimize the system. Efforts have primarily focused on increasing performance, selectivity, and stability through catalyst development. Additionally, research has been conducted to investigate the combined effects of the reaction environment, active sites, and the system configuration [15]. Yet a common thread present in most current studies is the coupling of the cathodic CO_2 reduction reaction (CO_2RR) with the anodic oxygen evolution reaction (OER) [12]. Although OER's prevalence in conventional CO_2 electrolyzers can be attributed to the easy accessibility of water and the well-known kinetics from water electrolysis studies [16], there are still challenges associated with having it as the anodic reaction in CO_2RR systems. These challenges arise from both intrinsic kinetics and thermodynamics, requiring high overpotentials, consuming a large amount of the energy input [12], producing a gas product that requires a costly separation step, and the financial insignificance of the produced oxygen [17, 18]. Moreover, using OER as the anodic reaction in highly-stable commercialized applications commonly requires rare and precious metal-based catalysts like iridium, which up the costs associated with the system significantly [19].

Given the abovementioned limitations, a considerable strategy is coupling alternative value-added anodic reactions with CO_2RR instead of OER. Coupling the anodic glycerol oxidation reaction (GOR) with the cathodic reduction of CO_2 is a promising approach among the various options available. Glycerol is an inexpensive byproduct of industrial biodiesel and soap production, and its oxidation can lead to the production of various value-added chemicals such as glyceraldehyde, glyceric acid, formate, oxalate, etc. [20]. Research on the electrochemical behavior of glycerol dates back to the 1960s [21]; however, it has only recently been explored for its capacity for co-electrolysis with CO_2 [12, 17, 22–24]. Glycerol oxidation reaction offers substantial advantages over the conventional oxygen evolution reaction in avoiding the costly gas separation step due to its liquid-to-liquid nature, producing commercially desirable products, and its potential to reduce cell potential, thus resulting in a decrease in electricity consumption of the system [12].

1.1. Knowledge Gaps

Glycerol oxidation alone is well-studied by coupling it with the cathodic hydrogen evolution reaction (HER); however, there are limited studies exploring coupling GOR with CO_2RR. A common thread in these studies is the utilization of noble metal-based catalysts such as Pt, Au, Ag, Pd, and Ru [21]. These catalysts were previously identified for their stability and high catalytic activity when GOR is coupled with HER [21]; however, their use in the disparate reaction environment formed when GOR is coupled with CO_2RR requires further investigation.

Moreover, these studies have only used electrolyzer configurations other than zero-gap electrolyzers which have been identified to be the most promising type for industrial applications due to their low ohmic resistances and high energy efficiencies [25]. Thus, there is inadequate knowledge of the effects of coupling GOR and CO_2RR in zero-gap electrolyzer configurations, and a study investigating this can provide valuable insights.

As of the start of this study, there have also been no current endeavors to explore the coupling of

GOR with CO_2RR using bipolar membranes (BPM). Considering bipolar membranes operating in reversed bias are proven to be better at reducing parasitic CO_2 losses than anion exchange membranes (AEM) and cation exchange membranes (CEM) [26], an investigation to understand the effect of replacing OER with GOR in BPM-fitted configurations is an exciting avenue of study. Therefore, further research must be performed on the topic to understand the coupling of GOR with CO_2RR to explore its potential in BPM configurations.

It should also be mentioned that the Materials for Energy Conversion and Storage (MECS) group has quite a lot of experience with CO_2 electrolysis; however, no prior experience with paired electrolysis is present. Therefore, this study also lays the groundwork for future paired electrolysis work by the MECS group.

1.2. Research Objectives

Determined through an analysis of the knowledge gaps, this thesis's primary goal is understanding and optimizing the paired electrolysis of glycerol oxidation with CO_2 reduction to CO in zero-gap electrolyzers. This is done by testing the performance of the paired electrolysis while utilizing different anodic catalysts in both AEM and BPM-utilized zero-gap electrolyzers.

To guide the study following sub-questions were identified:

- Do the platinum-group-metals (PGM) identified as best for GOR also perform better than their PGM-free alternatives in a CO_2RR-GOR paired electrolysis?
- Can replacing oxygen evolution reaction with glycerol oxidation reaction in CO_2 electrolysis studies performed realize a decrease in the system's energy needs?
- How does using bipolar membrane-fitted zero-gap electrolyzers affect the performance of GOR?

2

Theory

Electrochemistry is the branch of chemistry that focuses on the chemical changes that happen due to the flow of electrons and, conversely, electricity production due to chemical changes [27]. Therefore, the interrelation of chemical and electrical effects is at the forefront of this area of study. The understanding and application of electrochemical principles require the examination of electrochemical systems; of those, the electrochemical cell is a great starting point. The two primary types of electrochemical cells are electrolytic and galvanic cells, where the former converts electrical energy to chemical energy and the latter does vice versa. This work only concerns electrolytic cells where electrical energy is required to drive a non-spontaneous reaction; however, simple example schematics of both these types can be viewed in Fig. 2.1 below.

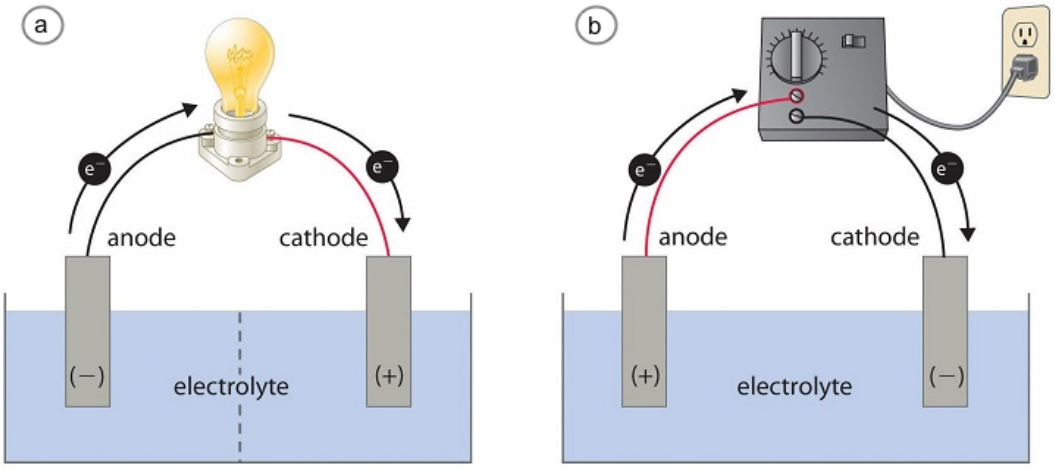

Figure 2.1: The schematic of (a) a galvanic cell where chemical energy is converted to electrical energy and (b) an electrolytic cell where the electrical energy supplied is used to drive a chemical reaction. Sourced from [28].

Electrochemical cells consist of two electrodes: an anode and a cathode. At the cathode, the reactants gain electrons leading to a reduction reaction, and at the anode, reactants lose electrons, causing an oxidation reaction. Both an oxidation and a reduction reaction are necessary to have a working electrochemical cell. Thus, the anodic and cathodic reactions are often described as half-cell reactions.

Typically, the electrodes are separated by a liquid electrolyte, and the electrochemical reactions

occur at the electrode-electrolyte interface. The electrodes transport charge by transporting electrons through an external circuit, whereas in the electrolyte phase, the charge is carried through the movement of ions [29]. Porous separators/membranes are often centrally present to transport and block specific charged species.

2.1. Electrochemical Reduction of CO_2

As mentioned before, using CO_2 to make value-added chemicals and fuels is a promising approach to achieving net-zero CO_2 emission systems. Thus, this study investigates the optimization of the electrochemical reduction of CO_2 through the approach detailed in Section 2.2. The half-reactions involved in this thesis are the CO_2 reduction reaction (CO_2RR) to CO, hydrogen evolution reaction (HER), oxygen evolution reaction (OER), and glycerol oxidation reaction (GOR). Of those listed, the first two are the reactions occurring at the cathode, while the last two occur at the anode. HER is an undesired reaction competing with CO_2RR in this system [14].

Below are the half-reactions and the standard reduction potentials of CO_2RR, HER, and OER. The alternative, GOR, will be discussed later in Section 2.2.4.

Hydrogen Evolution Reaction (HER): (E° = 0.00 V vs RHE)

$$2H^+ + 2e^- \rightleftharpoons H_2 \qquad (acidic) \tag{2.1}$$

$$2H_2O + 2e^- \rightleftharpoons H_2 + 2OH^- \qquad (alkaline) \tag{2.2}$$

CO_2 Reduction Reaction (CO_2RR): (E° = -0.11 V vs RHE)

$$CO_2 + 2H^+ + 2e^- \rightleftharpoons CO + H_2O \qquad (acidic) \tag{2.3}$$

$$CO_2 + H_2O + 2e^- \rightleftharpoons CO + 2OH^- \qquad (alkaline) \tag{2.4}$$

Oxygen Evolution Reaction (OER): (E° = 1.23 V vs RHE)

$$H_2O \rightleftharpoons \frac{1}{2}O_2 + 2H^+ + 2e^- \qquad (acidic) \tag{2.5}$$

$$2OH^- \rightleftharpoons \frac{1}{2}O_2 + H_2O + 2e^- \qquad (alkaline) \tag{2.6}$$

The chemical species' standard reduction potentials (E°) signify their tendency to gain electrons and get reduced [29]. And by looking at the three reactions listed above, it can be observed that the standard thermodynamic potential of HER is pretty close to that of CO_2RR. This is the reason behind HER's previously-mentioned presence in CO_2RR systems as an undesired reaction. Also, it should be noted that the standard thermodynamic potential of OER is significantly higher than HER and CO_2RR despite being the conventional anodic reaction in these systems which will be discussed further later in Section 2.2.1.

It should be mentioned that CO_2RR can lead to several other products depending on the reaction environment, applied potential, reactant concentrations, and especially the catalyst being used [30]. Some of the possible CO_2RR products (including CO, as denoted in equations 2.3 and 2.4) and their half-reactions that could have occurred are listed (in an alkaline environment) in Table 2.1.

Table 2.1: Possible CO_2RR half-reactions and their products

Product	Possible Half-Reactions for CO_2RR
CO	$CO_2 + H_2O + 2e^- \rightleftharpoons CO + 2OH^-$
$HCOOH$	$CO_2 + 2H_2O + 2e^- \rightleftharpoons HCOOH + 2OH^-$
$HCHO$	$CO_2 + 3H_2O + 4e^- \rightleftharpoons HCHO + 4OH^-$
CH_3OH	$CO_2 + 5H_2O + 6e^- \rightleftharpoons CH_3OH + 6OH^-$
CH_4	$CO_2 + 6H_2O + 8e^- \rightleftharpoons CH_4 + 8OH^-$
CH_3COOH	$2CO_2 + 6H_2O + 8e^- \rightleftharpoons CH_3COOH + 8OH^-$
C_2H_4	$2CO_2 + 8H_2O + 12e^- \rightleftharpoons C_2H_4 + 12OH^-$

Of these products, CO is known to be the smallest molecule with a well-understood and straightforward reaction route [31]. In addition, CO is a gaseous product making the choice of CO_2 reduction to CO as the cathodic reaction in this study attractive because it would minimize the addition of liquid products to the anolyte. Thus, CO_2 reduction to CO is the chosen cathodic reaction for this thesis. It should also be noted that, although in a minimal amount, production of formate (HCOO-) occurs in addition to CO from CO_2RR [32]. This will be accounted for while analyzing the liquid products of the electrochemical cell and discussed later in this report.

2.1.1. Thermodynamics

The thermodynamic equations governing the behavior of an electrochemical configuration are crucial in understanding both the cell and the system potentials. Therefore, this chapter will detail the thermodynamics associated with electrochemical cells.

All electrochemical reactions require a potential (E) to drive the reaction. This required potential can be calculated by subtracting the potential associated with the oxidation half-reaction ($E^\circ_{oxidation}$) from the one associated with the reduction half-reaction ($E^\circ_{reduction}$) as such:

$$E^\circ_{redox} = E^\circ_{reduction} - E^\circ_{oxidation} \tag{2.7}$$

where E°_{redox} is the standard thermodynamic potential to drive the total reaction in a cell. The sign of the redox potential calculated using Eq. 2.7 can be correlated to the spontaneity of the reaction in question. If the E°_{redox} is positive, the reaction is spontaneous, and the E° can be taken as the amount of generated potential difference from the occurrence of the chemical reaction [27]. On the other hand, if the E°_{redox} is negative, the reaction is said to be non-spontaneous, requiring a minimum of E° amount of potential from a voltage source to drive the reaction [27]. In this study, all half-reaction pairings result in negative E°_{redox} values meaning that the cell potential calculated is the minimum amount of potential needed to be supplied.

However, an additional potential (overpotential) is generally required to run and drive a reaction in experimental conditions [29]. This overpotential can be calculated as below:

$$\eta = E - E^\circ \tag{2.8}$$

where η is the overpotential needed, E is the applied potential in V, and E° is the thermodynamic potential to drive the reaction in volts. Without an applied overpotential, no net electrolysis can be observed in a system [27].

This prediction of the spontaneity of reactions can be obtained from the change in Gibbs free energy (ΔG) at constant temperature and pressure as given by:

$$\Delta G = \Delta H - T\Delta S \tag{2.9}$$

where ΔH is the change in enthalpy in J/mol, T is temperature in Kelvin, and ΔS is the change in entropy in J/mol · K [27]. The change in enthalpy can be viewed as the heat released from or the heat required for a reaction, and due to an increase in entropy, the change in Gibbs free energy is smaller than the heat requirement. Since the change in Gibbs free energy is the maximum amount of non-expansion work (w_{max}) done on the system, it is then equal to the required electrical work (w_{el}) in the context of electrochemistry [27].

$$\Delta G = w_{max} = w_{el} \tag{2.10}$$

In general, electrical work is described by the following relation:

$$w_{el} = E_{cell} \cdot I\Delta t \tag{2.11}$$

where E_{cell} is the cell voltage, I is the current, and Δt is the duration in seconds the current is applied. $I\Delta t$ is the amount of charge transferred when a reaction occurs and can also be given by nF where n is the number of transferred electrons and F is the Faraday's constant (96485 $\frac{C}{mol}$). Thus, the required electrical work and the change in Gibbs free energy (under standard and non-standard conditions) can be calculated as such:

$$\Delta G = -nFE_{cell} \tag{2.12}$$

Under standard conditions, Eq. 2.12 then is written as:

$$\Delta G^{\circ} = -nFE^{\circ}_{cell} \tag{2.13}$$

Unfortunately, this equation only applies in ideal conditions. However, the change in Gibbs free energy of a reaction in non-standard conditions can be related to the change in Gibbs free energy in standard conditions by including the effect of reaction mixture composition [27].

$$\Delta G = \Delta G^{\circ} - RT \cdot lnQ_{rxn} \tag{2.14}$$

where R is the universal gas constant (8.314 J/mol*K) and Q_{rxn} is the reaction quotient. Substitution of Eq. 2.12 and 2.13 into 2.14 leads to the Nernst equation as follows:

$$E_{cell} = E^{\circ}_{cell} - \frac{RT}{nF} \cdot lnQ_{rxn} \tag{2.15}$$

2.1.2. Kinetics

This section serves as a quick discussion of the kinetics of electrochemical reactions. Understanding kinetics is essential to interpreting the factors that affect the rate of these reactions and controlling them [27]. It is also highly linked to a current density of a system, which is the amount of electrical current passing through per unit area of a chosen material per second and a key performance indicator.

Let's consider the following simple reversible redox reaction that involves a single electron transfer:

$$O^+ + e^- \underset{k_b}{\overset{k_f}{\rightleftharpoons}} R \tag{2.16}$$

where O^+ and R are a redox couple's oxidized and reduced form, and k_f and k_b are rate constants for the forward (reduction) and backward (oxidation) reactions, respectively. The rates of the forward (v_f) and backward (v_b) reactions with their corresponding current densities can be described as:

$$v_f = k_f \cdot [O^+]_0 = \frac{j_f}{F} \tag{2.17}$$

$$v_b = k_b \cdot [R]_0 = \frac{j_b}{F} \tag{2.18}$$

where j_f is the forward current density, j_b is the backward current density, and $[O^+]_0$ and $[R]_0$ are the surface concentrations of the reactant species [33]. It can be assumed that the rate constants follow Arrhenius's law as such:

$$k_f = k^0_f \cdot exp[-\frac{\alpha F(\eta)}{RT}] \tag{2.19}$$

$$k_b = k_b^0 \cdot exp[\frac{(1-\alpha)F(\eta)}{RT}] \tag{2.20}$$

The k_f^0 and k_b^0 are the rate constants at standard conditions; α is the transfer coefficient, and η is the overpotential applied [33]. It should be noted that in equilibrium, the forward and backward reaction rates are equal; however, at non-equilibrium conditions, the net reaction rate (v) and the net current density (j) are:

$$v = v_b - v_f = \frac{j_b - j_f}{F} = \frac{j}{F} \tag{2.21}$$

By combining the Eqs. 2.17, 2.18 and 2.21, the Butler-Volmer equation can be reached:

$$j = j_0 \cdot exp[\frac{(1-\alpha)F\eta}{RT}] - exp[-\frac{\alpha F\eta}{RT}] \tag{2.22}$$

where j_0 is the exchange current density in A/m^2, which is the current density in the presence of no overpotential and net electrolysis. Thus, the Butler-Volmer equation can be used to understand the effect of applied overpotential on the current density of an electrode. At highly positive overpotentials, the oxidation reaction becomes dominant; at highly negative overpotentials, the reduction reaction dominates [33].

2.1.3. Electrolyte Effects

Electrolytes used in CO_2RR systems can significantly affect performance and efficiency. Factors such as the electrolytes' concentration, species, and pH value can influence the local reaction conditions and impact the products produced by the electrocatalyst [34].

The local pH at the electrode plays a crucial role in determining electrocatalytic selectivity. At the cathode, low pH conditions increase the favorability of HER over CO_2RR. This reduces CO_2 utilization and increases inefficiencies in the system [35]. Moreover, low pH conditions at the anode in conventional CO_2RR electrolyzers require using PGM such as iridium and ruthenium. These catalysts are necessary to prevent an increase in overpotentials and the slowing down reaction kinetics that would otherwise occur if catalysts like nickel were used for the anodic oxygen evolution reaction [35].

To avoid these negative consequences, a high local pH can be imposed as a natural conclusion; however, alkaline conditions created by using electrolytes such as KOH also come with some drawbacks. At the cathode, alkaline conditions can be induced to suppress HER and increase multi-carbon product formation, but this increase in the local pH can lead to a reduction in CO_2 availability due to parasitic (bi)carbonate formation [35]. The reaction of dissolved CO_2 with OH^- ions formed by both CO_2 reduction and the competing HER will result in the following reactions:

$$CO_{2(g)} \rightleftharpoons CO_{2(aq)} \tag{2.23}$$

$$CO_{2(aq)} + OH^-_{(aq)} \rightleftharpoons HCO^-_{3(aq)} \tag{2.24}$$

$$HCO^-_{3(aq)} + OH^-_{(aq)} \rightleftharpoons H_2O_{(l)} + CO^{2-}_{3(aq)} \tag{2.25}$$

The formation of (bi)carbonates depicted above has many consequences. The acidic (bi)carbonates will cause the electrolyte pH to decrease gradually, which can result in the adverse effects of lowered pH, as discussed above, appearing in the system [36]. Their reaction with the cation of the electrolyte can also cause salt formation at the cathode, which increases the likelihood of flooding [35]. Flooding of the cathode electrode will be detailed later, but it mainly decreases CO_2 availability leading to an increase in HER [36].

Studies have also been investigating the effect of different cations in the electrolyte. It was found that the larger a cation is, the smaller its hydration shell is, and the smaller its repulsion will be near the electrode [37]. This reduced repulsion will lead to a higher concentration of cations at the electrode and a larger surface charge density. And finally, the increased surface charge density will cause stabilization of the CO_2RR intermediates, resulting in decreased overpotentials, higher activities, and a change in selectivity [38]. The cations of interest were: Cs^+, K^+,Na^+ and Li^+ listed here decreasing in size, and

thus decreasing in performance. However, the use of K^+ is more common than Cs^+ in CO_2RR studies, which is the case due to the higher price of Cs^+ containing electrolytes [37].

Lastly, it was reported that increased cation concentrations could be leveraged in MEA configurations using bipolar membranes to promote CO_2RR over HER. This indicates that the electrolyte concentrations can be critical in optimizing CO_2RR applications besides the pH environment they create [39].

2.1.4. CO_2RR Electrolyzer Configurations

As described, electrolyzers are the carriers for CO_2RR applications. They allow the testing of electrocatalysts under similar reaction conditions to those found in the industrial practice (i.e., high current densities, pressures, temperatures) [35]. Throughout this thesis, a membrane electrode assembly (MEA) was used for testing; however, H-cell and flow cell are also widely used electrolyzer configurations and will be briefly covered in this section.

H-Cell Electrolyzer

In CO_2RR studies, preliminary research typically starts in an H-cell when investigating fundamental processes and novel catalyst materials. A schematic of this type of CO_2 electrolyzer can be seen in Fig. 2.2.

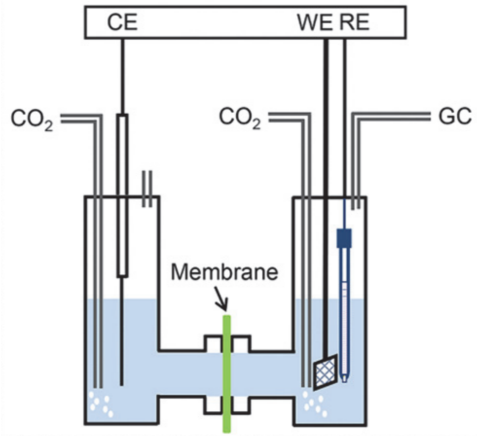

Figure 2.2: Schematic diagram of H-cell type CO_2RR electrolyzer where the working electrode (WE), reference electrode (RE), counter electrode (CE), and the path of the gas output to the gas chromatography (GC) is denoted. Sourced from [40].

In this configuration, the CO_2 and its products diffuse to and from the catalyst through the liquid electrolyte. However, this significantly restricts the current density and selectivity of CO_2RR. Due to the low solubility ($\sim$ 34 mmol/L) and diffusivity ($\sim$ 2x10^{-9} m^2/s) of CO_2 in the aqueous electrolyte, only low maximum current densities can be achieved [41]. If higher current densities were to be applied (>200 mA $\cdot$ cm^{-2}), mass transport limitations would result in an undesirable uptick of HER in the cathode [41] that competes with CO_2RR. H-cell electrolyzers are simple, cheap, and allow rapid screening of new catalysts and electrolyte solutions; however, such limitations restrict their use to lab-scale experiments and hinder their potential in practical applications [41]. To address this issue, gas diffusion electrodes (GDE) that allow CO_2 to reach the catalyst surface in its gaseous form have been developed [35].

Gas Diffusion Electrode (GDE)

As shown in Fig. 2.3, there are two main components of a GDE: the catalyst layer and the diffusion medium that consists of a microporous layer and a gas diffusion layer. The catalyst layer is formed by depositing catalyst particles onto the microporous layer and is the active site for the electrochemical reaction [42]. On the other hand, the diffusion medium acts as the porous medium that allows the gaseous CO_2 to diffuse toward the catalyst layer. It also mechanically supports the catalyst layer and conducts electrons to ensure their flow from the current collector to the active catalyst site [42].

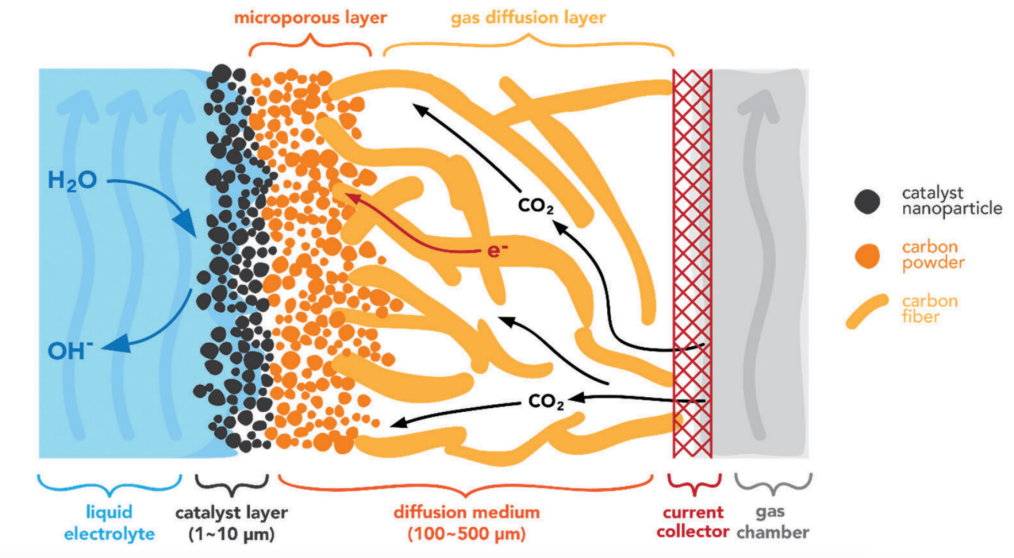

Figure 2.3: Schematic of a gas diffusion electrode. Sourced from [42].

The use of GDEs for CO_2RR systems has allowed current densities an order of magnitude larger than those of H-cell configurations as described above [43]. Their utilization, unfortunately, comes with some stability challenges associated with the flooding of GDEs [43]. Ideally, the gas diffusion layers are made hydrophobic with polytetrafluoroethylene (PTFE) treatment, and electrolyte leakage to the cathodic gas chamber is minimized [42]; however, it was discovered that some applied potentials could still lead to GDE instability [43].

As discussed previously in section 2.1.3, in alkaline environments, CO_2 can go through a side reaction with the OH^- ions to form (bi)carbonates. These (bi)carbonate ions can then react with the potassium ions that were dragged through the membrane in their hydrated form due to osmotic drag and electrostatic forces [44]. These reactions cause salt precipitates to form in low-water regions of the GDE, and their hydrophilic nature attracts water molecules to these areas [45]. Thus, flooding occurs, the diffusion length of CO_2 molecules increase, and active catalyst sites experience CO_2 accessibility issues [46]. This shift ultimately leads to a rise in the undesirable HER, reducing CO_2RR selectivity [46]. Further research is necessary to develop effective protocols for flooding prevention in GDEs due to the limited knowledge about the causes and mechanisms behind flooding and the gradual shift towards HER. [44].

However, despite these issues, using GDEs as catalytic support in CO_2RR systems can improve activity, selectivity, and stability, making its use necessary for scaling up and establishing this electrochemical process in the industry. Two configurations in which GDE is present and have been widely used in CO_2RR studies are flow-cell and MEA-type electrolyzers.

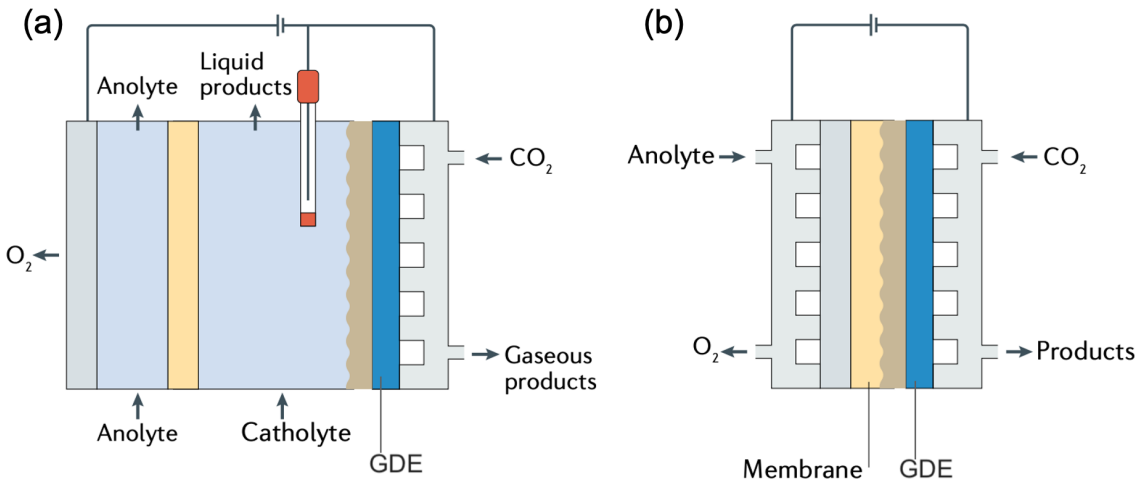

Figure 2.4: Schematics of (a) flow cell and (b) membrane electrode assembly (MEA) type electrolyzer. Modified from [35].

Flow Cell Electrolyzer

As it can be seen from Fig. 2.4 (a) above, the flow cell electrolyzer is composed of an anode, a cathode GDE, a flowing anolyte and catholyte, a reference electrode, and a membrane. As described above, the utilization of GDE solves the CO_2 solubility issues. In fact, through the use of flow cell electrolyzers, very high (>600 mA $\cdot$ cm^{-2}) current densities can be achieved; however, due to the presence of the catholyte, some stability issues arise [46]. The presence of the catholyte increases the risk of flooding in the GDE as described above, and any impurities present in the catholyte have the potential to reduce the performance efficiency and the stability of the system [46]. Flow cell electrolyzers also suffer from high ohmic resistivity and low energy efficiencies due to their sizeable interelectrode separation (in the order of a few millimeters) [40].

Another disadvantage of flowing electrolyte CO_2RR systems is that they experience a gradual lowering of bulk electrolyte pH due to an accumulation of highly acidic (bi)carbonates [36]. In flow cell electrolyzers, the parasitically formed (bi)carbonates don't get a chance to react with the H^+ ions to revert to CO_2 before flowing away from the electrolyzer, thus slowly turning the bulk electrolyte acidic. This creates stability issues in the system and limits the types of catalysts used on the anode [36].

Membrane Electrode Assembly (MEA) Cell Electrolyzer

MEA-cell electrolyzers are the most likely configuration for cost-effective industrial CO_2RR applications [40]. As it can be seen in Fig. 2.4(b), the MEA cell can also be described as a zero-gap electrolyzer cell due to its compact configuration where the anode, the membrane, and the cathode are stacked one after another with no gaps in between. In an MEA cell, the membrane works as a solid electrolyte, reducing the distance between the two electrodes to the membrane thickness (in the order of tens of micrometers) [40]. Whereas both flow cells and MEA cells can deliver high currents, this reduction in the interelectrode distance in the MEA configuration lowers the ohmic resistances, and the system's energy efficiency is increased [25]. Additionally, the simple and thin structure of MEA makes it easier to scale up, allowing researchers to investigate the system in various sizes [47].

A disadvantage of MEA cells is that the sandwiching of the electrodes and the membrane causes parasitically formed (bi) carbonates to reach the anode catalyst layer directly. This leads to high (bi)carbonate concentrations at the anode, creating a lower local pH at the anode than the bulk electrolyte [36]. The lowered local pH can then contribute to catalyst deactivation and lowered stability [36]. Nonetheless, MEA's scalability and higher efficiencies make it still the most attractive for further studies on the way to industrial-level applications; hence it is the chosen electrolyzer configuration in this study.

2.1.5. Ion Exchange Membranes

Ion exchange membranes are an essential part of electrolyzer systems. Their main functions are: (1) to allow the passage of the desired ionic charge carriers, (2) to ensure the separation of reactants and products between anode and cathode, and (3) to provide a regulated environment for electrode reactions [48]. They are manufactured to contain immobilized ionic groups and aid in the transport of hydroxide anions in the case of anion-exchange membranes (AEM) and protons along with cations species like K^+ in the case of cation-exchange membranes (CEM). A third type of ion-exchange membrane called bipolar membrane (BPM) consists of both a cation exchange layer (CEL) and an anion exchange layer (AEL) laminated together. Usually, there is also a water dissociation reaction (WDR) catalyst in this interface layer. Due to the presence of both types of exchange layers, BPMs prevent the transport of ions across its two layers and allow for the evolution of distinct reaction environments at the anode and cathode sides [48].

The specific species that can travel through these membranes vary with the type and other specifications of the membranes. Still, they are mainly determined by the size, and the valence of the species trying to pass through [49]. A driving force, such as a concentration, potential, or pressure gradient, causes transport within the membrane. For electrochemical cells, migration and diffusion are the most common transport mechanisms [49]. As this thesis focuses on the investigation of a glycerol oxidation reaction in MEA cells using both AEM and BPM, a more detailed explanation of the different categories of ion exchange membranes can be found below.

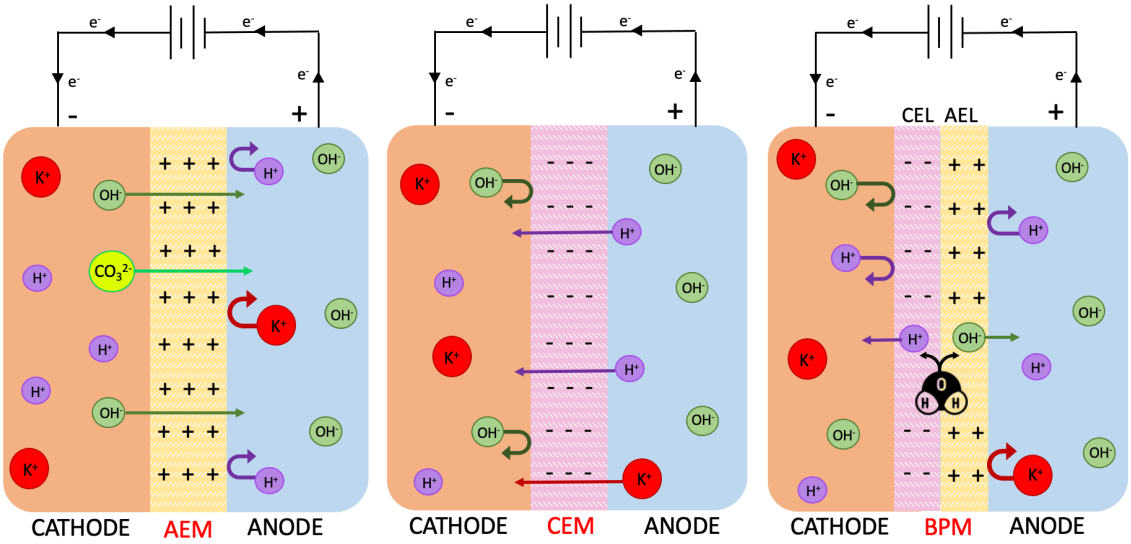

Figure 2.5: Schematic representations of zero-gap electrolyzer cells with (left) an anion exchange membrane where anions can travel from the cathode to the anode through the positively charged AEM, (middle) a cation exchange membrane where cations can travel from anode to the cathode through the negatively charged CEM, (right) a bipolar membrane under reverse bias where neither cations nor anions can pass through the BPM.

Anion Exchange Membrane (AEM):

AEMs are semipermeable membranes designed to conduct anions such as hydroxide and prevent the passing over of cations. This selective permeability is achieved through the positively charged functional groups anchored to the membrane's hydrophobic polymer backbone [50]. When an electric field is applied to the system, anions are driven to move from the cathode (negative electrode) to the anode (positive electrode). In contrast, cations are driven to move from the anode (+) to the cathode (-). However, AEM blocks the transport of cations, as shown on the left in Fig. 2.5. This allows for the reaction environment for the cathode to stay alkaline, which is beneficial for CO_2RR systems since HER becomes more favorable and competes with CO_2 RR in an acidic environment [35]. Thus when AEMs block the cations, this undesired reaction that lowers the faradaic efficiency of the system can

be suppressed. This benefit of AEM is why it is the most commonly used ionic exchange membrane in CO_2RR setups [35].

Given the previous discussion on the effects of pH on the system, a foreseeable disadvantage of the basic environment created on the cathode side due to the use of AEMs is that it favors the formation of catalytically inactive carbonates (CO_3^{2-}) and bicarbonates (HCO_3^-) [35]. Especially at high current densities (reaction rates), these (bi)carbonate ions maintain the ionic conductance of the system, increasing ohmic losses because of the significantly lower ionic mobility of (bi)carbonates compared to OH^- [35]. Moreover, (bi)carbonates acting as the charge carriers lead to a locally acidic surface pH at the anode and cause them to react back to CO_2, decreasing its utilization in the system [51].

A final remark about AEMs is that while they are expected to hinder the transport of cations from the anode to the cathode, this exclusion is imperfect in practice [52]. In the case of KOH based anolytes, the K^+ cation is in its hydrated form in the system. Due to the consumption of water by the CO_2RR, water dragging is present towards the cathode, making K^+ cations crossover. Moreover, the K^+ crossover is also enhanced in the system to provide electroneutrality to deal with the imbalance created by the (bi)carbonate crossover towards the anode [50, 52]. Thus, it is common to observe K^+ salt formation at the cathode GDE leading to gas flow blockage, catalyst surface obstruction, and flooding when AEMs are used [52].

Cation Exchange Membrane (CEM):

CEMs are semipermeable membranes that favor the transport of cations from the anode (positive electrode) to the cathode (negative electrode). This selectivity is realized due to the negatively charged functional groups attached to the membrane's polymeric backbone [50]. The anions driven to migrate toward the anode are prevented from crossing the membrane, as shown in the center in Fig. 2.5. Cation exchange membranes exhibit low ohmic losses and high conductivities because they transport H^+, which are known to be highly mobile ions [35]. Unfortunately, CEMs are not commonly used in CO_2RR systems because the salt precipitation tends to occur too quickly due to K^+ transport. Additionally, they tend to create acidic conditions at both the anode and the cathode unless specifically treated to be selective for K^+ transport and reduce H^+ crossover. As described before, at the cathode, low pH conditions result in the favoring of HER over CO_2RR. At the anode, the acidic conditions tend to increase the anodic reaction overpotentials and require expensive catalysts like iridium and ruthenium [35].

Bipolar Membrane (BPM):

Bipolar membranes can be viewed as a hybrid of AEMs and CEMs. They are composed of an anion-exchange layer (AEL) that transports anions like OH^- and a cation-exchange layer (CEL) that transports cations like H^+ [48]. The presence of both types of layers inhibits the crossover of ions through the whole of the BPM but allows for the creation of distinct reaction environments at either side [48]. A schematic of this behavior can be seen on the right side in Fig. 2.5 above. The junction between AEL and CEL is called an interface layer (IL) and, when operating in reverse bias, becomes a reaction site for water dissociation reaction (WDR), which can be seen in equation 2.26 below. [39].

$$H_2O = H^+ + OH^- \tag{2.26}$$

Since the ions in the bulk electrolyte cannot provide the ionic current due to BPM blocking their passage, the produced H^+ and OH^- carry the ionic current in BPM systems [53]. Orienting the BPM so that the CEL faces the cathode and the AEL faces the anode allows the flux of OH^- to the anode and H^+ to the cathode [53]. This characteristic of BPMs is an attractive feature for its use in CO_2RR systems. Since the water dissociation provides the protons, the parasitic CO_2 crossover described before, a prevalent issue in AEM-based systems, can be eliminated through the use of BPMs [48]. This elimination allows for an increase in the single pass utilization rate of CO_2 (the ratio of the CO_2 converted to the total CO_2 inputted), which results in lower amounts CO_2 crossover that mixes with the anodic outlet and lower amount of energy required for the downstream separation of CO_2.

Due to its hybrid nature, BPM has a few other intrinsic advantages over the monopolar membranes, such as better separation of products and/or reactants and increased stability of electrolytes (reaction environments) at either side of the membrane [48]. This characteristic of BPM makes it commercially

interesting for CO_2 electrolysis applications since the optimal pH is commonly different for the two electrodes [48] in these systems. Formation of these distinct reaction environments (acidic at the anode and alkaline at the cathode) can reduce the overpotential associated with performing OER (or GOR) in acidic anodic reaction environments. However, this characteristic also results in a favorable reaction environment for HER which lowers the faradaic efficiency of CO_2RR products significantly [39]. Recent studies suggest that by using a buffer or decreasing the acidity of the CEL, the undesired HER can be suppressed, but further optimization is required [48].

Another aspect of BPM-based CO_2RR systems is the increased energy cost since the water dissociation reaction requires an applied potential of 0.83 V (the standard reduction potential in V vs. RHE). This increase makes the overall cell potential higher and causes significant energy losses in the system [35]. Some recent studies suggest that such drawbacks can be improved by incorporating catalysts like TiO_2 [54]. However, improvements are still necessary to implement BPMs in CO_2RR applications in commercially relevant conditions.

2.2. Anodic Half-Reactions

As the focus of this thesis is to investigate the optimization of CO_2RR processes through modifying the anodic half-reaction, this section introduces the main subject of this research. The following subsections will discuss the challenges associated with the conventional OER, criteria for potential alternative reactions, and glycerol oxidation reaction as the proposed anodic reaction alternate.

2.2.1. Challenges Associated with OER

As mentioned briefly in the introduction, despite being the most conventionally coupled anodic reaction in CO_2RR processes, oxygen evolution reaction (OER) has many associated challenges. Performing OER on the anode has been made prevalent so far based on two main reasons: no mass transfer limitations are expected due to abundant reactant presence in the system, and the extensive body of knowledge is present for water electrolysis, making this anodic reaction and its catalysts, supports, binders, etc. well-understood [16].

However, quite a few limitations come from OER acting as the anodic reaction in CO_2RR. These constraints are:

OER requires expensive materials as catalysts.

Commercialized OER catalysts that can maintain low overpotentials, desirable kinetics, and high stability are mainly precious metal-based ones such as IrO_2 and RuO_2. Both ruthenium and iridium are among the rarest metals and suffer from high costs and limited supplies [17].

OER is thermodynamically unfavorable.

As briefly mentioned in Section 2.1, the standard thermodynamic potential of OER (1.23V vs. RHE) is significantly higher than the standard thermodynamic potentials of CO_2RR and HER. This potential value causes the total cell voltage to be substantially high [17], making the choice of OER thermodynamically unfavorable.

OER is kinetically unfavorable.

By looking at Equations 2.5 and 2.6, it can be noticed that making 1 molecule of O_2 requires 4 electron transfers. This requirement makes the reaction kinetically sluggish and accounts for 50% of the imposed overpotential to the cell [17, 55].

OER consumes a significant amount of the energy input.

When the standard Gibbs free energies of electroreduction of CO_2 to CO and OER is calculated using Hess's law, it can be concluded that 92.2% of the total energy is being consumed to drive the OER at the anode [12].

Produced O_2 requires a separation step.

In most conventional CO_2RR electrolyzers, a significant amount of CO_2 crosses the membrane from the cathode side to the anode side as bicarbonate/carbonate. Later when these compounds encounter the protons generated from the anodic reaction, they get converted to CO_2 [56]. This

crossover CO_2 then mixes with gaseous O_2 that has been produced via OER to make up an anodic outlet composition of 60-80% CO_2 to 40-20% O_2 [57]. Direct recycling of this gaseous output to the cathode is not feasible due to oxygen reduction likely taking over at the cathode [22]; thus, a costly gas separation step is needed downstream of the anode when OER is the anodic reaction.

Produced O_2 is financially worthless.

The value of the produced oxygen is approximately 30€ per ton, which is quite insignificant and doesn't contribute to the economic viability of the CO_2RR process [16].

2.2.2. Alternatives to OER

Considering the limitations associated with having OER as the anodic reaction mentioned above, the search for alternative anodic half-reactions to couple with CO_2RR has been suggested and investigated in the past few years. However, it is vital to keep in mind that choosing an oxidation reaction that satisfies some of the shortcomings of OER but derails from the overarching efforts of making CO_2 electrolyzers commercially viable is not adequate. Thus, it is necessary to have some guidelines while searching for alternatives to OER for CO_2 electrolysis. In 2019, Verma et al. came up with a few simple principles that can guide the replacement anodic reaction selection process. These process design rules can be sorted under three main categories [12], and these are:

1. Cost.
   - Is the anodic feed expensive?
   - Is there a well-sized market demand for the anodic product?
2. Production of Feed
   - Is the production of the anodic feedstock energy intensive?
   - Does it involve additional CO_2 emissions?
3. Scale
   - Does the anodic feedstock have enough availability to match the scale of projected CO_2 utilization?

The abovementioned criteria are quite encompassing; however, there are a few other requirements that should also be mentioned. First is the compatibility of the reaction to be coupled with CO_2RR. The chosen alternative anodic reaction should be able to handle the current densities required for commercial application of CO_2 electrolysis ($\geq$100 mA/cm^2). Second is the preferred lower thermodynamic potential than OER so that the thermodynamic unfavorability issue can be handled, and the third is the suitability of operating conditions for the reaction to be coupled with CO_2RR.

Keeping the standards discussed above in mind, one group of candidate anode reactions that have recently been investigated due to their mild reaction conditions, catalyst availability, flexible product range, etc. are organic oxidation reactions (OOR). Recent techno-economic analyses have suggested that utilizing OORs would reduce the total cell voltage and produce profitable products from both sides of the cell [12, 22]. These include the oxidation of glucose [22], glycerol [12], alcohols [58], furfural [59], methane [12], etc. Among these alternatives, glycerol is a highly promising choice for numerous reasons. Consequently, this thesis centers on investigating the oxidation reaction of glycerol as the selected anodic reaction.

2.2.3. Viability of Glycerol Oxidation Reaction as the Anodic Reaction

Various reasons make glycerol oxidation reaction (GOR) a promising alternative to OER as the anodic reaction in CO_2RR systems. The first notable advantage of GOR is its potential to significantly reduce the electricity input required in CO_2RR systems [17]. This lower energy cost is due to the lowered cell potential of the total reaction. See table 2.2 below for the standard reduction potentials of OER and a few reaction routes of the glycerol oxidation reaction.

Table 2.2: Possible anodic half-reactions and their standard reduction (thermodynamic) potentials in V vs. RHE[12]

Anodic Half-Reactions	Standard Thermodynamic Potential E°_{anode} (V vs. RHE)
Oxygen Evolution Reaction $2OH^- \rightleftharpoons \frac{1}{2}O_2 + H_2O + 2e^-$	1.23
Glycerol $\rightarrow$ Glyceraldehyde $C_3H_8O_3 + 2OH^- \rightleftharpoons C_3H_6O_3 + 2H_2O + 2e^-$	0.41
Glycerol $\rightarrow$ Lactic Acid $C_3H_8O_3 + 2OH^- \rightleftharpoons C_3H_6O_3 + 2H_2O + 2e^-$	0.25
Glycerol $\rightarrow$ Formic Acid $C_3H_8O_3 + 8OH^- \rightleftharpoons 8HCOOH + 5H_2O + 8e^-$	0.14

Note the significant difference between the standard thermodynamic potential of OER and the standard thermodynamic potential of the listed possible GOR products. This notable divergence of the values indicates the anticipated decrease of the cell potential ($\sim$0.96 V), and thus the required energy input when OER is replaced with GOR in CO_2RR systems. A groundbreaking study by Verma et al. demonstrated a reduction in the system's electricity consumption by 37-53% through coupling CO_2RR with glycerol oxidation to formate and lactate [12].

The second significant advantage of GOR is its liquid-to-liquid nature, which would simplify the overall process design of the CO_2RR systems. As mentioned before in the limitations of OER, due to bicarbonate/carbonate formation, conventional CO_2RR electrolyzers regularly have to deal with CO_2 crossover on the anode side [56]. And because OER involves a gas evolution, the anode gas outlet is a mixture of CO_2 and O_2. Direct recycling of this mixture back to the cathode is impossible since this would cause oxygen reduction to compete with CO_2RR. However, this complex and expensive gas separation step can be avoided by replacing GOR with OER, thanks to its all-liquid nature.

The third notable advantage of glycerol is its potential to produce commercially desirable products in mild conditions, expanding the market potential of CO_2RR systems [12]. Glycerol oxidation reaction can produce many value-added compounds such as aldehydes, carboxylic acids, and other functional groups [21]. Each of these products has various applications in industries from pharmaceuticals to food & beverage industries, thereby increasing the economic viability of CO_2RR systems [21]. More details about the potential products from GOR will be discussed later in this chapter.

And the final advantage of glycerol oxidation over the other potential alternative anodic reactions is its availability and affordability. A more detailed examination of glycerol as a feedstock is discussed below, but it is necessary to mention that in recent years, the growing biodiesel industry has led to an abundance of glycerol, resulting in decreasing prices [60]. This means that utilizing glycerol instead of another chemical like glucose or methane as the feedstock for the anodic reaction not only ensures a readily available and cost-effective resource but also contributes to the valorization of a surplus waste product.

2.2.4. Glycerol

Having discussed the viability of glycerol as an alternative to OER, a quick introduction to glycerol as a potential feedstock is necessary. Glycerol ($C_3H_8O_3$) is an inexpensive by-product of industrial biodiesel and bioethanol production (approximately US\$0.24 kg^{-1} for 80% purity) [60]. As efforts to find less CO_2 emitting alternatives to gasoline and diesel have accelerated, more attention has been given to biodiesel and bioethanol due to their renewable and eco-friendly nature [61]. Crude glycerol is produced via the trans-esterification of triglycerides with methanol, as shown in Fig. 2.6. It makes up about 10 wt% and 7-8 wt% of the products in the process of manufacturing biodiesel and bioethanol, respectively [62].

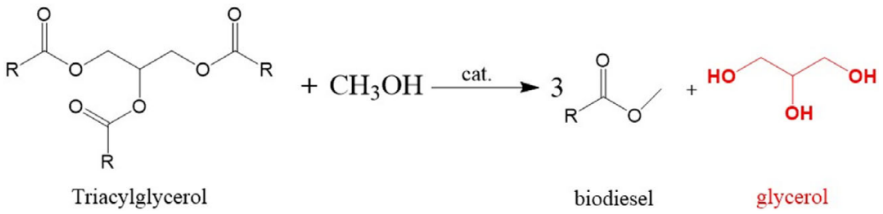

Figure 2.6: Trans-esterification of triglycerides with methanol to make biodiesel and glycerol [21]

The global glycerol market is estimated at around 3000 kilo-tons per year and is expected to increase to 6000 kilo-tons by 2025 [60]. It is expected that as the global production of biodiesel increases, glycerol will be brought into the market, making its price plunge [21] and making glycerol more financially attractive to buy. However, it is important to note that this is significantly smaller in scale compared to the vast magnitude of excess global CO_2 emissions, which currently amount to 14.7 gigatons of CO_2 per year [12]. A substantial increase in biodiesel adoption in the transportation sector could improve this limitation; however, the system is still likely to be limited by the size of this market.

Glycerol can be used as a feedstock to make the necessary chemicals for producing medicine, cosmetics, military equipment, coating, and so on.[21]. Various methods exist to make these value-added products from glycerol, but most are energy-intensive and require intricate processes [21]. On the other hand, electrocatalytic glycerol oxidation is a promising approach to producing these high-value products that have been getting more attention in the past few years.

The high functionality of glycerol comes from its chemical structure. Looking at the chemical structure of glycerol depicted in red in Fig. 2.6, its symmetrical nature and the presence of three hydroxyl groups (OH^-) can be observed. These symmetrical primary and secondary hydroxyl groups can react with different substances and can lead to the production of a wide range of products [21] like formate, oxalate, lactate, dihydroxyacetone, etc. These products can be considered high-value (higher than glycerol) and are desired in various industries. Table 2.3 below summarizes some potential products from glycerol oxidation and their potential applications.

Table 2.3: Various common products of glycerol oxidation and their applications.

Potential GOR Product	Applications
Dihydroxyacetone (DHA)	Chemical intermediate in the pharmaceutical industry [63], sweetener in the food & beverage industry [63], humectant and self-tanning agent in the cosmetic industry [64]
Formic Acid (FA)	Starting material or intermediate in the chemical and pharmaceutical industry, surface treatment agent, fuel in fuel cells, and a potential medium for hydrogen storage [65]
Glyceraldehyde (GLAD)	Fuel for fuel cells [66], a substrate in the study of enzymatic reactions and metabolic pathways [67], and a precursor in the production of pharmaceuticals and fine chemicals [68].
Oxalic Acid (OA)	Bleaching agent, rust remover, a mordant in dying textiles [69], and a chelating agent to remove calcium from wastewater and dissolve metal oxides [70].
Acetic Acid (AA)	A solvent [71], reactant to make synthetic fibers and plastics [72], antiseptic and rust remover.
Tartronic Acid (TA)	Building block for compounds useful in medicine and a precursor in the formation of sugars [21].

Continuation of Table 2.3

Potential GOR Product	**Applications**
Lactic Acid (LA)	A humectant in cosmetics, a preservative and flavoring agent in the food industry [73], and a mordant in textile dyeing [74].
Glyoxylic Acid(GLOX)	A synthetic intermediate in pharmaceuticals and dyeing agent in the textile industry [75].
Glyceric Acid (GA)	Used as a precursor in a wide range of chemical syntheses [76], found in skincare products, and its derivatives are used in the medical industry [77].
Glycolic Acid (GLO)	An acidifier in cleaning agents and wastewater treatments [78], a component in topical treatments for various skin conditions and in the cosmetic industry [79].
Mesoxalic Acid (MA)	Reference material in analytical chemistry [80], a precursor in the production of fine chemicals like dyes and pharmaceuticals, chelating agent or complexing agent for metal ions in wastewater treatment [81].

Electrocatalytic glycerol oxidation reaction is a complex multi-electron transfer process. Fig. 2.7 showcases the complex reaction pathways in making the previously listed GOR products.

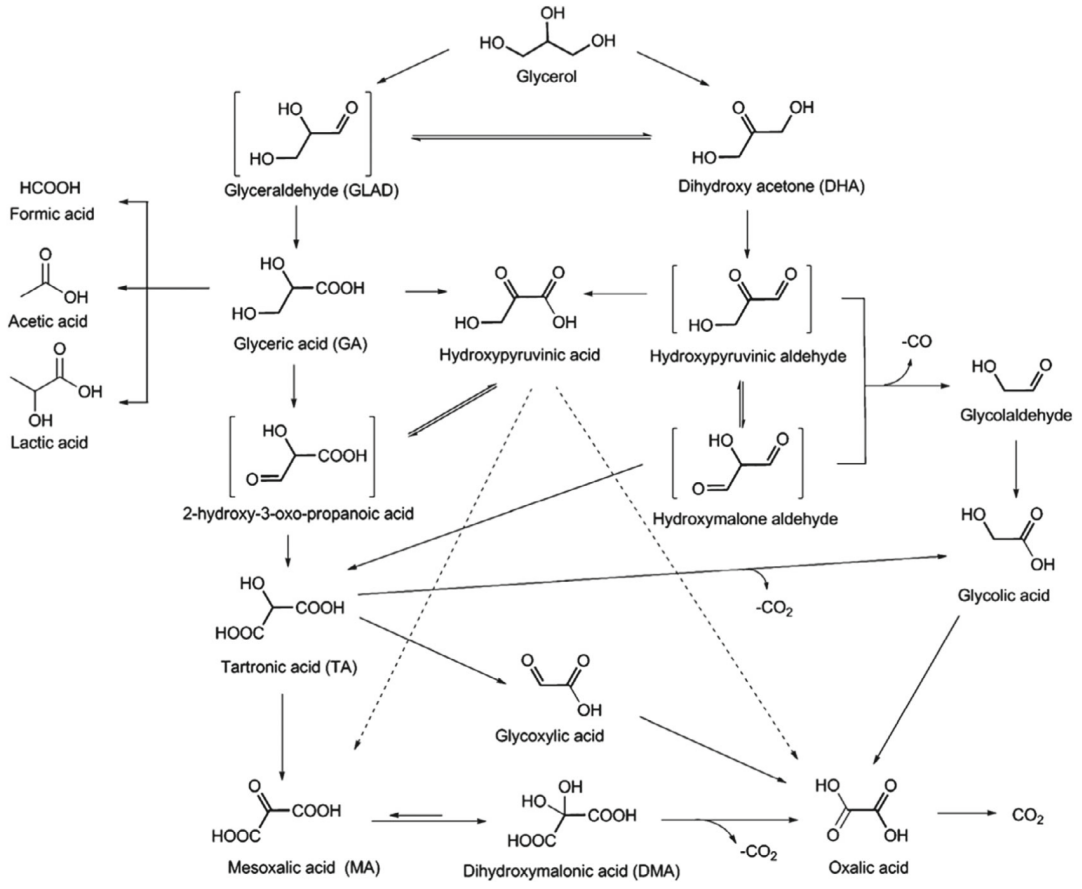

Figure 2.7: The main reaction pathways of the glycerol oxidation reaction. Sourced from [21].

For the production of C_3 products, the primary -OH of the glycerol can be oxidized to GLAD and

GA, and the secondary -OH can be oxidized to DHA. Further oxidization of GLAD and DHA can then lead to TA, MA, and hydroxypyruvic acid. The formation of C_2 products such as LA, AA, and OA, on the other hand, is mainly caused by the further oxidization of GA through the breaking of on C-C bond [21]. Various pathways can also lead to the production of one product, which is the case for OA, as seen in Fig. 2.7. As a C_1 product of GOR, formate is formed through the C-C bond cleavage of GA [21]. The complete oxidation of glycerol can also result in CO_2 production; however, the sluggish oxidation kinetics and the high energy barrier for C-C bond cleavage make this quite tricky [82]. The variety of pathways briefly described here depends on the catalytic activity, reaction environment, and selectivity of the catalysts used for the GOR reaction. The different pathways also lead to ongoing debates, creating a challenge in achieving highly selective catalysis towards a single GOR product in specific environments [21].

2.3. Catalysts

Since catalysts play an essential role in the stability and selectivity of many multiproduct reactions, they have been a focus topic for many researchers aiming to optimize CO_2RR systems.

Cathodic Catalysts

As mentioned in section 2.1, CO_2 electroreduction can result in various products. The selectivity of these value-added products depends on many factors, such as the reaction environment, system configuration, and, most significantly, the chosen catalyst for the cathodic reaction. The available literature has reported a wide range of CO_2 reduction catalysts. Although homogeneous catalysts can also be used in CO_2RR systems, they suffer from solubility issues in aqueous electrolytes. Heterogeneous catalysts, on the other hand, do not face that issue and can reach much higher activities due to their proximity to the current collectors [83].

In particular, metal-based catalysts such as Au, Ag, Cu, and Pd show excellent activity and selectivity in CO_2RR applications [84]. For CO_2RR, where multiple products and pathways are possible, the binding strength of the CO intermediate has a significant effect on product selectivity. For instance, Ag binds to the CO intermediate too weakly; thus, CO has a short residence time on the catalyst surface, insufficient to undergo the C-C coupling necessary for producing C_2 products [84]. However, this makes it a suitable catalyst for single-carbon products such as carbon monoxide and formate. On the other hand, copper has the unique ability to produce a wide range of higher carbon products (e.g., methane, ethylene, alcohols, etc). This is due to its moderate binding strength to CO, which increases the residence time of CO and makes the necessary reduction reactions possible [84].

As previously stated, this thesis investigates the paired electrolysis of glycerol oxidation reaction with CO_2RR towards CO. This was done to minimize the different types of liquid products that could be mixed into the electrolyte since GOR would also produce various compounds. Hence, the chosen cathodic catalyst in this study is Ag. Besides being a catalyst with good CO selectivity ($\sim$81%), silver also costs significantly less than other precious metal catalysts making it a suitable option for industrial applications [85].

Anodic Catalysts

Until recently, little attention has been given to the anode reaction and the anode itself. In conventional CO_2RR systems, the anodic catalysts were chosen to minimize the overpotential, increase the efficiency and enhance the stability of OER in the electrolyzer. In the published works, almost half of the studies have thus utilized Ir (47%), while 30% and 14% of the studies employed Ni and Pt, respectively [86].

The prevalence of Ir and Ni is caused by their stability and high performance for OER in acidic and alkaline aqueous electrolyzers, respectively [86]. Nonetheless, since electrolytes tend to be driven towards a neutral pH regardless of their initial acidity or alkalinity, oxygen evolution reaction requires Ir-based catalysts like IrO_2 to maintain efficient kinetics and low overpotentials. Ni goes through dissolution in near-neutral pH environments when Ir is stable and active [86]. Yet iridium is still far from being the perfect catalyst since it is among the rarest metals on earth. When the overarching goal of

making CO_2RR systems large scale is considered, the dependency on catalysts like iridium becomes economically unfeasible and potentially leading up to availability issues [87]. This limitation is a driving factor in the search for alternative anode reactions to OER and a motivation for this thesis.

GOR Catalysts

Separate from GOR's potential to be coupled with CO_2RR, glycerol valorization is a topic that has been getting more attention with the increase of glycerol influx into the market. Thus, there exists an extensive area of study that investigates the various methods of GOR optimization outside of the CO_2RR context [21]. As with most electrochemical processes, the electrocatalysts' composition, structure, and morphology play an essential role in the selectivity and activity of GOR [21]. Thus, this section aims to summarize existing GOR catalysts that informed the selection of the anodic catalysts in this thesis.

A list of some existing electrocatalysts and their GOR performance from previous studies can be seen in Table 2.4 below. Noble metal-based catalysts such as Pt, Au, Ag, and Pd have been widely employed in GOR studies due to their remarkable stability, excellent corrosion resistance, high-temperature oxidation resistance, and high catalytic activity [21]. Especially platinum has been receiving significant attention for its excellent catalytic activity and stability in both acidic and alkaline environments despite being one of the rarest materials [21].

Table 2.4: The GOR performance and electro-oxidation parameters of GOR electrocatalysts.

Catalyst	Electrolyte	E_{onset} (V)	Products	Ref.
Pt (111)	0.1M H_2SO_4 + 0.1M GLY	0.35 V vs. RHE	DHA, GLO	[88]
	0.1M H_2Cl_4 + 0.1M GLY	0.35 V vs. RHE		
Pt (100)	0.1M H_2SO_4 + 0.1M GLY	0.55 V vs. RHE	DHA, GLO, FA, CO_2	
	0.1M H_2Cl_4 + 0.1M GLY	0.55 V vs. RHE		
Au	0.1 M NaOH + 1 M GLY	0.65 V vs. RHE	DHA, TA, MA, GLOX, CO_2	[89]
	0.1 M H_2SO_4 + 0.1 MGLY	-	TA, FA, CO_2	
Pt	0.1 M NaOH + 1 M GLY	0.5 V vs. RHE	TA, GLO, FA, CO_2	
	0.1 M H_2SO_4 + 0.1 M GLY	0.5 V vs. RHE		
PtAg	0.1 M KOH + 1 M GLY	0.51 V vs. RHE	OA, TA, GLOX, GA, GLAD, DHA	[90]
$Pd_{52.4}Cu_{38.7}Pt_{8.9}$	1 M KOH + 1 M GLY	0.41 V vs. Hg/HgO	GLO, FA	[91]
$Pd_{51.4}Cu_{39.2}Pt_{9.4}$		0.36 V vs. Hg/HgO		
$Pd_{49.5}Cu_{41.4}Pt_{9.1}$		0.34 V vs. Hg/HgO		
$Pd_{50.2}Cu_{38.4}Pt_{11.4}$		0.32 V vs. Hg/HgO		
$PdAu_{irr}$	0.1 M NaOH + 0.1 M GLY	0.5 V vs. RHE	GA, GLO, FA, CO_2	[92]
$Pt_{0.24}Cu_{0.76}$/C	0.1 M NaOH + 1 M GLY	-	DHA, GLAD	[93]
$Pt_{0.31}Cu_{0.69}$/C				
$Pt_{0.62}Cu_{0.38}$/C				
$Pt_{0.74}Cu_{0.26}$/C				
PtBi/C	0.5M H_2SO_4 + 0.1M GLY	-	GA, TA, GLO, OA	[93]
PtSb/C				

Continuation of Table 2.4

Catalyst	Electrolyte	E_{onset} (V)	Products	Ref.
Ni electrode	1.0 M KOH + 0.1 M GLY	1.2 V vs. RHE	GLAD, carbonyl, carboxylate ions	[94]
Ni-CA	1.0 M KOH + 0.1 M GLY	1.32 V vs. RHE	-	[95]
Ni-TBr	1.0 M KOH + 0.1 M GLY	1.33 V vs. RHE	-	[95]
Ni-Mo-N/CFC	1.0 M KOH + 0.1 M GLY	1.30 V vs. RHE	FA	[96]

Early studies have mainly focused on studying the effect of different facets and alloys of various noble metals on GOR selectivity and performance. Pt(111) was found to be more active for GOR, more likely to produce C_3 products, and less affected by CO-poisoning compared to Pt(100) and Pt(101). This was attributed to the difficulty of breaking C-C-C bonds at low potentials in the Pt(111) facet [88]. Later, tuning the components and structure of catalysts has interested many researchers. Examples include the formation of 3D nanoporous PtAg skeletons with primarily Pt(111) facets that produced DHA with high selectivity (82.6%). This improved performance compared to Pt/C was attributed to the high surface area and the abundance of Pt(111) [90].

In addition to Pt-based catalysts, other noble metals such as Au and Pd have also been studied for GOR. Au-based studies mainly focused on the influence of potential and pH and found that polycrystalline Au had higher selectivity for C_3 products and a higher GOR activity in alkaline environments [89]. Pd studies were primarily performed in tandem with other catalysts such as Au or Pt, and it was observed that deposited onto Au, Pd particles could enhance the complete oxidation of glycerol significantly [92].

Another approach was to create hybrid electrocatalysts combining the noble metal catalysts with non-precious metals, such as Cu, Sb, Co, and Bi. The aim was to create multi-component catalysts that harness the advantages of each component while avoiding their shortcomings [21]. It worked for some combinations and not so much for others. For instance, Yang et al. were able to create Pd–Cu–Pt particles in various metal ratios and observed that $Pd_{50.2}Cu_{38.4}Pt_{11.4}$ was able to circumvent CO-poisoning better than others because it was able to easily convert intermediates of GOR into CO_2 [91]. In contrast, another study focusing on introducing Bi to Pt and Pd-containing catalysts was only able to influence the selectivity of Pt-containing catalysts at low potentials but observed no changes in Pd-containing catalysts [93].

Recently, due to their low costs and abundance, non-noble metal catalysts have been getting the spotlight in GOR studies. Especially Ni-based catalysts have been garnering quite a bit of attention [21]. Due to their simplicity, electrodeposited Ni-based catalysts are the most commonly used; however, some studies also report that through the use of structure-directing agents like citric acid (CA) and tetrabutylammonium bromide (TBr), specific morphologies can be enhanced, and higher catalytic activities can be achieved [95]. Like noble-metal-based catalysts, hybrid catalysts such as Ni–Mo–N/CFC were also tested to enhance GOR performance [21] and found nearly unity selectivity for formate [96].

Given the studies described above, the two catalysts whose performance will be tested in this thesis are chosen to be Pt and Ni. This choice compares the most commonly preferred platinum group metal catalyst, Pt, and its up-and-coming non-noble alternative, Ni, in a paired electrolysis MEA configuration.

2.4. Previous Studies Coupling GOR with CO_2RR

The paired electrolysis of GOR with CO_2RR has been getting increasing attention due to the benefits of GOR over OER, as described before. Across these studies, various catalysts have been tested in different cell configurations and potential control strategies. Interestingly, none of the studies have utilized zero-gap electrolyzers for this reaction pairing. A review of the literature reveals that while some groups focused on improving the performance of the paired electrolysis via the maximization

of valorization and reduction of anodic gas products, others focused more on ensuring reduced cell potentials. As standard with other research areas, each study offers its suggestions for optimizing this paired electrolysis system while having drawbacks.

The study by Pei et al. demonstrated FEs of over 90% to formate from paired synthesis at current densities of 10 and 22.4 mA/cm². They also reduced cell potentials compared to OER when utilizing Ni-Co-OH-based anodes. However, their discontinuous batch cell configuration is limited by low electrolyte volume and small electrodes, and the absence of a GDE at the cathode is not applicable for high-rate production required in industrial scales [97]. Verma et al.'s study reported formate and lactate formation alongside a potential reduction of up to 53% in electricity demand. However, their use of Pt-black as the anode catalyst poses cost challenges due to its cost and rare nature [12]. Similarly, Vehrenberg et al. have simultaneously achieved reduced cell voltages and the production of value-added GOR products (mainly lactate) while utilizing the expensive Pt catalyst [98].

In contrast, Junqueira et al. employed a nickel-based anode and achieved formate FEs of 96% at the cathode and 45% at the anode at a current density of 200 mA/cm². Unexpectedly, despite these promising results, their study did not show a reduction in cell potential compared to OER [99]. It is worth noting that a separate investigation, which utilized a Pt/C catalyst on carbonaceous support, reported an unanticipated increase in energy consumption by 25-50% upon replacing OER with GOR [24]. However, no detailed explanation was provided as to why this was observed, and the behavior was simply attributed to the higher anode potentials measured. Moreover, a recent study utilizing Ni_3S_2 on nickel foam achieved exceptional formate FEs of up to 90%, reported on potential adverse effects of high formate concentrations on GOR. Yet, no reduction in cell potential was reported [100].

Aside from formate, there has also been interest in producing other potential GOR products due to their high value and demand. For instance, Bajada et al. developed a molecular catalyst on an indium tin oxide scaffold to ensure high FEs to glyceraldehyde (83%) from GOR while CO and H_2 were produced at the cathode [101]. But these studies were found to be limited and generally had significant formate FEs despite efforts to minimize them.

A comprehensive compilation of these existing studies, including those discussed here and others, is available in Table 2.5 below. The array of previous studies underscores the diverse efforts and challenges in the paired electrolysis of GOR and CO_2RR. These investigations reveal the complex relationships of catalysts, configurations, and potential controls while highlighting the need for innovative approaches to address limitations. Within this context, the investigation into paired electrolysis using the zero-gap electrolyzer configuration is identified as an unexplored and promising area of study which is what is pursued in this thesis.

Table 2.5: Reported studies in literature coupling GOR with CO_2RR according to: (a) anodic electrode; (b) cathodic electrode; (c) the composition of the anolyte; (d) the composition of the catholyte; (e) the cell configuration; (f) the main cathodic products; (g) the main anodic products; (h) the cell voltage; and (i) the total current density applied.

Anode	Cathode	Anolyte	Catholyte	Cell Configuration	Cathodic Product	Anodic Product	E_{cell} (V)	j ($mA \cdot cm^{-2}$)	Ref.
CoP-NF[1]	AgBOC[2] GDE	KOH (1.0 M) + GLY (0.1 M)	$KHCO_2$ (0.5 M)	Two-compartment flow cell with AEM	FA	FA	2	50	[102]
Co-Se on CC[3]	Ni GDE	KOH (2.0 M) + GLY (2.0 M)	$KHCO_2$ (2.0 M)	Two-compartment flow cell with CEM	CO	FA	2.2	111.1	[103]
Ni-Au/C-GDE	Ag GDE	KOH (2.0 M) + GLY (2.0 M)	KOH (2.0 M)	Two-compartment flow cell with AEM	CO	FA	1.55	-	[104]
Pt-black GDE	Ag GDE Cu GDE Sn GDE	KOH (2.0 M) + GLY (2.0 M)	KOH (2.0 M)	Two-compartment flow cell with AEM	CO, FA C_2H_4 C_2H_5OH	FA, LA	1.5 1.5 1.5	94.67 99.19 72.95	[12]
Pt/C on CP	Bi/C GDE	KOH (1.0 M) + GLY (1.0 M)	KCl (0.5 M) + $KHCO_3$(0.45 M)	Continuous filter press cell with CEM	FA	FA, GLAD, CARB[4], GLO, LA, MA, DHA	3.46 4.51	45 90	[24]
Ni-Co-OH on NF	BiOI on CP[5]	KOH (1.0 M) + GLY (0.1 M)	$KHCO_3$ (0.5 M)	Discontinuous batch flow cell with CEM	FA	FA	1.74 1.9	10 22.4	[97]
STEMPO[6] on ITO[7] scaffold	CNT[8] -CoPPc on CP	$KHCO_3$ (0.3 M) + GLY (50 mM)	$KHCO_3$ (0.5 M)	Two-compartment cell with AEM	CO	GLAD	-	-	[101]
Ni_xB on NF	BiOBr GDE	KOH (1.0 M) + GLY (1.0 M)	KOH (1.0 M)	Two-compartment flow cell with CEM	CO, FA	FA, OX, TA, GA, GLO, LA, AA	4.5	100	[99]
Ni_3S_2 on NF	InBi-GDE	KOH (1.0 M) + GLY (1.0 M)	$KHCO_3$ (0.1 M)	Two-compartment flow cell with BPM	FA	FA	3.4	100	[100]
Pt/C on GDE	Sn/C GDE	KOH (1.0 M) + GLY (2.0 M)	$KHCO_3$ (0.5 M)	Two-compartment flow cell with CEM	FA	LA, FA, GLO	4.4	50	[98]

[1] NF = Nickel foam
[2] BOC = Bismuth subcarbonate
[3] CC = Carbon cloth
[4] CARB = carbonates
[5] CP = Carbon Paper
[6] STEMPO = (2,2,6,6-tetramethylpiperidin-1-yl)oxyl modified with a silatrane-anchor
[7] ITO = Indium tin oxide
[8] CNT = Carbon nano tube

3

Experimental Method and Materials

3.1. Experimental Method

The main objective of the experimental study is to understand and optimize the coupling of glycerol oxidation with CO_2 reduction to CO in zero-gap electrolyzers. Since both sides of the cell yield valuable compounds, this coupling is paired electrolysis; therefore, both anodic and cathodic products are measured throughout the experiments. However, minor performance changes in CO_2RR are not the primary concern of this thesis, and the cathodic products are mainly measured to ensure reasonable CO_2RR selectivities are achieved. This assumption that the CO_2RR performs as expected is made to simplify the analysis of experiments and direct the focus on the anodic reaction.

The anodic catalyst, glycerol concentration, applied cell potentials, and applied current densities all affect the selectivity of the GOR products and the amount of glycerol that can be valorized. Cyclic voltammetry can be used to determine the potential of a catalyst to be active for GOR. Chronopotentiometry (when the current density is applied) or chronoamperometry tests (when the cell potential is applied) can be used to evaluate the performance of the MEA cell for different catalysts and different glycerol concentrations in the anolyte.

Starting with the state-of-the-art AEMEA cell configuration, the plan was to test the paired electrolysis at seven potentials (1.8, 2.1, 2.4, 2.7, 3.0, 3.3, 3.6V) in a stepwise process with twenty-minute increments. It was designed to observe the effect of different applied cell potentials on the performance of the two GOR catalysts in question (Pt and Ni). However, most experiments showed high levels of salt precipitation at the 3.3V and 3.6V steps, rendering the data unreliable for those potentials. Then, to investigate the effect of glycerol concentration on GOR selectivity and activity, three different glycerol concentrations (0.1 M, 0.5 M, 1.0 M) were added to the anolyte (0.5 M KOH) and tested in the aforementioned stepwise process using both catalysts.

In addition to completing all the previously mentioned tests, the catalysts were tested at one commercially relevant rate ($\sim$ 100 mA/cm^2) for CO_2RR. Moreover, an equal mole amount of the Ni catalyst was sputtered on the same support material as the Pt anode to level their electrochemical active surface areas and investigate the cell performance with less uncontrolled variables. Finally, the Ni catalyst was tested in the BPMEA cell configuration to understand the impact of BPMs on the system performance. It should also be mentioned that in BPMEA stepwise experiments, instead of applying the potentials listed above, five current densities (25, 50, 100, 150, 200 mA/cm^2) were applied to ensure comparability with the available literature.

3.2. Experimental Setup

Fig. 3.1 shows a process flow diagram for the experimental setup used in this thesis. A membrane electrode assembly (MEA) from Dioxide Materials was utilized for all experiments. A potentiostat powers

the MEA to facilitate the electrochemical reactions. The potentiostat allows the application of desired current densities and cell potentials based on the specific test.

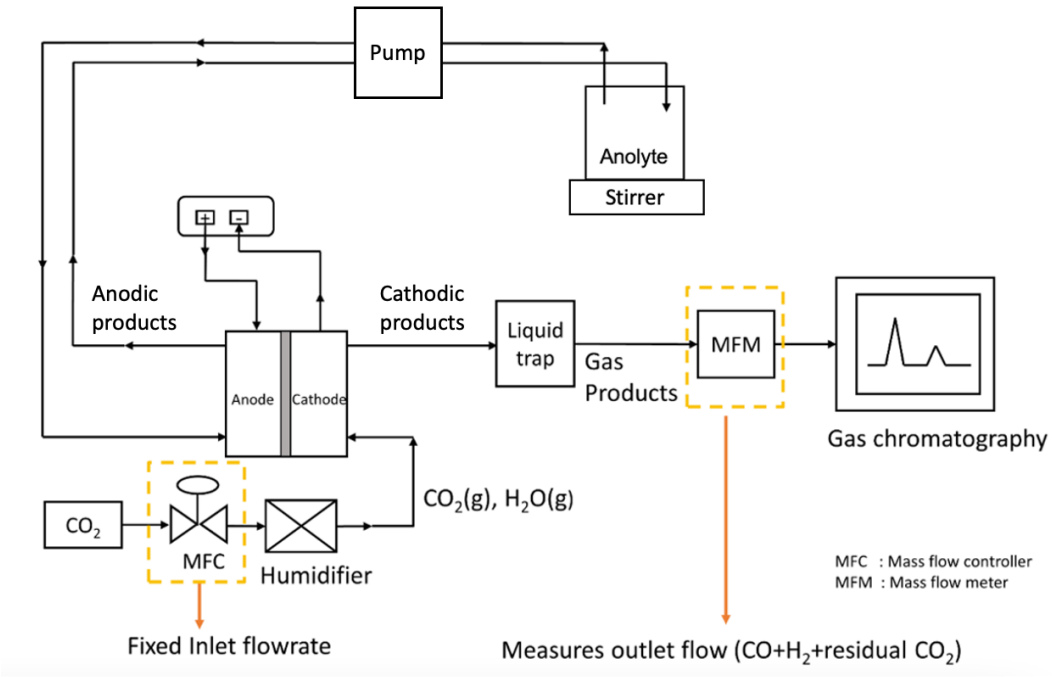

Figure 3.1: Process flow diagram of the experimental setup used for paired electrolysis of GOR with CO_2RR in an MEA. Modified from [105].

The MEA has inlet and outlet connections on both sides to supply reactants to the respective reactions and remove products from the reaction sites. On the cathode side, the MEA is fed with humidified CO_2 by bubbling dry CO_2 from a cylinder into a water bath at room temperature. This step ensures the membrane remains humidified and maintains low ohmic resistances associated with MEAs [106]. The flow rate of CO_2 is controlled by a mass flow controller (MFC), and in this study, it is set at a fixed flow rate of 50 sccm.

The gaseous cathodic products, such as CO and H_2, are removed from the MEA through the cathodic outlet. The products first pass through a liquid trap to capture any anolyte that may have flooded through the gas diffusion electrode (GDE). Then, their flow rate is measured using a Bronkhorst mass flow meter (MFM) as shown in Fig. 3.1. The MFM is connected to a gas chromatograph (GC) that separates the chemical components of a sample, enabling the detection of specific compounds [107]. The concentrations of gaseous cathodic products can be obtained from gas chromatography. The GC available can only accept a single stream of gas flow, samples are collected every 5 minutes using the GC, and the average values for each applied reaction condition are used to calculate FEs.

On the anode side, anolyte is fed into the MEA via a peristaltic pump at a constant flow rate of 20 mL/min. Since the pump continuously circulates the anolyte through the cell, the liquid anodic products formed on the reaction site are able to be removed from the anodic outlet and join the bulk anolyte. The anolyte container is sealed with Parafilm to avoid acidification by atmospheric CO_2. The anolyte is kept well-mixed throughout the experiments using a stirrer, and liquid samples are collected from the bulk for each applied current density/potential. These samples are then analyzed using H-NMR.

Regarding the electrolyte in the system, it is essential to consider the type and concentration to optimize the experimental conditions. In AEMEA experiments, an anolyte with a concentration of 0.5 M KOH was selected to create an alkaline environment within the cell, considering factors such as membrane compatibility and performance. This concentration was chosen to minimize the formation of salts and prevent flooding, which can negatively affect the experimental outcomes. However, for

BPMEA experiments, a higher concentration of 1.0 M KOH was utilized to promote CO_2RR over HER, as BPMs have been found to exhibit reduced susceptibility to salt formation [48].

Moving onto the components that comprise the membrane electrode assembly, Fig. 3.2 shows the schematic view of the MEA configuration used in the experiments.

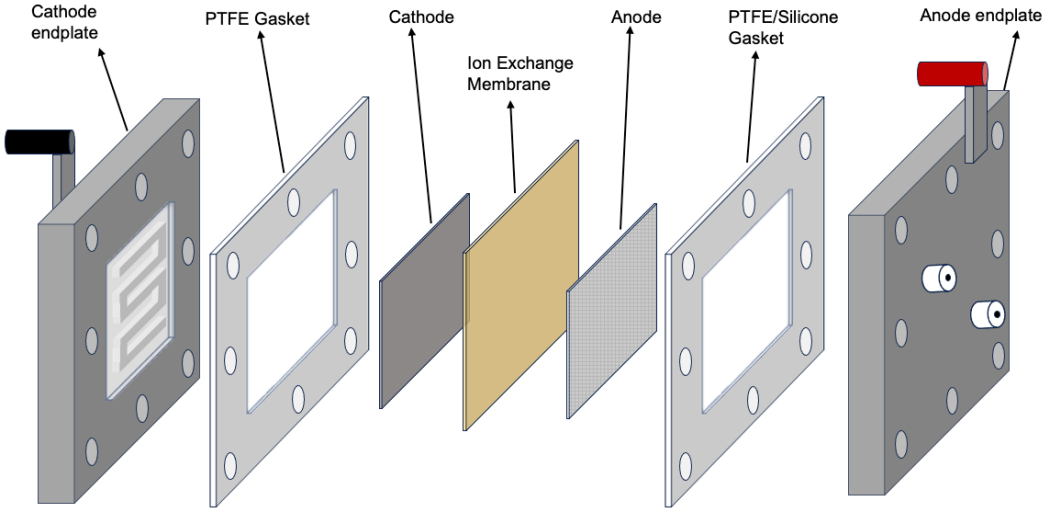

Figure 3.2: Schematic of the membrane electrode assembly configuration used in the experiments.

The figure depicts the seven main components of the MEA cell used in this thesis. The cathode and anode endplates that can be seen at both ends of the image are the current collectors of the cell. The black and red connections at the top are used to attach the MEA to the potentiostat, and the white channels coming out of the back of the endplates are the inlets and outlets for the reaction components. Although only the cathodic endplate's inside is shown in this schematic, both endplates have flow channels that allow for the flow of reactants and products through them to reach the reaction sites of the electrodes.

The cathode was kept the same throughout experiments. A Sigracet 39 BB gas diffusion layer (GDL) of 5.06 cm^2 area (2.25cm x 2.25cm) was used as the porous transport layer. To make the cathode active, a 100 nm thick Ag catalyst layer was sputtered on top of the microporous layer of the GDL using direct current magnetron sputtering. On the anode side, two different electrodes were tested. The first type is a Nickel foam with an area of 5.29 cm^2 (2.3cm x 2.3cm). The second type is a platinized titanium fiber felt sputtered with a 200 nm layer of Pt on one side. The titanium support was picked due to its excellent stability. Due to only one side being catalytically active, the size of the Pt anode was chosen to be 8.41 cm^2 (2.8cm x 2.8cm) to ensure a larger surface area than the cathode. This size increase was unnecessary for the Ni foam anode because the activity is not limited to only one electrode side.

For each experiment, a fresh ion exchange membrane and a fresh Ag GDE were used to enhance the accuracy of the results. For AEMEA tests, Sigracet anion exchange membranes were used, whereas, for BPMEA tests, Fumasep bipolar membranes were used and positioned to ensure the cation exchange layer faces the cathode.

Gaskets are positioned between the endplates and the electrodes to secure the electrodes in position and ensure a tight seal in the electrochemical cell. Each gasket used is fitted with appropriately sized openings, and they are made of either PTFE or silicone, chosen based on the required thickness to securely hold the electrodes in place. PTFE gaskets were used for Pt and Ag GDE electrodes, but for Ni foam, the silicon gasket was used.

Around the perimeter of the endplates and the gaskets, eight openings can be observed. These openings allow for the passage of bolts that can be used to physically compress the MEA cell compo-

nents together. Tightening was achieved using a torque wrench set to 2.5 N·m. This compression was chosen to ensure no damage to the Ag GDE while providing full contact between the electrodes and the membrane.

3.3. Analysis

3.3.1. Analysis of Products

Faradaic efficiency (FE) describes the selectivity of an electrochemical process toward the production of a specific product. It is one of the essential parameters used to quantify the performance of an electrochemical system since it is common for multiple reactions to occur at a single electrode where one is the desired reaction and the other is the side reaction (i.e., CO2RR and HER or GOR and OER in this study) [27]. As seen from Eq. 3.1 below, FE is defined as the amount of the desired product with respect to the amount possible to produce from the total charges passed [27].

$$FE = \frac{\text{amount of desired product produced}}{\text{amount that could be produced with the coulombs supplied}} \tag{3.1}$$

For this study, the FEs of gaseous and liquid products need to be determined. The analysis of cathodic gaseous products was done using a gas chromatograph (GC) to ensure reasonable CO_2RR selectivities are achieved. Since Ag was used as the cathodic catalyst for all CO_2RR experiments, it was assumed that the output gas was made up entirely of CO, H_2, H_2O and CO_2. Based on a study by Subramanian et. el. using the same electrolyzer setup and gas flow conditions, the humidity of the output stream was taken as 78% (x_{H_2O} = 0.023) [105].

The GC is equipped with two thermal conductivity detectors and a flame ionization detector, and it measures the different gaseous compounds in the sample. A homemade Excel file was created to correct the outlet flow rate data reported through the mass flow meter monitoring system calibrated only for CO_2 and the part per million (ppm) data given by the GC. These values were then used to calculate FEs of gaseous products as seen in Eq. 3.2. A sample calculation of the FEs of gaseous products and the correction calculations performed can be found in Appendices A.1 and A.2, respectively.

$$FE_x = \frac{(ppm_x \cdot 10^{-6} \cdot \frac{P}{R \cdot T} \cdot \dot{V}) \cdot n^e \cdot F}{I} \cdot 100\% \tag{3.2}$$

where:
FE_x is the FE of the gaseous product x,
ppm_x is the corrected parts per million amount of x,
P is the standard pressure in Pa,
R is the gas constant (8.314 $J \cdot mol^{-1} \cdot K^{-1}$),
T is the standard temperature (273.17 K),
$\dot{V}$ is the corrected volumetric flow rate of the outlet stream in m^3/s,
n^e is the number of electrons involved in the reaction,
F is the Faraday's constant (96485 C/mol),
I is the current (A) applied.

Although minimal, the Ag catalyst used in these experiments can also produce liquid formate [32]. This can be assumed to be the case if the FEs of CO and H_2 do not add up to 100%. The missing FE can thus be attributed to formate made from CO_2RR, which will be discussed more when detailing the FE calculations of liquid products.

The liquid products from the anolyte were analyzed using proton nuclear magnetic resonance (H-NMR) spectroscopy. This method allows for both a qualitative analysis to detect the types of compounds present in the sample as well as a quantitative one. For the quantitative analysis, the internal standard was maleic acid (Sigma Aldrich), per the MECS group H-NMR protocol. The NMR samples were

created by mixing 550 μL of the anolyte with 40 μL of the maleic acid solution (0.047 g in 10 mL D_2O) and 10 μL D_2O (Sigma Aldrich). D_2O is used to sharpen the maleic acid NMR signal by exchanging deuterium atoms with carboxyl protons and to eliminate the hydroxyl signals from the KOH anolyte that can overwhelm the rest of the signals. The NMR facility utilized is Agilent-400 MR DD2 operating at 400 MHz, and measurements were made using H-PRESAT experiment mode to suppress the water peak.

Once the spectra were measured, quantitative analysis for all the detected and identified compounds was performed using the MestReNova software. Quantitative analysis entails integrating the area under all the signals identified and calculating the desired concentration via the known concentration of the reference standard in the NMR sample via Eq. 3.3 below.

$$C_x = \frac{I_x}{I_{std}} \cdot \frac{N_{std}}{N_x} \cdot C_{std} \tag{3.3}$$

where:
C_x is the molar concentration of the product,
I_x is the integral (areas under the signal) of the product,
I_{std} is the integral of the reference standard,
C_{std} is the concentration of maleic acid in the NMR sample,
N_{std} is the number of represented protons of the reference standard,
N_x is the number of represented protons of the product.

Once the molar concentration of the product was calculated, it was used to calculate the FE of the liquid products as shown in Eq. 3.4:

$$FE(\%) = \frac{C_x \cdot \frac{V_{NMR\,tube} \cdot V_{anolyte}}{V_{NMR\,sample}} \cdot n^e \cdot F}{I \cdot t} \cdot 100\% \tag{3.4}$$

where:
$V_{NMR\,tube}$ is the total liquid volume in the NMR tube (600 μL),
$V_{anolyte}$ is the total anolyte volume circulated throughout the experiment,
$V_{NMR\,sample}$ is the volume of the anolyte sample in the NMR tube (550 μL),
t is the time in which the current, I, has been applied in seconds.

Since most of the experiments were performed stepwise as described in section 3.1, the C_x parameter inputted into Eq. 3.4 should be replaced with ΔC_x to only account for the concentration increase of the product at a specific applied electrical condition. A sample calculation for the FEs of liquid products can be found in Appendix A.3.

Although the procedure described above gives a comprehensive method to calculate the FE of most liquid products through H-NMR, the calculations are more complex for formate. This is because formate can be produced through both the anodic and cathodic reactions, as mentioned before. Therefore, a modified method of calculation is necessary for the formate FEs, which accounts for the different amounts of electrons required for formate production via GOR vs. CO_2RR, the different sampling frequencies for gaseous vs. liquid products, and more. A detailed explanation for the calculation of FE of formate can be found in Appendix A.4.

Besides NMR, some high-performance liquid chromatography (HPLC) measurements were also completed to check whether any products that are invisible to H-NMR (such as oxalate) were present in the anolyte; however, no trace of them was found in the samples, and HPLC measurements were not pursued further.

3.3.2. Analysis of Cell Performance

The performance analysis of the electrochemical cells was executed using the data acquired from the VersaStudio software, which allows for the control and monitoring of the potentiostat used as part of the setup. As discussed before, most experiments performed for this thesis were realized by supplying

the working electrode (the anode) with either a fixed current and monitoring the cell potential or a fixed cell potential and monitoring the current passing through the external circuit.

Unfortunately, in the setup used for this study, no reference electrode is present to read the anode potential. Therefore, only the total cell potential can be applied or monitored, causing the evaluation of cell performance in terms of changes in energy efficiency and activity to be quite complex.

Moreover, the cell potential (or current density) readings can be impacted by the unexpected and expected side reactions occurring in electrochemical cells, such as: competing HER, water dissociation when using BPM, (bi)carbonate formation, competing OER, and phase changes in catalysts [35, 39]. Thus, the evaluation of cell performance is a complex matter that needs to account for the presence of unintended reactions.

4

Results

This chapter showcases the experimental findings and results obtained during this study. The findings will be explored in Section 5. A total of 33 experiments were performed in the laboratory during this thesis. Appendix B can be referred to for the experiment numbers and their applied experimental parameters. The FEs of the cathodic products (CO and H_2) for each experiment measured to ensure reasonable CO_2RR can be found in Appendix C and the results of the supplementary experiments that did not significantly contribute to the primary conclusions are presented in Appendix E.

4.1. NMR Measurements

As discussed before, the catalyst, reaction environment, and cell configuration are all factors affecting the selectivity of GOR. Therefore, identifying the compounds produced is an essential task tackled first and improved upon throughout this study. In Fig. 4.1 below, an example H-NMR spectra for an anolyte sample where GOR was performed as the anodic reaction can be seen.

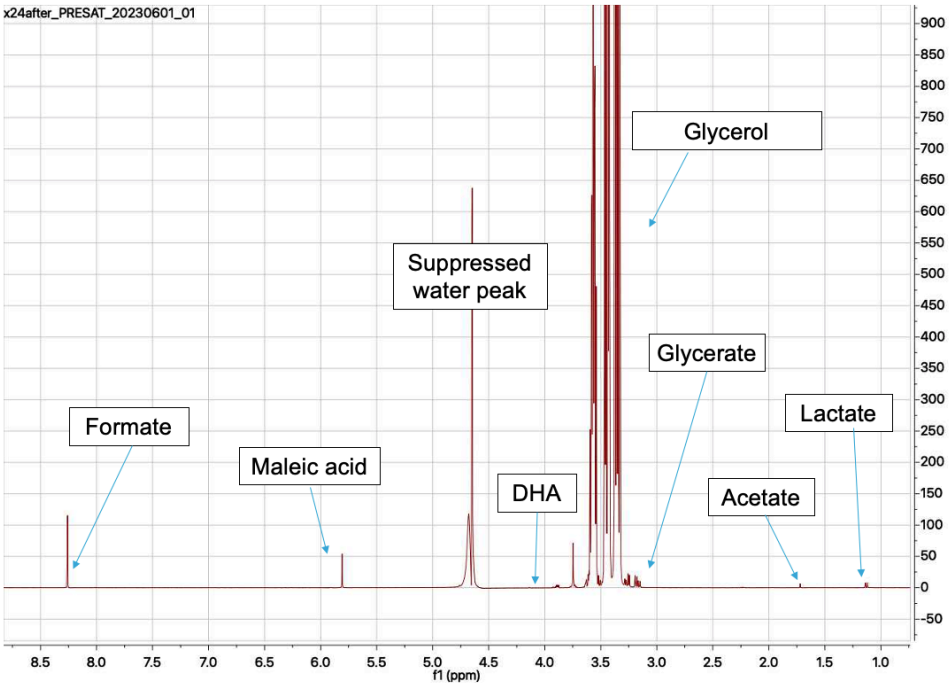

Figure 4.1: H-NMR spectra of the anolyte sample for Exp. 24 and the identified peaks

While the presented spectrum is from a single experiment, it is essential to note that the same signals were consistently observed in measurements taken from samples of other experiments where OER was replaced with GOR, regardless of the anodic catalyst used. All samples were measured to be highly alkaline, and for the experiments where GOR was intended, slight yellowing was observed. Most signals were identified using the available literature in GOR studies or NMR databases such as the Human Metabolome Database [108]. The identified peaks, their chemical shifts, peak type, and proton locations in the compound are shown in Table 4.1 below.

Table 4.1: H-NMR signal values for identified compounds in the anolyte

Chemical Name	Proton Location	Chemical shift (ppm)	Peak type
Maleic Acid	$HO_2CCH{=}CHCO_2H$	5.8	Singlet
	HOCHH-CHOH-CHHOH	3.57	Multiplet
Glycerol	HOCHH-CHOH-CHHOH	3.45	Doublet of doublets
	HOCHH-CHOH-CHHOH	3.35	Doublet of doublets
Formate	HCOOH	8.25	Singlet
DHA	$HOCH_2C{=}OCH_2OH$	4.1	Singlet
Glycerate	$HOCH_2CHCO_2H$	3.22	Multiplet
Acetate	CH_3COOH	1.72	Singlet
Lactate	$CH_3CHCOOH$	1.13	Doublet

Aside from the reference standard (maleic acid) and the reactant (glycerol) still present in the sample, the compounds listed are the products of glycerol oxidation observed in zero-gap electrolyzers when using Ni foam or Pt as the anode. The balanced half-reactions below correspond to the conversion of glycerol into these specific GOR products in alkaline solutions.

$$C_3H_8O_3\,(glycerol) + 11\,OH^- \rightarrow 3\,HCOO^-\,(formate) + 8\,H_2O + 8\,e^- \tag{4.1}$$

$$C_3H_8O_3\,(glycerol) + 2\,OH^- \rightarrow C_3H_5O_3^-\,(lactate) + 2\,H_2O + 2\,e^- \tag{4.2}$$

$$C_3H_8O_3\,(glycerol) + 5\,OH^- \rightarrow C_3H_5O_4^-\,(glycerate) + 4\,H_2O + 4\,e^- \tag{4.3}$$

$$C_3H_8O_3\,(glycerol) + 7/2\,OH^- \rightarrow 3/2\,C_2H_3O_2^-\,(acetate) + 7/2\,H_2O + 2\,e^- \tag{4.4}$$

$$C_3H_8O_3\,(glycerol) + 2\,OH^- \rightarrow C_3H_6O_3\,(DHA) + 2\,H_2O + 2\,e^- \tag{4.5}$$

4.2. Cyclic Voltammetry Tests

The cyclic voltammetry responses presented below in Fig. 4.2 are part of the examination of the two chosen catalysts, Ni & Pt, regarding their performance for glycerol oxidation compared to oxygen evolution reaction. Peaks are already labeled in the figure; however, a discussion regarding their assignments will be explained in Section 5.2.

The CV response of the Pt electrode under anodic conditions on Fig. 4.2a demonstrates notable differences with the addition of glycerol into the electrolyte. An increased anodic current density is observed at all applied potentials in the presence of glycerol. Furthermore, this presence leads to a reduction of 1.2 V in the onset potential compared to the OER case. In the presence of glycerol, the Pt electrode exhibits two reversible redox pairs centered at 1.0 V and 2.05 V. A comparison between the OER and GOR responses at 5 mA·cm^2 reveals a reduction of approximately 1.32 V in the anodic half-reaction. When glycerol is absent in the electrolyte, an oxidation peak centered around 1.0 V and a reduction centered around 0.2 V is observed.

In the Ni anode measurements, as seen in Fig. 4.2b, the presence of glycerol reduces the onset potential of oxidation in CV by 0.3 V. Ni electrode exhibits a reversible redox pair centered at 1.3 V in

the absence of glycerol. The redox pair disappears in the presence of glycerol; however, an irreversible oxidation peak centered around 0.9 V can be observed instead. A comparison between the OER and GOR responses at 5 mA·cm^2 shows around 0.33 V reduction in the anodic half-reaction for the Ni anode.

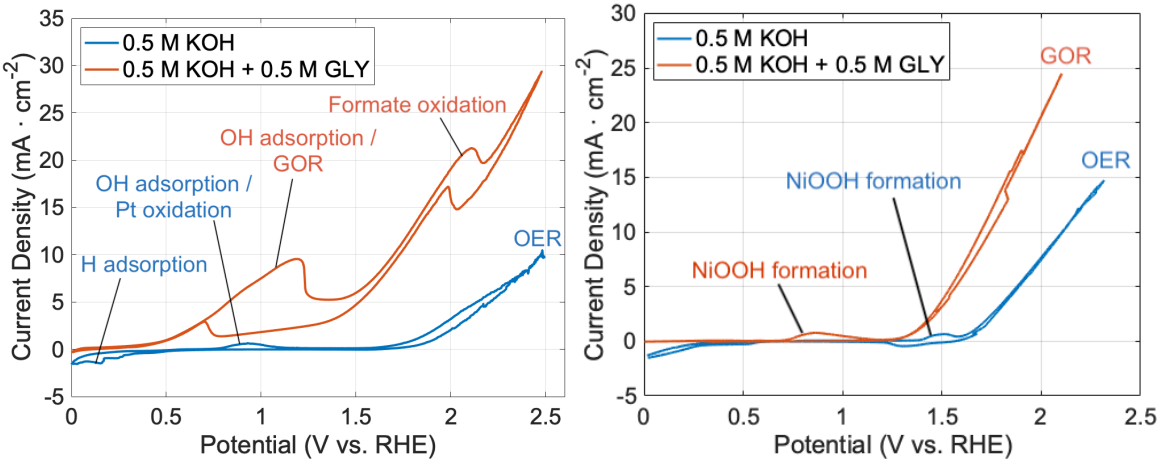

(a) CV response of the Pt anode

(b) CV response of the Ni foam anode

Figure 4.2: Cyclic voltammetry (CV) responses of Pt and Ni foam electrode recorded in a single compartment three-electrode cell using RHE as the reference electrode in the presence and absence of glycerol in 0.5 M KOH. Measurements were made at a scan rate of 0.1 V/s in an Ar-saturated environment using Ni foam as the cathode. 5th cycle responses are displayed.

4.3. Investigating GOR Product Selectivity

Although information about system activity and product selectivity can both be extracted from the experiments, the results presented in this section primarily pertain to the GOR product selectivity performance concerning the tested parameters. Only main products (>10% FE) are presented in the figures. The data for 2.1 V samples are not displayed due to unreliable results caused by improper anolyte mixing. The FEs of minor products for each measurement shown in the figures can be found in Appendix D.

4.3.1. Influence of Varying Applied Potential

Given that many previous studies showed the impact that applied potential could have on the selectivity of GOR [23], this chapter presents the results regarding the effect of varying applied potential on the product selectivity of glycerol oxidation for both Pt and Ni anodes in an AEMEA cell. Combined bar and scatter plots present the faradaic efficiencies and the achieved current densities. The following results do not include the 2.1, 3.3, and 3.6 V applied potential steps. This is due to the unreasonably high concentration measurements at 2.1 V and the common occurrence of salt formation and blockages at the cathode. Fig. 4.3 shows the formed salt precipitates and blockages.

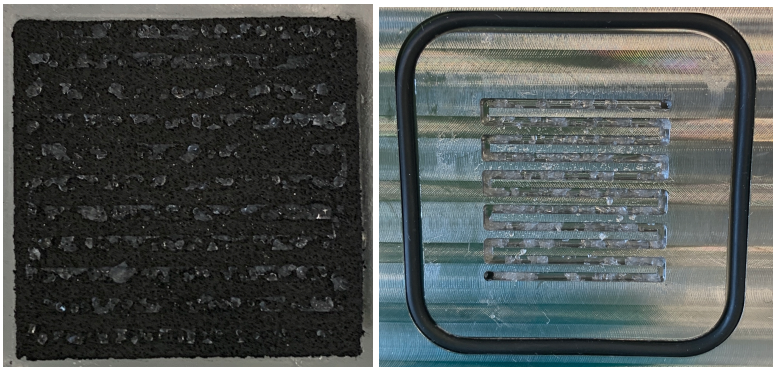

(a) Salt formation on the back of the Ag-GDE

(b) Blockages caused by salt in the cathodic gas flow channel

Figure 4.3: Picture of the cathode and the cathode end plate after salt formation issues were observed in an experiment

Figure 4.4 reveals a few things about the product selectivity of GOR while using Pt in an AEMEA cell. The faradaic efficiency of formate from GOR is the highest (averaging 70%), making it the main product of this reaction. With much lower FEs (averaging 5%), lactate is the second major product of GOR. Additionally, when Pt is used as the catalyst, all three samples show similar FEs to formate and lactate combined at around 70 %. Also, no Pt dissolution was detected in these studies through EDX measurements performed at the end of these experiments. Corresponding SEM images are in Appendix F.

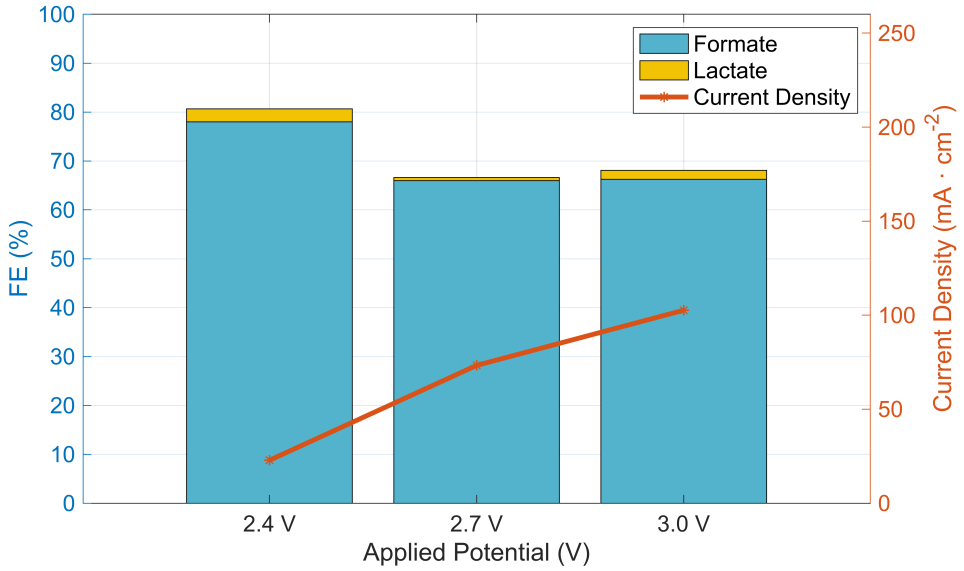

Figure 4.4: Faradaic efficiency and current density as a function of applied cell potential in 0.5 M KOH and 0.5 M glycerol using the Pt anode in an AEMEA cell. See Table D.1 for FEs of minor products.

Similar to the Pt anode, the major products of GOR on Ni foam are formate followed by lactate, as evidenced by the FEs denoted in Fig. 4.5. However, in contrast to the consistency in performance seen when using Pt, the FE of formate has a sharp decline for Ni from around 80% to 20% in 3.0 V applied potential conditions. But, before that decrease, the FE of formate and lactate is higher for Ni than Pt, suggesting better GOR activity on Ni catalysts. Moreover, when Ni anode is used, the cell consistently performs at higher current densities, up to 200mA·cm^{-2} at 3 V. In fact, before 3.0 V is applied, the Ni-utilizing cell has significantly higher partial current densities of formate (53 and 85 mA·cm^{-2}) compared to the Pt-utilizing cell (18 and 48 mA·cm^{-2}). At 3.0 V, however, the Pt-utilizing cell achieves 68 mA·cm^{-2} the partial current density of formate whereas the Ni-utilizing cell has 42 mA·cm^{-2}.

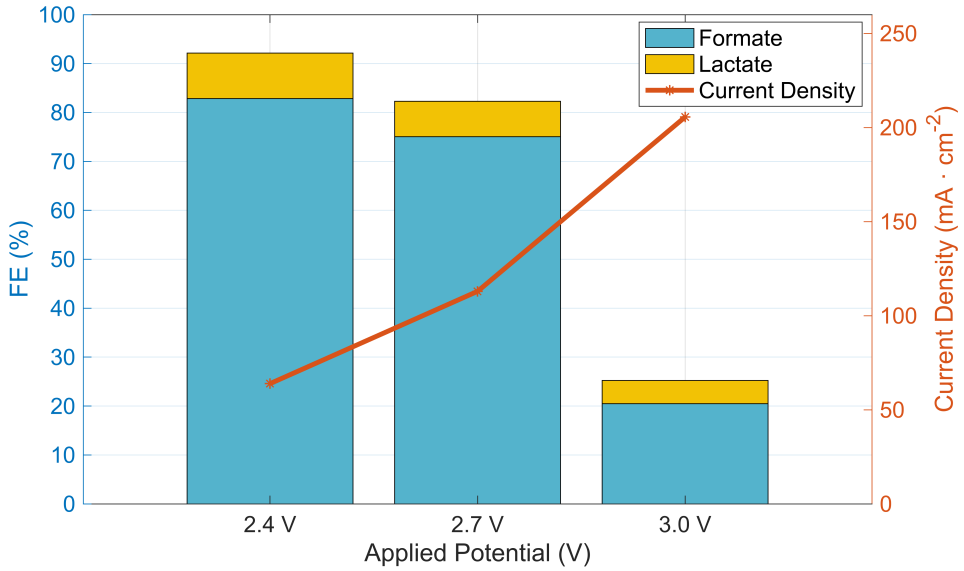

Figure 4.5: Faradaic efficiency and current density as a function of applied cell potential in 0.5 M KOH and 0.5 M glycerol using the Ni foam anode in an AEMEA cell. See Table D.2 for FEs of minor products.

4.3.2. Influence of Varying Glycerol Concentration

It has been shown in previous reports that the concentration of glycerol in the electrolyte affects the GOR process, and it does not necessarily have a linear relationship with reactivity, unlike most other catalytic reactions [21]. Thus, this section presents product selectivity as a function of different glycerol concentrations. During experimentation, three glycerol concentrations (0.1 M, 0.5 M, and 1.0 M) were tested; however, the product analyses for the 0.1 M samples could not be completed due to equipment limitations. Therefore, the following product selectivity results will only include the results of the 0.5 M and 1.0 M tests.

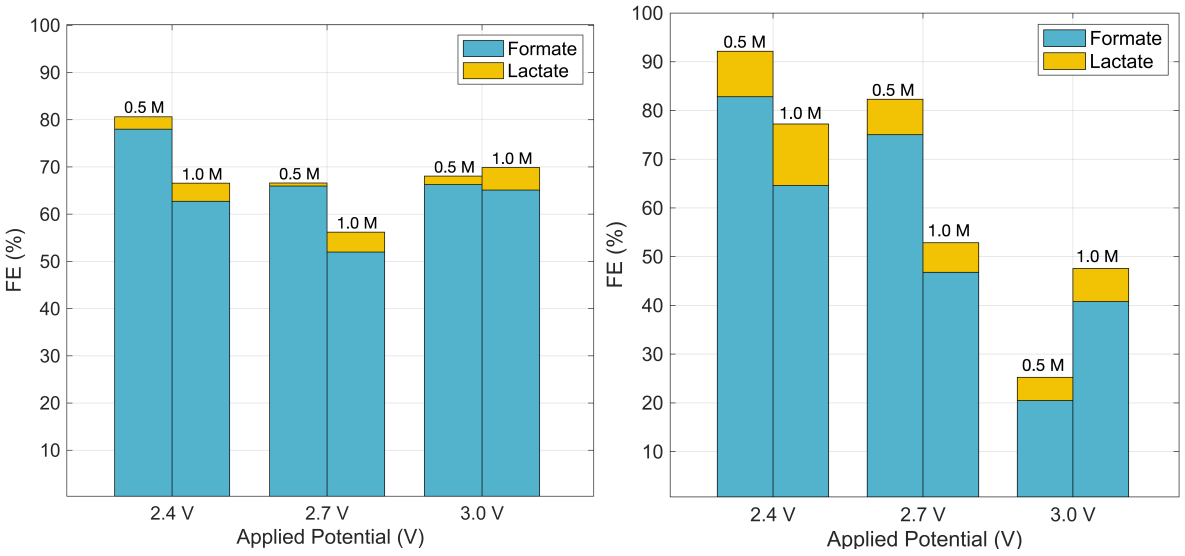

(a) Utilizing Pt anode. See Table D.3 for FEs of minor products.

(b) Utilizing Ni anode. See Table D.4 for FEs of minor products.

Figure 4.6: Faradaic efficiency as a function of applied cell potential with different glycerol concentrations added to the 0.5 M KOH electrolyte in an AEMEA cell.

Fig. 4.6a above displays the effect of glycerol concentration on the faradaic efficiency of major GOR products at different applied potentials when Pt anode has been used. FE of formate is higher for all applied potentials when 0.5 M glycerol is present in the system. Moreover, the formate FEs are relatively consistent across different applied potentials regardless of the glycerol concentration in the anolyte when Pt is used as the anode.

On the other hand, this consistency in FEs across different applied potentials is not present for the cell utilizing the Ni anode. Fig. 4.6b showcases the effect of glycerol concentration on GOR selectivity for this cell, and a few observations can be made. First, a decrease in total FEs can be observed for both glycerol concentrations at higher applied potentials, and the reduction in FEs is significantly steeper when the electrolyte contains 0.5 M glycerol. In fact, before the 3.0 V is applied, the formate FEs are considerably larger in tests circulating electrolytes containing 0.5 M glycerol than 1.0 M glycerol. The FEs are also more consistent across different applied potentials in the presence of 1.0 M glycerol.

4.3.3. Influence of Electrochemical Active Surface Area

Given that the efficiencies of reactions that utilize catalysts are highly dependent on the active surface area available for compounds to react, a comparative anode was created by sputtering an equal mole amount of Ni onto the same type of support Pt was sputtered on. This method yielded an anode featuring a 150 nm layer of Ni on one side of the titanium support. This electrode was tested, and the following leveled surface area comparison regarding GOR product selectivity, as shown in Fig 4.7, was created.

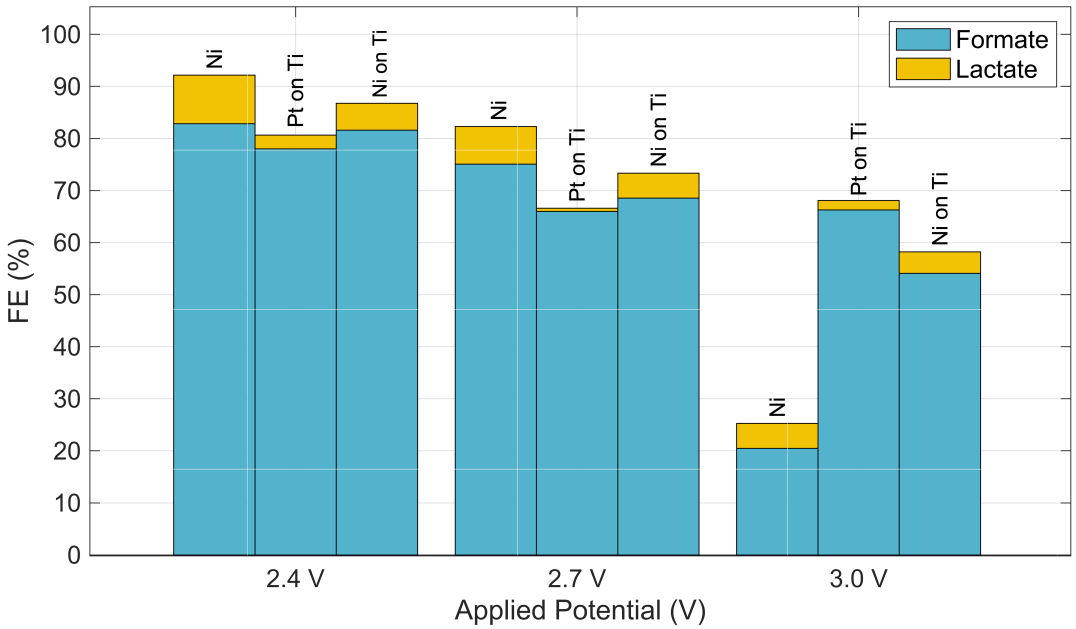

Figure 4.7: Faradaic efficiency as a function of applied cell potential for Ni foam, sputtered Ni on Ti and sputtered Pt on Ti as the anodes in an AEMEA cell. The anolyte utilized was 0.5 M KOH and 0.5 M glycerol. See Table D.5 for FEs of minor products.

This figure shows that the Ni on Ti anode exhibits lower FEs than the Ni foam anode while exhibiting higher FEs than the Pt on Ti anode for the 2.4 and 2.7 V applied voltages. Ni on Ti anode also demonstrates a relatively small reduction in the total FEs with increasing applied potential. Although not as pronounced as the substantial reduction seen with the Ni foam anode at 3.0 V, this decrease still leads to lower FEs than the Pt anode under the same applied potential.

4.3.4. Selectivity at Commercially-Relevant Rates

Since a catalyst's selectivity and activity are highly dependent on reaction rate due to its effect on the reaction environment [14], an evaluation of GOR catalysts has been conducted at the commercially relevant current density of 100 mA·cm^{-2}. Additionally, instead of integrating this current density as part of a step-wise test, it was applied alone for 1 hour. Thus, any undesired effect of step-wise tests was removed from these measurements.

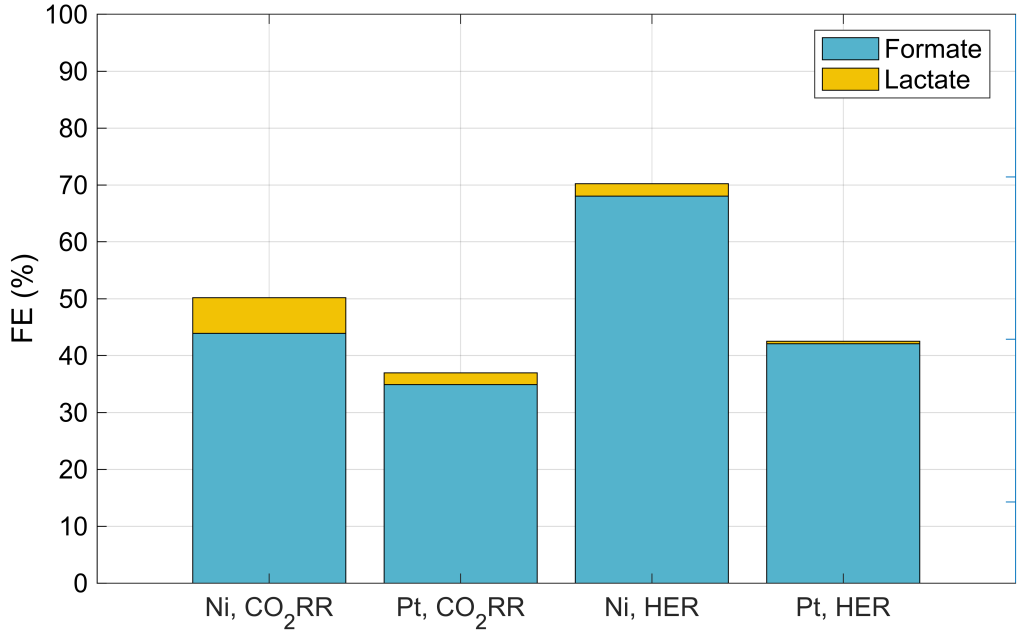

Figure 4.8: Faradaic efficiency and full cell potentials at 100 mA·cm^{-2} for Pt and Ni catalysts in the presence and absence of CO_2RR in the cathode side using 0.5 M KOH and 0.5 M glycerol in an AEMEA system. See Table D.6 for FEs of minor products.

Fig 4.8 above makes a comparison of Ni and Pt anodes in terms of GOR product selectivity when coupled with either CO_2RR or HER on the cathode side at 100 mA·cm^{-2}. The data indicate that, for both cathodic reactions, Ni foam exhibits higher GOR faradaic efficiencies (50% and 70%) compared to the Pt anode (37% and 43%) at this specific current density. Furthermore, GOR faradaic efficiencies to formate and lactate are higher when coupled with HER for both Pt and Ni, suggesting possible oxidation of products under CO_2RR conditions.

4.3.5. Selectivity in BPMEA Cells

Given the benefits of BPMs for use in CO_2RR systems, this section compares the results of the chronopotentiometry tests done using Ni foam as the GOR electrode in AEMEA and BPMEA cells. Based on the experimental data displayed in Fig 4.9, it is apparent that at lower current densities, the AEMEA system shows higher total FEs from GOR than the BPMEA system. Yet GOR products show a less significant decrease in FEs at higher current densities when BPMs are used. In fact, the total FEs of the BPMEA system is higher at 100 mA·cm^{-2} than at 50 mA·cm^{-2}. A slight decline can still be observed at 200 mA·cm^{-2}; however, it is significantly smaller than the reduction observed in the AEMEA system.

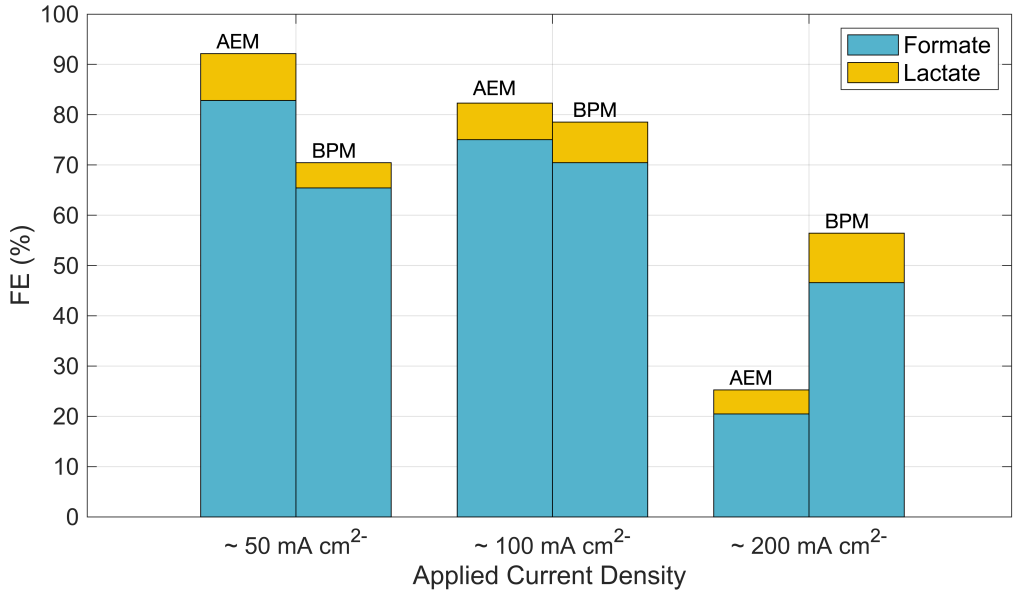

Figure 4.9: Faradaic efficiency as a function of applied current density when using different ion exchange membranes in an MEA cell. For the AEMEA and BPMEA tests, an anolyte composed of 0.5 M KOH with 0.5 M glycerol and 1.0 M KOH with 0.5 M glycerol was used, respectively. See Table D.7 for FEs of minor products.

Following the trends observed in the BPM experiment, an investigation was devised to determine what could be causing the reduction of FEs at higher current densities in BPMEA systems. As mentioned before, the GC utilized in this study is designed to accommodate only one gas flow stream. This inherent limitation prevents the feasible measurement of gas concentrations like O_2 and CO_2 in the anodic stream, as measuring the cathodic products with the GC is essential to confirm the occurrence of CO_2RR. Therefore, to detect the presence (and the hypothesized suppression) of gas compounds like O_2 exiting the anodic end-plate, a few experiments were performed using the setup in the Transport Phenomena (TP) group's laboratory that can accommodate two gas flow streams.

The experiments were conducted using a BPMEA cell, where Ni foam served as the anode, Ag-GDE as the cathode, and the anolyte comprised either 1.0 M KOH or a mixture of 1.0 M KOH and 0.5 M glycerol aiming to induce OER or GOR as the anodic reaction, respectively. Table 4.2 summarizes the detection results of these experiments.

Table 4.2: The O_2 detection results of BPMEA experiments utilizing Ni foam as the anode.

Intended Reaction	Anolyte	Test Performed	Detected O_2
GOR	1.0 M KOH + 0.5 M GLY	Chronopotentiometry test at 100 mA·cm^{-2}	X
OER	1.0 M KOH	Chronopotentiometry test at 100 mA·cm^{-2}	✓
GOR	1.0 M KOH + 0.5 M GLY	Stepwise chronopotentiometry test at from 25 to 200 mA·cm^{-2}	X

Besides the lack of detection of O_2 by the GC when glycerol was added into the anolyte, no gas bubbles were observed exiting the anodic outlet throughout these three experiments, suggesting the complete suppression of OER.

4.4. Investigating System Activity & Energy Efficiency

The results presented in this section are about system activity and the reduction in the energy requirements hypothesized to occur with the paired electrolysis of GOR with CO_2RR. The data presented complements the results already showcased concerning product selectivity in the previous chapter. Due to the lack of a reference electrode, the potentials measured and applied are all total cell potentials.

4.4.1. Influence of Varying Applied Potentials and Glycerol Concentration

Fig 4.10 presents chronoamperometry results of AEMEA cells using the Ni anode in various glycerol concentrations. Looking at the entire applied potential range in Fig 4.10a, no apparent increase in activity could be observed when glycerol was incorporated into the anolyte. Except for the 0.1 M glycerol case, measurements done without glycerol (where OER acts as the anodic reaction) show a higher current density than the GOR-coupled cells. A closer comparison of the no glycerol and the 0.1 M glycerol measurements also reveals a modest improvement in current density of about 15 $mA{\cdot}cm^{-2}$.

A convergence of current densities can be observed at lower applied cell potentials when looking at the entire range. Therefore, Fig 4.10b on the right highlights the increased activity observed at low current densities with glycerol. The results indicate that an absence of glycerol in the anolyte causes the system's lowest current density (hence activity) at low cell potentials. When activities of tests with glycerol presence are compared, it can also be said that activity decreases with increased glycerol concentration in this applied potential range.

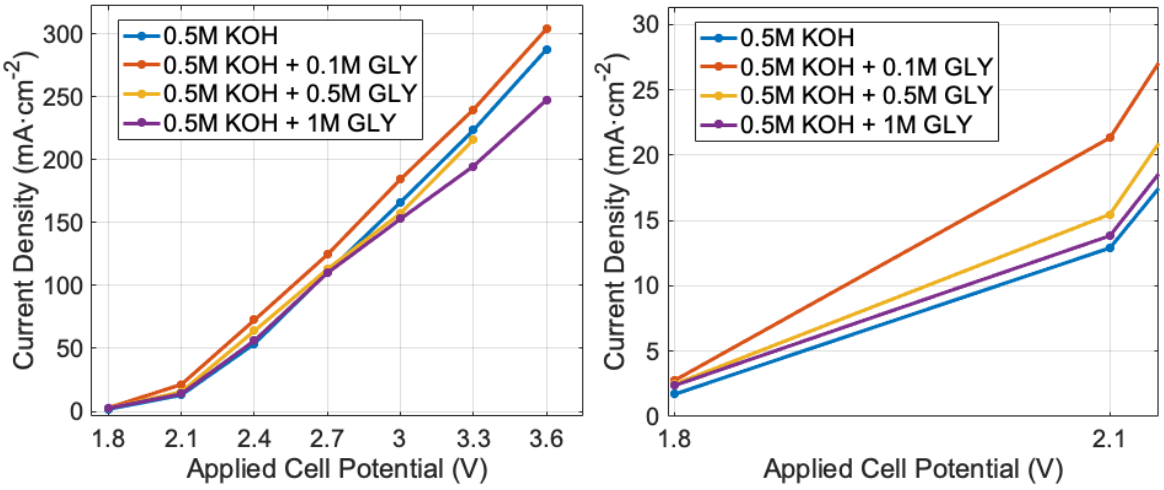

(a) The experimental range from 1.8 V to 3.6V

(b) The experimental range from 1.8 V to 2.1V

Figure 4.10: Current density as a function of applied cell potential in the absence and various glycerol concentrations in a Ni anode utilizing AEMEA cell.

Fig 4.11 below showcases the chronoamperometry results of the Pt anode in an AEMEA cell for various glycerol concentrations. Based on the experimental data, it is apparent that the no glycerol cell where OER is the anodic reaction shows the highest activity for all applied potentials. Another thing to note is that similar to the trend observed with the Ni anode, amongst the glycerol present experiments, the test with 0.1 M glycerol has the highest activity for all applied potentials; however, the tests with 1.0 M glycerol outperforms the one with 0.5 M glycerol at some applied potentials.

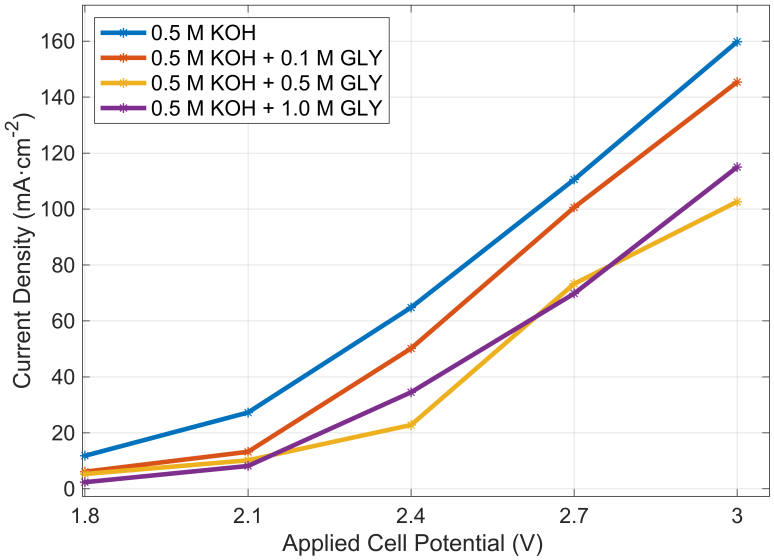

Figure 4.11: Current density as a function of applied cell potential in the absence and presence of various glycerol concentrations in an AEMEA cell utilizing a Pt anode. The potential range from 1.8 V to 3.0 V is shown, and the experimental steps where salt blockages were encountered are not presented.

4.4.2. Influence of Electrochemical Active Surface Area

Fig 4.12 below presents the energy performance results of Ni foam, Pt on Ti, and Ni on Ti tested to investigate the performance when the effect of the catalyst surface area is minimized. The figure highlights the significant impact of surface area on energy performance: Ni foam (an anode whose active surface area is not limited to one side) operates at substantially higher current densities of formate for most applied cell potentials. When a comparison of the sputtered catalysts is made, it can be observed that Ni on Ti can operate at higher current densities than Pt on Ti for applied potentials up to 2.7 V. At 2.7 V applied cell potential, Pt on Ti anode has the best performance towards formate production at 70 $mA{\cdot}cm^{-2}$ closely followed by the Ni on Ti anode with 64 $mA{\cdot}cm^{-2}$ partial current density to formate.

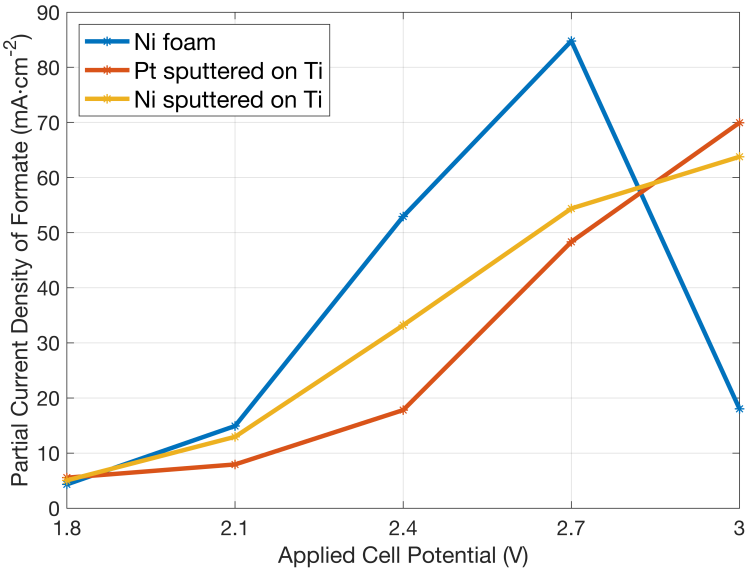

Figure 4.12: Partial current density of formate as a function of applied cell potential using differing anodes in 0.5 M KOH and 0.5 M glycerol in an AEMEA cell.

4.4.3. Influence of BPM

The energy performance results for BPMEA tests are below in Fig 4.13. Note that the cell potentials measured for the BPMEA cells are higher than those presented for the AEMEA cell. This increase is associated with the water dissociation reaction occurring at the BPM interface.

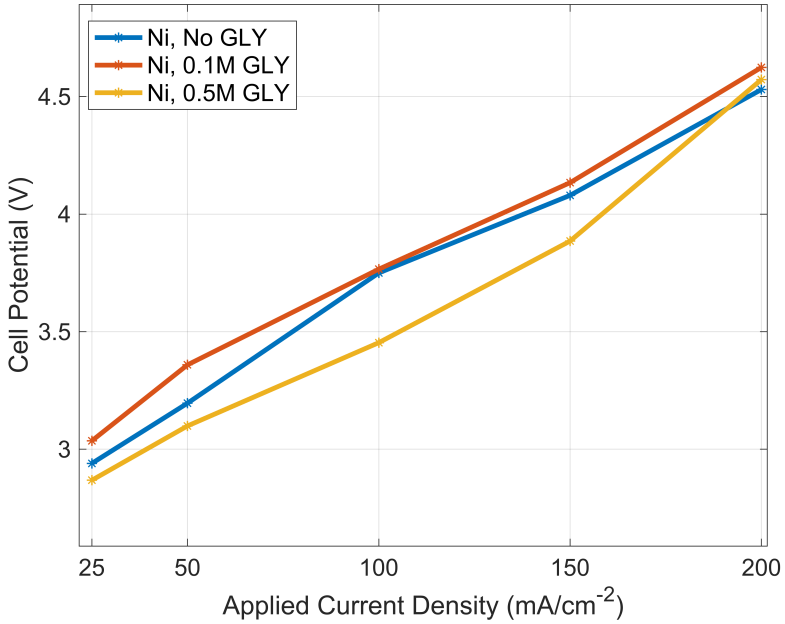

Figure 4.13: Cell potential as a function of applied current density in the absence and various glycerol concentrations in 1 M KOH for the Ni anode utilizing BPMEA cell. The entire experimental range is shown from 25 to 200 mA·cm^{-2}.

The data indicates that the system's best performance is achieved with 0.5 M glycerol added anolyte, evident from the lower cell potentials. In contrast, the performance in the presence of 0.1 M glycerol operates at higher cell potentials than when glycerol is absent. The difference is minimized at 150 mA·cm^{-2} but gets as high as 0.17 V at 50 mA·cm^{-2}.

4.4.4. Impact of Various Reaction Pairings on Effective Cell Potential

Table 4.3 below is a big-picture view of different reaction pairings' impact on cell potential at the commercially relevant rate of 100 mA·cm^{-2} for both Ni and the Pt catalysts tested. The tests were performed with Ag-GDE as the cathode. The anolyte composition was varied based on the cell type and whether or not GOR was intended, with 1.0 M KOH + 0.5 M GLY used for BPMEA cells and 0.5 M KOH + 0.5 M GLY for AEMEA cells where GOR was the intended anodic reaction. If the intended anodic reaction was OER, 0.5 M KOH was used for AEMEA, and 1.0 M KOH was used for BPMEA tests. The cathodic inlet was modified according to the intended cathodic reaction as well, and it was either CO_2 to initiate CO_2RR or N_2 to initiate HER.

The tabulated results indicate that for tests performed in AEMEA cells, regardless of which catalyst is utilized, the GOR provided no improvements in energy efficiency (no decrease in the cell voltage measured) when coupled to CO_2RR. Moreover, when GOR was coupled with HER, an increase of 0.2 V was observed. As already showcased in graphical form in Fig. 4.8, it can also be observed that the FEs of formate from GOR were significantly higher when Ni catalyst was used. On the other hand, the BPMEA tests suggest a 0.1 V decrease in cell potential with GOR when Ni is used as the anode.

Table 4.3: Formate faradaic efficiency and cell voltage measurements for Ni and Pt anodes in various electrolysis pairings performed at 100 $mA \cdot cm^{-2}$ applied current density.

	Coupled Rxns	**Anode**	**$FE_{FA,\ GOR}$(%)**	**Cell Potential (V)**
AEM	GOR + HER	Ni	68.0	2.82
	GOR + HER	Pt	42.1	2.81
	GOR + CO_2RR	Ni	75.0	2.60
	GOR + CO_2RR	Pt	34.9	2.62
	OER + CO_2RR	Ni	-	2.61
	OER + CO_2RR	Pt	-	2.62
BPM	GOR + CO_2RR	Ni	71.0	3.53
	OER + CO_2RR	Ni	-	3.62

5

Discussion & Recommendations

The results of this research have provided an exploration and understanding of the paired electrolysis of glycerol with the electroreduction of CO_2 to CO in zero-gap electrolyzers. Through detailed analysis and interpretation of the obtained results, this chapter aims to assess and shed light on the product selectivity of GOR and the impact this coupling has on the system energy demand while also conducting a comprehensive comparison of Ni and Pt as anodic catalysts for this reaction pairing.

5.1. Product Determination via NMR Spectroscopy

In this study, NMR analysis confirmed the presence of formate, lactate, acetate, glycerate, and dihydroxyacetone as value-added products resulting from glycerol oxidation. Identifying and quantifying these products are necessary to understand the effects of various factors like glycerol concentration and applied cell potential on GOR product selectivity. NMR Spectroscopy was selected as the primary analytical technique for liquid analysis due to its widespread application in previous GOR studies for product identification and quantification [103]. With NMR, identifying various compounds within a chemical mixture is possible without a specific calibration for detecting individual GOR products. Although this method proved invaluable in qualitatively identifying and quantitatively analyzing the products resulting from glycerol oxidation in our study, some limitations were associated with its use for product and selectivity analysis.

While H-NMR has been commonly employed in product analysis for numerous GOR studies, the limited documentation of measured spectra and peak assignments poses a challenge. To address this, we utilized NMR databases, such as Human Metabolome Database (HMDB) [108] and NMRShiftDB Project [109], in two distinct approaches. On the one hand, the peaks of molecules that could be GOR products were searched by their names, allowing for a direct comparison of reported peaks with those observed in our measurements. On the other hand, peaks already present in the measured spectra were searched to generate a list of possible corresponding compounds. However, many databases only provide H-NMR signals of compounds recorded under neutral pH conditions. Since the pH of the sampled solution significantly influences chemical shifts, they can only be approximated to an extent without measuring the compound in the appropriate alkaline environment. The anolyte samples in this study are highly alkaline, and the chemical shifts do not align appropriately with the available NMR data.

Moreover, the glycerol signal has a strong presence in the spectra, as evidenced in Fig. 4.1. It spans from 3.30 ppm to 3.62 ppm (in pH 14) in three different clusters and poses difficulties in distinguishing signals from certain GOR products, such as glycolate. This limitation was initially suspected to be the case when the chemical shifts of the possible GOR products were identified via NMR databases. Then NMR analyses were performed on anolytes with varying and known initial glycerol concentrations after their experimental runs. The glycerol signal measured was integrated to determine the glycerol

concentrations in the anolytes, and the measured glycerol amount was consistently higher than the initial glycerol concentration put into the electrolyte despite the newly formed presence of GOR products like formate. These higher-than-initial concentrations suggest the presence of peaks associated with compounds other than glycerol in the span that was being integrated. And this indicates the presence of GOR products that have not been able to be quantified and accounted for in the faradaic efficiency calculations for GOR. To mitigate this issue, a discussion with Dr. Stephen Eustace was initiated to investigate alternative methods for quantifying these products. C-NMR measurements with large sample volumes were identified for their potential; however, when trial samples were tested, it was determined that a week of measurement time was required to get signals clean and robust enough for quantitative measurements. Due to the time limitations associated with this thesis, this method was not pursued further.

Lastly, a limitation that appeared towards the latter half of the experiments was the repeated errors (60+) the NMR machine started giving, causing the samples to be left unmeasured. It is suspected that the issue is due to the high ionic strength of samples, causing them to affect the tuning and the matching of a probe, especially at high frequencies [110]. As for the NMR spectroscope utilized in this study, when the dip in the tuning frequency isn't big enough, it stops the measurement and sends an error message to the user. As per Dr. Eustace's suggestions, several attempts were made to dilute the samples and turn off the tuning during the measurements to tackle this issue; however, several samples still could not be measured. This resulted in a lack of information about the product selectivity performance for samples with 0.1 M glycerol. To get around this problem, HPLC was calibrated with the available compounds (formate, glycerol, lactate, oxalate) in the lab. However, the delays in this step resulted in discrepancies in the trial samples between the concentrations measured directly after the experiment via NMR and measured via HPLC after calibration was completed. This discrepancy is speculated to be a consequence of the possible evaporation of the water content in the anolyte samples that could not be measured.

To address the limitations of conventional H-NMR for selectivity analysis described above, all possible GOR products can be acquired and used to calibrate HPLC before the start of experimentation. This way, HPLC can be used as the primary analytical technique for liquid product detection. If utilizing the H-NMR approach is still preferred for comparison with previous literature, neutralizing samples with acid before NMR measurements can overcome the limitations of NMR databases in identifying products under only neutral conditions. Lastly, access to an NMR spectroscope fitted with coils designed to handle high ionic strength samples can be arranged to prevent issues related to tuning errors.

5.2. Electrochemical Examination of GOR Catalysts via CV

The cyclic voltammetry measurements have been valuable in evaluating the potential of the Pt and Ni catalysts in terms of electrocatalytic performance.

Pt Anode in the Absence of Glycerol

Starting with the CV response of the Pt anode displayed in Fig. 4.2a, it can be said that in the absence of glycerol, Pt goes through phase changes before OER takes over at its onset potential of 1.7 V. This change in surface chemistry can be observed by the presence of the oxidation peak at 1.0 V as commonly identified in previous studies investigating the OER mechanism on Pt electrodes [111, 112]. It has been widely accepted that in alkaline media, this peak corresponds to the binding of hydroxide ion onto the activated Pt site (forming Pt^{δ}–OH_{ads}) coupled with a one-electron oxidation step is followed by the formation of the surface oxide species for OER on Pt [111].

A recent *operando* study by Favaro et al. aiming to investigate the surface chemistry of Pt during OER reveals that the active species for oxygen evolution is the subsurface layer of Pt^{δ}–OH_{ads} formed. In contrast, Pt oxides like $Pt^{(II)}O$ and $Pt^{(IV)}O_2$ that are present in outer layers are found to not contribute to OER [112]. Moreover, they identify a diversion from the thermodynamically predicted stable phases of Pt as seen by the Pourbaix diagram in Fig. 5.1 below. In alkaline conditions, upon increasing potentials (up to 1 V vs. NHE), the Pourbaix diagram predicts Pt to first partially oxidize to $Pt(OH)_2$ and then be present in the form of PtO_2 as it is the only stable phase. However, their experimental results indicate

the presence of Pt^{δ}–OH_{ads} and $Pt^{(II)}$ up to 0.5 V and the presence of PtO_2 only after 0.9 V, which is higher than the potentials predicted in the Pourbaix diagram. This deviation is hypothesized to be due to kinetic effects not considered in a thermodynamic investigation of Pt phases. As we are operating in similar reaction environments without glycerol, it can be inferred that these mechanistic steps are also occurring in our experimental setup.

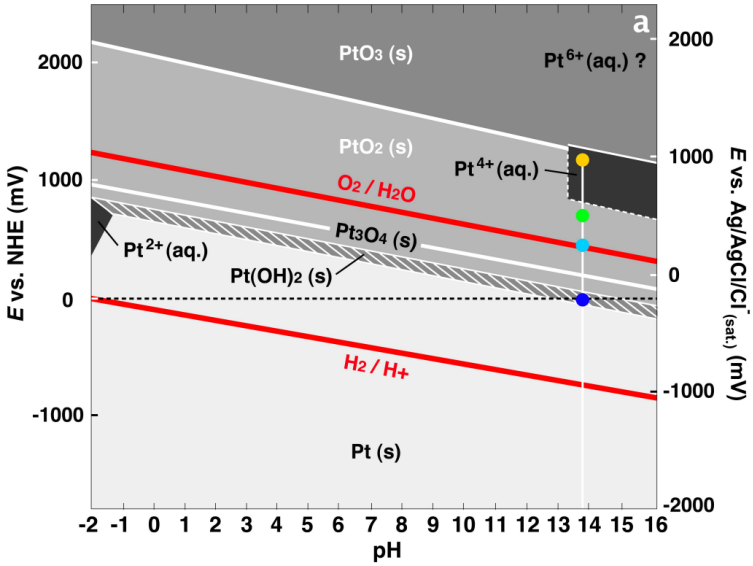

Figure 5.1: Pourbaix diagram of Pt at 298 K. Sourced from [112].

Note that the small redox pair centered at 0.2 V is associated with hydrogen adsorption onto the Pt. This peak is observed less prominently in our measurements, but it is in agreement with the CV responses reported in other studies and [113, 114].

Pt Anode in the Presence of Glycerol

The cyclic voltammetry results of the Pt anode in the presence of glycerol indicate a significant improvement in catalytic activity compared to OER performed on Pt. The higher current densities observed and the 1.2 V reduction in onset potential both show that Pt has an improved activity for glycerol oxidation. The two redox pairs observed can be inferred to be related to the GOR process occurring on the Pt anode. The mechanism of GOR on platinum in alkaline media is a complex process that is not yet fully understood. However, the first redox pair centered at 1.0 V is expected and has been reported in the literature before [114]. Identifying the mechanistic process this peak corresponds to for GOR on Pt is still elusive; however, it is often associated with a combined electrochemical effect of OH^- adsorption and the cascading steps of glycerol oxidation.

The GOR is hypothesized to occur via O-adsorption on Pt, which involves the deprotonation of the primary or secondary hydroxy group of glycerol, and C-adsorption on Pt, which consists of the chemisorption of a glycerol carbon [115]. The prevalence of each pathway is highly dependent on the reaction conditions. The O-adsorption pathway involves the formation of alkoxides, a second deprotonation step to DHA and glyceraldehyde, and further oxidation to other GOR products such as glycerate and lactate [115]. On the other hand, the C-adsorption pathway is highly dependent on the Pt interface the adsorption happens. For instance, Pt(100) is reported to only chemisorb the terminal carbon atoms and produce glyceraldehyde, whereas Pt(111) is said to chemisorb both terminal and non-terminal carbon atoms [115].

An observation to note is that in addition to the complex network of products possible from GOR as illustrated in Fig. 2.7, the results derived from different research groups on the subject of GOR pathways on Pt seem to be contradictory to each other. Therefore, standardization of reporting on this subject to include elemental compositions, morphologies, and crystal planes is needed in future studies [115].

The presence of the second redox pair observed and centered at 2.05 V is unexpected and has not been reported often in GOR studies. A detail to mention is that the cyclic voltammograms of Pt for GOR reported in the literature do not reach as high anodic potentials. The maximum is generally around 1.5 V vs. RHE. It can be concluded that this peak is unrelated to any impurities present on the Pt surface because a similar redox pair does not appear in the absence of glycerol. A plausible explanation for the second redox pair is the further oxidation of glycerol in the form of formate oxidation to CO_2 [100]; however, more detailed analyses that include identifying the products formed in situ should be performed to clarify this ambiguity.

Despite the elusive understanding of what is happening on the Pt anode, the above results highlight opportunities to decrease the energy input requirement in the CO_2RR systems when the Pt anode is used as the anode and the OER is replaced with GOR.

Ni Anode in the Absence of Glycerol

The cyclic voltammetry response of Ni in the absence of glycerol in Fig. 4.2b reveals a phase transition of Ni before the onset potential of OER at 1.65 V vs. RHE. The redox pair centered at 1.3 V vs. RHE can be associated with the formation of a nickel oxyhydroxide (NiOOH) film on the surface of the Ni electrode. This rapid conversion was observed to occur prior to OER and determined not to be a reaction step limited by kinetics of diffusion [116]. This NiOOH film is also well-reported to be the active species for OER in Ni [117]. Moreover, previous studies have shown that this transformation either occurs at the surface leading to core-shell type structures, or throughout the bulk anode leading to higher surface areas of NiOOH [118]. The formation of this Ni species can also be thermodynamically predicted by the alkaline and high potential region of the Pourbaix diagram seen in Fig. 5.2 below.

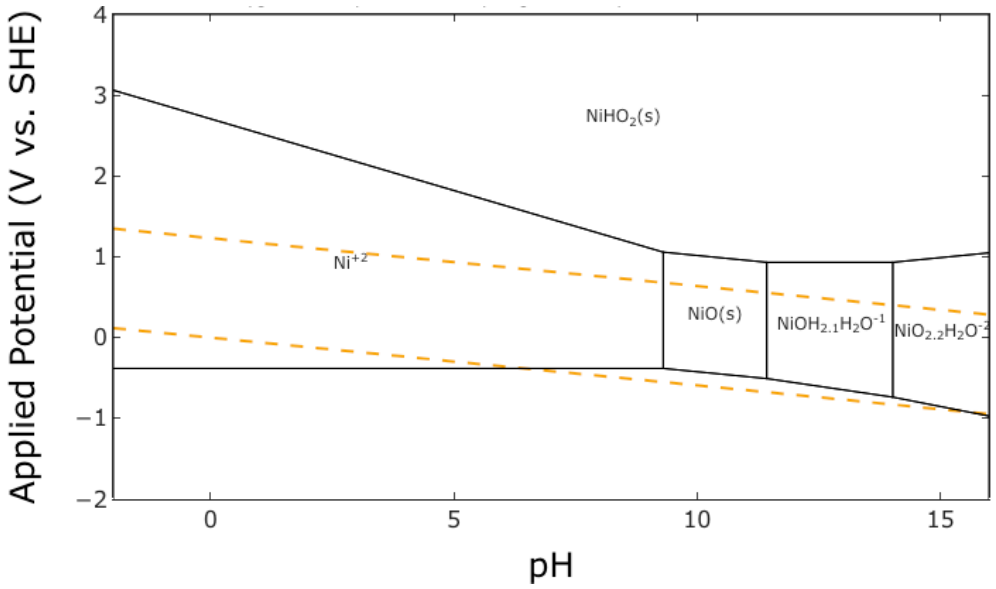

Figure 5.2: Pourbaix diagram of Ni at 298 K. Sourced from [119].

Ni Anode in the Presence of Glycerol

The CV measurement of Ni in the presence of glycerol shows a decent improvement in activity, as observed by the reduction in the onset potential and the steeper increase in current density once oxidation begins. Previous literature indicates that the oxidation peak around 1.0 V without a reduction peak during the cathodic scan is a significant indication of the GOR process [120]. Fundamental investigations have revealed that many types of alcohols, including glycerol, were found to oxidize at the same potential at which the nickel anode is oxidized [116]. Therefore, it was concluded that the catalytically active NiOOH is the species responsible for GOR, and the peak observed is the evidence for the oxidation of hydroxy groups in glycerol through the reduction of NiOOH [95, 120] as such:

$$NiOOH + \text{glycerol} \rightarrow Ni(OH)_2 + \text{glycerol oxidation products} \tag{5.1}$$

It was also reported that when glycerol is present, the oxygen evolution on NiOOH occurs at higher potentials [121], indicating that NiOOH has a preference for producing intermediates of GOR rather than generating the adsorbed OH species ($Ni-OH_{ads}$) which explains the improvement in the onset potential.

Limitations of the CV Measurements

A limitation to be mentioned regarding the CV measurements discussed above is the lack of predetermined areas in the single-compartment cell to place the working electrode (WE), counter electrode (CE), and reference electrode (RE). Because the cell needs to be emptied, cleaned, and fitted with electrodes for each catalyst, slight differences in the electrode separation in the Ni vs. Pt tests can be present, changing the ohmic resistance of the system and leading to changes in the overpotential required to perform a reaction. To remedy this issue, attention has been paid to keeping the locations of the electrodes as constant as possible. Therefore it is believed that such differences have not significantly affected the primary outcomes of these measurements, yet the potential impacts should still be recognized when comparing the catalysts. In future studies, the cell can be modified to include slots at the bottom that ensure the locations of the three electrodes are kept constant. Keeping this limitation in mind, it can be said that the Pt electrode shows a more significant improvement in the energy requirement to perform GOR compared to the Ni electrode. However, this difference in improvement is relatively small, and Ni anode still shows significant energy demand improvements for GOR compared to OER.

To gain a more comprehensive understanding of the CV responses when glycerol is present, further research can also be conducted by measuring the CV using electrolytes containing GOR reaction intermediates, such as DHA or glyceraldehyde. This approach would enable researchers to independently identify and analyze the electrochemical responses of these intermediates, thereby aiding in understanding the mechanism with which GOR happens in a more focused manner.

5.3. Investigating Performance of GOR and CO_2RR Co-Electrolysis in MEA Cells

Before discussing the changes in product selectivity and system activity concerning each parameter tested, a few key findings can be presented. First and foremost, this study finds that the glycerol oxidation reaction performed in zero-gap electrolyzers when using Ni or Pt as the anode formate and lactate are the major products, and acetate, glycerate, and dihydroxyacetone are the minor products of GOR. The main products are not known to be the most value-added products of GOR but still have a higher market value than glycerol itself, as seen in Table 5.1 below.

Table 5.1: Market price values of the GOR products in this study [114]

Product	Market Price ($/kg)
Glycerol	0.24
Formate	0.97-1.08
Lactate	1.58-1.87
Acetate	0.68-0.92
Glycerate	12-17
DHA	37-60

The production of formate and lactate up to combined faradaic efficiencies of 92% is still significant since the profit made from the sale of these products can be used to offset the costs associated with some of the system inefficiencies in CO_2RR on top of making up for the cost associated with acquiring glycerol.

However, the sale of these compounds requires separating the liquid products in the anolyte. Product separation is a significant technical challenge slowing down the development of catalytic glycerol oxidation processes because GOR tends to result in various products at once [122]. Despite this typical

behavior and the apparent costs this step would add to the price of such systems, not many studies are available evaluating and discussing how these products can be separated. Overall, the methods suggested for these purposes are liquid-liquid extraction and distillation [12].

5.3.1. Effects of Varying Applied Potential

Looking at the impact of applied potential on the product selectivity of GOR in Pt, several key findings come to light. The first notable observation is the considerably higher FEs of formate with the highest value of 78% at ∼25 mA/cm², which strongly indicates formate as the primary product of this process. Considering the observed products and the available literature on the reaction pathway of GOR on Pt, it can be suggested that, at first, glycerol was oxidized to produce glyceraldehyde and DHA. Then glyceraldehyde was further oxidized to glycerate and lactate and then to formate, acetate, and glycolate through C-C bond cleavage [114]. This possible product formation pathway can be illustrated as such:

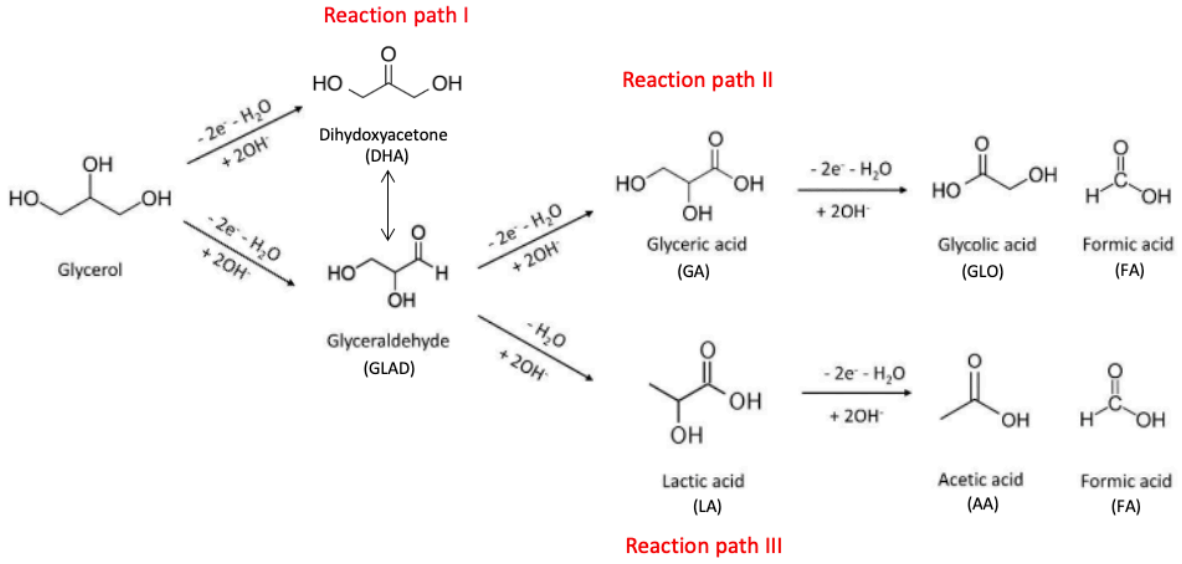

Figure 5.3: Electrochemical reaction mechanism for GOR on Pt catalyst. Modified from [114]

The results also suggest that the FEs of the major GOR products appear to be produced primarily independently to the applied potential when a Pt catalyst is utilized. This independence in product formation with varying potential signifies the consistent performance of Pt in GOR reactions.

It is crucial to compare these selectivity outcomes with those obtained using Ni anode to comprehend the overall performance and identify potential areas for catalyst enhancement. Like Pt, Ni also exhibits higher FEs for formate than lactate, with the highest FE to formate of 83% at ∼65 mA/cm². These FEs suggest that formate is the primary product of GOR on Ni. This kind of selectivity is expected since existing reports indicate that Ni anode has a demonstrated ability to cleave the C−C bond and that the catalyst is likely to produce C1 products like formate and CO_2 from glycerol [121]. But the reaction pathway that includes this C-C bond breakage is still not fully understood for Ni. However, the GOR products formed are the same for both catalysts. Thus the path illustrated in Fig. 5.3 can also be assumed to apply to Ni catalysts.

Prominent differences are present for the two catalysts when examining the effect of higher applied potentials on their GOR product selectivity. For both catalysts, the effective current densities are smaller, and the FE of GOR tends to be closer to 100% at lower cell potentials. But in the case of Ni, there is a considerable decrease in the FEs of GOR products with increasing applied potentials, a phenomenon not prominently observed in Pt. This unique behavior raises the possibility that the oxygen evolution reaction (OER) may take precedence over GOR at higher potentials on Ni [24]. Unfortunately, access to a GC that could be used to detect the components of the anodic gas stream was not available for these experiments, but gas bubbles were observed on the anode outlet with increasing potential, possibly

confirming the occurrence of an unintended reaction.

It should also be noted that for all applied potentials, the cell activity is higher for Ni than for Pt, with the effective current densities reaching up to 200 mA/cm² at 3.0 V. Considering that the Ni anode's partial current density of formate is lower than Pt only at this applied potential, the higher cell activity could signify the potential increase in side reactions such as OER and/or the increased production of CO_2 from the complete oxidation of glycerol at high potentials, as given in Eq. 5.2 below:

$$C_3H_8O_3\,(glycerol) + 14\,OH^- \rightarrow 3CO_2 + 11\,H_2O + 14\,e^- \tag{5.2}$$

The formation of O_2 or CO_2 gasses can explain the shift in liquid product selectivity. This decrease in FEs was also documented by Irabian et al. around 200 mA/cm² while utilizing Pt/C catalyst as the anode [24], indicating that the phenomenon observed is not unique to the Ni anode. However, since the tests discussed here are chronoamperometry tests and the Pt anode used in this study does not reach current densities of 200 mA/cm² within this range of potentials, we do not have the empirical data to confirm whether the Pt sputtered on Ti anode would also face this issue.

Notably, before the significant decrease in FEs at the 3.0 V applied potential, the Ni catalyst exhibited better FEs (and higher partial current densities of formate) than Pt, further underscoring the complexity of the interplay between catalyst activity and product selectivity in the coupled electrochemical system. These results indicate that Ni anode might be the better catalyst for coupling GOR with CO_2RR in zero-gap electrolyzer systems at certain cell potentials. The overall lower selectivity performance of Pt can be explained through the notorious issue of CO-poisoning by strong CO adsorption that is common with the use of Pt for glycerol oxidation [123]. In this study, it was assumed that CO is not due to a flux of the species through the membrane but originating from the glycerol oxidation itself [114]. Surface poisoning species such as $Pt-COads$ can either form through C-C bond cleavage of adsorbed GOR intermediates such as $Pt-COOHads$ or get adsorbed onto the Pt from the electrolyte [124]. These surface poisoning species are reported to exacerbate selectivity and catalytic activity even at low concentrations (<100 ppm) [125, 126]. Moreover, in the case where $Pt-OH_{ads}$ is widely present on the active surface, the $Pt-COads$ reacts with $Pt-OH_{ads}$ to form CO_2 leading to an increased catalytic activity [115] but no changes in the FE measurements of liquid products.

5.3.2. Effect of Different Glycerol Concentration

This section will discuss the effects of various glycerol concentrations on the GOR product selectivity and system activity/energy requirement. As mentioned before, the selectivity data for the tests with 0.1 M glycerol content are unavailable due to equipment limitations; thus, no examination will be presented in this section regarding the product selectivity performance of these samples.

The selectivity results of various glycerol concentrations presented in section 4.3.2 indicate that the anode has no apparent limitations in glycerol availability at the measured concentrations. This is evidenced by the generally higher FEs for the main GOR products in the presence of 0.5 M glycerol compared to 1.0 M for both catalysts. This decrease in the FEs in the presence of 1.0 M glycerol can be attributed to the reduced diffusivity for all species due to the higher viscosity of the electrolyte with 1.0 M of glycerol [114]. Moreover, the consistency of FEs observed and discussed in section 5.3.1 for the Pt catalyst was again observed when 1.0 M glycerol was added to the anolyte. On the other hand, an improvement can be observed in the presence of 1.0 M glycerol for the Ni anode regarding the reduction of FEs measured at the 3.0 V applied potential. The decline in FEs for Ni is significantly larger when 0.5 M glycerol is present in the anolyte, indicating that perhaps with the increased availability of glycerol, the presence of the liquid-to-gas side reactions can be suppressed at high cell potentials. It can be suggested that the abundant glycerol and its intermediates might occupy the active sites on Ni and decrease the likelihood of side reactions common around high current densities such as 200 mA/cm².

Moving on to results presented in section 4.4.1 about the effects various glycerol amounts have on the activity and the system's energy requirements for these same experiments, a few points can be made. Overall, the system activity results of these experiments indicate no overall improvement in

the AEMEA system's energy requirements when GOR is coupled to CO_2RR instead of OER for either catalyst.

For the Ni anode, this is because the current densities observed without glycerol are not the lowest across the entire range of applied cell potentials. The data visualized in Fig. 4.10a reveals that the system's activity was highest in the presence of 0.1 M glycerol, followed by the measurement taken in the absence of glycerol. A comparison of only these two concentrations might suggest that the presence of glycerol is improving the system activity, but the cells with higher glycerol concentrations (0.5M and 1.0M) have lower activities than the no glycerol cell. This decrease in activity could be due to the increased viscosity of the electrolyte with enough addition of glycerol. The increased viscosity is reported to impair the transport of species away from the electrode resulting in higher electrode potentials (or lowered activities in chronoamperometry tests) [98, 127]. Likely, the 0.1 M glycerol cells do not suffer from this issue since this amount of glycerol is too little to make a significant difference in the viscosity [127].

When using the Ni anode, the cell with the poorest overall activity differs from the cell exhibiting the poorest performance at lower applied potentials, as shown in Figure 4.10b. Within this cell potential range, the replacement of OER with GOR shows some improvements in cell activity since any amount of glycerol in the electrolyte leads to higher activity. However, comparing the experiments with glycerol presence within themselves reveals that increasing the glycerol amount decreases cell activity at this potential range. This can again be explained by the increased viscosity of the electrolyte, which causes a slower species turnover on the Ni anode [98]. The dampening effect of the viscosity on mass transport is suspected to be less intense but still present in this range because of the slower reaction kinetics.

The system activity results of the Pt anode show a different trend from what was discussed for the Ni anode. The glycerol absent experiment has the highest activity throughout this catalyst's applied potential range. The results indicate that adding any amount of glycerol to the anolyte in the presence of the Pt anode does not improve the system's activity. Moreover, comparing the Pt-utilizing cells with glycerol in the electrolyte reveals that those with 0.1 M glycerol concentration show more activity than the rest. Once again, this phenomenon can be attributed to higher viscosities in electrolytes with increased glycerol concentration, which hinders species' transport from the anode [98]. The difference in the Pt and Ni results also indicates the varying effect viscosity increase can have for different catalysts.

Looking solely at the system activity results of various glycerol concentrations discussed here, it can be said that the 0.1 M glycerol amount seems to be the better-performing concentration of the three tested. However, as explained before, the product selectivity data for the 0.1 M cases could not be acquired due to equipment limitations. Since valorization of glycerol is an integral part of this paired electrolysis study and the product selectivity results indicate that the 0.5 M glycerol concentration in the anolyte offers the most favorable conditions for achieving optimal product selectivity, the decision was made to select the 0.5 M glycerol amount as the standardized concentration in the anolyte for the remainder of the studies. This choice was made to ensure consistency in the comparisons between catalysts and electrolysis conditions, ultimately leading to a more informative study.

Two key improvements can be made to enhance the understanding of how glycerol concentration influences the performance of this paired electrolysis system. The first improvement is the completion of liquid product analyses for electrolytes containing 0.1 M glycerol. It is essential to acquire the GOR selectivity results of cells with this glycerol concentration to understand the cell performance better and check the conclusions made regarding the effect of viscosity on GOR product selectivities. This endeavor should be guided by the recommendations described in Section 5.1, such as initiating access to an NMR spectroscope that can handle high ionic strength samples. The second improvement is the pursuit of viscosity measurements. By carefully measuring the viscosity of the electrolytes, we can better evaluate our results using the existing literature. This step is essential in understanding how the viscosity of the electrolyte changes with the addition of glycerol and can provide a more comprehensive perspective for future research pathways.

5.3.3. Effect of Electrochemical Active Surface Area

Considering the significant influence of active surface area on catalytic efficiencies, the Ni and Pt catalysts were compared after their surface area was leveled by sputtering them on the same Ti support.

Interestingly, even with a leveled active surface area, Ni still demonstrated higher FEs (around 6.5%) to the major products compared to Pt at lower cell potentials, firmly establishing its superiority as a catalyst for GOR in zero-gap electrolyzers within this range. Additionally, the Ni sputtered electrodes exhibited a decrease in overall FEs at 3.0 V applied potentials, but this reduction was significantly smaller than what was observed with the Ni foam anode. Potentially, this behavior can be explained by the decrease in the availability of active sites to form O_2 in the Ni anode's lowered surface area form. This also aligns with the previous report indicating that in the presence of glycerol, NiOOH has a preference for producing intermediates of GOR rather than adsorbed OH species [121]. It is likely that with the lowered active surface area, the blocking of active sites by the bulkier glycerol intermediates becomes more effective in preventing the formation of $Ni-OH_{ads}$ species [118]. This finding offers a promising avenue for future GOR studies, indicating a potential approach to mitigate the FE decrease when employing Ni catalysts. By investigating this aspect, Ni catalysts can become more attractive and competitive for enhanced GOR selectivity.

The system activity results of the Ni and Pt catalysts (found in section 4.4.2), compared at their leveled active surface area form, also reveal the superior activity of the Ni catalyst for formate production via GOR in zero-gap electrolyzers. As anticipated, the system's activity for formate production is lower when the anode is the Ni catalyst sputtered on the titanium support than when the anode is Ni foam. This difference persists until the Ni foam activity sharply declines at 3 V. Nonetheless, the sputtered Ni anode continues to surpass the performance of the Pt anode sputtered on the same support material, remaining more effective up to the applied cell potential of 2.7 V.

The Pt anode unquestionably performs worse than the Ni alternatives in both parameters. As discussed, various reports suggest that CO poisoning can worsen catalytic activities and product selectivities on the Pt catalyst. Thus, CO poisoning is suspected to be responsible for the inferior performance observed for Pt in these tests [125].

Overall, this analysis underscores that Ni catalysts, even in their lowered active surface area form, demonstrate superior performance for GOR in zero-gap electrolyzers. They also highlight future avenues that can be pursued to improve the product selectivities using Ni at higher cell potentials, paving new ways for the continued advancement of GOR catalysts.

5.3.4. GOR Selectivity at 100 mA/cm²

All the results discussed before were obtained as part of stepwise chronoamperometry experiments. This means that the anode's performance was evaluated on a 20-min basis. Although this duration is long enough to understand the product selectivity of a catalyst in given experimental conditions, longer-duration tests can allow for the testing of durability while providing more reliable data. Thus, the following discussion focuses on the GOR product selectivity performance of the Ni and Pt electrodes tested at the commercially relevant reaction rate of 100 mA/cm² applied for one hour. For both the HER and the CO_2RR coupling case, it can be observed that due to higher overall FEs, Ni is the better-performing catalyst compared to Pt at this current density. Although the results of this study alone cannot explain why that is the case, it can be reasoned that lowered FEs are a consequence of the presence and perhaps the buildup of surface poisoning species (CO) on the Pt surface [126].

The lower FEs measured when the CO_2RR is paired with GOR suggest that a paired electrolysis with CO_2RR might negatively affect the GOR product selectivity. This is not an unexpected behavior and can be explained by the likely lowering of local pH at the anode due to the parasitic (bi)carbonate formation and crossover towards the anode when CO_2RR is employed in MEA configurations [36]. Moreover, this interpretation also explains why the FE reduction is more significant when Ni anode is utilized. Pt is well-known to be a stable catalyst at both acidic and alkaline environments [21] whereas Ni's activity is lowered in acidic environments [86]. While these tests enable a comparison of catalysts at a high reaction rate for an hour, future studies should conduct even longer duration tests (2-3 hours)

to confirm this interpretation and check the impact of changing local alkalinity on the catalyst GOR performance.

In conclusion, the product selectivity results obtained from this test using AEMEAs unmistakably support the already growing understanding that Ni catalysts outperform Pt below 200 mA/cm² current densities. While traditionally, PGMs such as platinum were considered superior catalysts for GOR; these findings indicate that Ni, a PGM-free alternative, performs better in this cell configuration and coupling. These results underscore the potential of non-PGM catalysts and suggest the need for further exploration of Ni-based alternatives in future research concerning CO_2RR-GOR paired electrolysis. By shedding light on the superior GOR selectivities of Ni in zero-gap electrolyzers, this study contributes valuable insights that can pave the way for more sustainable and economically viable electrochemical conversion processes.

5.3.5. Performance of Ni anode in BPMEAs

Having identified the better catalyst to be Ni in the AEMEA tests, the focus was shifted to addressing a limitation related to using Ni along with AEMs in zero-gap electrolyzers. Ni is incompatible to use in AEMEA systems because of the progression of the electrolyte towards neutrality near the anode with the formation of (bi)carbonates. Ni goes through dissolution at these reaction environments and becomes unsuitable for use [86]. Thus, it was determined that the Ni anode should be tested in a BPMEA cell.

The results of the BPMEA tests reveal that the overall GOR product selectivity performance is better with the use of AEMs at lower applied current densities. However, this decrease in FEs of desired products is less significant than what is commonly observed on the cathodic side with the use of BPMs [39] and only becomes more significant at 200 mA/cm². On top of that, the reduction in the performance of BPMEA cells is significantly less than that observed for AEMEA cells signifying a potential avenue of optimization for utilizing Ni in reaction rates of approximately 200 mA/cm².

To understand the origin of these reductions in FEs, the interpretations behind the decreased CO_2RR selectivities in BPMEA systems were considered. The information that the decrease in the CO_2RR selectivities was due to the increased presence of H^+ at the cathode enhancing the HER side reaction [39] led to the hypothesis that the anode side might be experiencing a possible takeover of OER due to the increased presence of OH^-. To test this hypothesis, access to a GC with two gas inlets was requested from the TP group, and a few Ni-BPMEA cells were tested in this setup. However, the anodic outlet results of these measurements presented in Table 4.2 indicate a lack of O_2 presence in the anode outlet, suggesting total OER suppression.

Although this was not aligned with our hypothesis, this finding can be explained by interpretations made by previous studies also experiencing a total decrease in GOR selectivity below 100%. As mentioned before, OER is not the only potential reaction suggested to drive the measured FEs below their expected range. CO_2 production via formate oxidation as part of the total glycerol oxidation could also reduce FEs for the liquid products [24]. It is feasible that with the increased presence of OH^- near the anode, the likelihood of the complete glycerol oxidation that requires 14 OH^- groups increases the production of CO_2, which would explain the lowered liquid product FEs. The GC data from the setup in the TP lab also provided some information regarding the amount of CO_2 in the anodic outlet; however, this data was deemed unreliable because of the highly probable presence of CO_2 leftover from the cathodic outlet during the anodic outlet measurements. This problem is because of the GC's way of sampling, which was designed to accommodate two gas flow streams by switching from one to the other, thus suffering from the presence of unwanted gas species. Alternative methods need to be devised to measure CO_2 on the anode side. Because no gas bubbles were observed leaving the cell, it is likely that the produced CO_2 was dissolved in the electrolyte [128].

Moving on to the system activity results for the BPMEA cells: they do not show the clear improvement in the effective cell potential expected due to GOR's significantly lower half-cell standard potential compared to OER. Thus, no clear reduction in the energy requirement of the electrochemical cell can be concluded with glycerol in BPMEA cells from Fig. 4.13. In fact, the cell with 0.1 M glycerol-added

electrolyte operates at a higher cell potential than the cell without any glycerol present in its electrolyte, suggesting that this amount of glycerol hinders the system's energy efficiency. This is unexpected and unlike the behavior examined in the AEMEA cells utilizing the Ni anode. However, it can be speculated that this is due to the water dissociation reaction at the BPM interface, leading to an excess of OH^- at the membrane-anode interface. When there is insufficient glycerol availability (0.1 M) in the electrolyte, these high concentrations of OH^- could be causing OER to be preferential to GOR and resulting in lower activities. Unfortunately, there is no available data regarding the O_2 presence in the anode outlet for cells with 0.1 M glycerol presence; thus, the data acquired in this study cannot be used to confirm or deny this claim.

On the other hand, a higher concentration of glycerol in the electrolyte (0.5 M) seems to lower the effective cell potential by up to 0.3 V for current densities up to 150 mA/cm². This decrease in cell potential indicates a reduction in the energy requirement of the BPMEA system with 0.5 M glycerol despite the previously suggested presence of excess OH^-. A similar improvement in the reduction of energy consumption was reported by Junqueira et al., which was reasoned by the lower expected total cell potential due to replacing OER with GOR [99].

This discussion indicates that further studies must be completed to clarify the behavior observed in the BPMEA cells. The limited number of experiments performed utilizing the TP setup is due to the time limitations of this thesis and the access issues to the TP lab during the summer period. In further studies, to enhance the comprehensive understanding of the anode behavior and the potential presence of liquid-to-gas reactions, it is crucial to either gain access to a GC capable of measuring the anodic gas outlet from the beginning or modify the existing experimental setup to capture and analyze the anodic gas. This modification would enable the detection of all of the gaseous compounds formed in the cell, providing valuable insights into the anodic processes. The detection and analysis of gaseous products would complement the liquid product analysis, leading to a more thorough understanding of the electrochemical reactions occurring at the anode and their impact on the overall glycerol oxidation reaction (GOR) performance.

5.3.6. Impact of Various Reaction Pairings on Effective Cell Potential

Analyzing the effective cell potentials for various reaction couplings recorded during one-hour experiments with 100 mA/cm² applied current density leads to several conclusions. Table 4.3 reveals that in the AEMEA cell, replacing GOR with OER does not result in a reduction in cell potential regardless of the catalyst utilized. This is unexpected as many previous reports comparing the replacement of OER with GOR have recorded reduced effective cell potentials [12, 97, 103, 104] However, all of these studies have utilized two-compartment flow reactors which involve the flow of anolytes and catholyte. It is possible that this flow of electrolytes might benefit the system energy requirement by aiding in the removal of GOR products from the active surface area. Thus, the absence of a flowing electrolyte layer in this study utilizing the MEA configuration can be the reason for the lack of reduction in the effective cell potential. On the other hand, some previous papers also report similarly nonexistent reductions in the system's energy consumption with the replacement of GOR with OER [24, 99]; however, no adequate explanations are provided to explain the unexpected response.

Moreover, the results in this study indicate that coupling GOR with HER instead of CO_2RR causes a 0.2 V increase in the cell potential. This increase can be interpreted in two ways. First, this could indicate the reaction environment the CO_2RR created positively impacts the cell potential. This is entirely unexpected since the decrease in local pH caused by the bicarbonate formation due to CO_2RR can be expected to decrease the reaction efficiency of GOR [36]. The other interpretation could be that the presence of GOR intermediates and products in the anolyte negatively affects the HER reaction. However, the data obtained in this study is inadequate to address how changes in the local reaction environment might affect the cathodic reaction. Thus, future paired electrolysis studies should simultaneously evaluate the performance of both anodic and cathodic reactions using a reference electrode.

Finally, the BPMEA measurements of effective cell potential for one-hour experiments show a 0.1 V decrease in the cell potential by replacing OER with GOR. This is a less pronounced reduction in the effective cell potential than what was observed for the stepwise experiments. The difference could

indicate a buildup of OH^- near the anode due to the longer duration of this experiment, which makes the excess OH^- have detrimental effects like increasing the effective potential even in 0.5 M glycerol concentrations [129].

5.4. Additional Recommendations

Having interpreted and analyzed the results of this study with regard to product selectivity and system activity, this section aims to provide some additional general recommendations and directions for future research. The future directions detailed here are meant to complement the recommendations already highlighted as part of the discussions.

Considering that the paired electrolysis of GOR with CO_2RR in this study results in a mixture of liquids containing KOH, glycerol, formate, lactate, glycerate, acetate, and DHA, the separation of this mixture is a step that needs to be accounted for in the analysis of this coupling for future applications. The requirement and the complexity of this liquid separation step can be minimized in two ways. The first is by improving the GOR product selectivity to get closer to 100% for a single GOR product such as formate, and the second is by maximizing the total oxidation of glycerol resulting in the formation of CO_2. Although the production of CO_2 in this way can seem counterproductive in the overarching goal of reducing CO_2 emissions at first glance, it can actually be recycled back into the system. The CO_2 formed on the anode would be mixed with the CO_2 crossover from the cathodic side and can be directly recycled back to the cathode. Assuming no liquid products are formed from CO_2RR, the total conversion of glycerol to CO_2 would mean that the electrolyte could be kept as KOH and glycerol and be reused.

A recent report by Van den Bosch et al. also suggested the potential inhibiting effects of high formate concentrations ($\sim$10 wt%) on the product selectivity of electrochemical glycerol oxidation. They observed a dramatic decrease in the FE to formate and a reduction in formate concentration at these high concentrations. They identified this as a significant bottleneck in the commercialization of this process [100]. Therefore such limitations should be checked for if maximizing formate production is pursued in future studies.

If optimizing the formate oxidation is prioritized, then future work should also investigate the impact of retention time and how further formate oxidation can be prevented. By varying the retention time through electrolyte flow rate adjustments, researchers can investigate how different residence times influence product selectivity. Previous studies have demonstrated that changes in retention time can lead to variations in the types of GOR products formed [24]. Such an investigation is not possible in the setup utilized in this study because the anolyte is being circulated. The circulation of the anolyte makes it challenging to distinguish the effect of retention time via the modification of the electrolyte flow. Adopting a flow-through system like Irabien et al. [24] would allow for a systematic exploration of this parameter, enabling a deeper understanding of its influence on product distribution and overall GOR performance.

Aside from modifying the way electrolyte flows through the system to test new parameters, adjustments can be made in the setup to improve the liquid product analysis. A limitation related to the liquid sampling in this study is that in the step-wise experiments, the samples are taken from the anolyte while the electrochemical reaction continues. Although the anolyte is mixed throughout experiments, this method still results in aliquots that are not entirely representative of the bulk anolyte. Therefore, differential electrochemical mass spectrometry (DEMS) should be used in future studies. This method allows for the quantitative analysis of reactants/products from electrochemical reactions in situ, reducing the uncertainty in the aliquots and allowing for a more comprehensive understanding of the reaction mechanisms and the kinetics of complex reactions [130].

While DEMS can also be utilized alongside CV measurements for the improved identification of peaks and a better understanding of structure-activity relationships [130], utilization of in situ FTIR measurements to investigate the presence of various species on the catalyst surface could also be pursued in future CV studies. As reported by Jeffrey et al., in situ FTIR can allow the detection of surface poisoning species like adsorbed CO and any decrease in the local alkalinity at the electrode surface

via the detected presence of the OH- species [131]. By implementing either of these techniques, more light can be shed on the many unknowns faced when reviewing the CV responses measured during this study, and further improvements can be made by the utilization of anti-poisoning methods such as the strategic introduction of defects [132]

Additionally, improvements can be made in future studies in how currents or potentials were applied on the cell. Due to time constraints, many experiments were conducted stepwise, as mentioned before. This way of testing the cell performance potentially introduces variations like salt formation and already modified starting local reaction environments at later steps. Future studies should consider performing continuous and uninterrupted tests that cover a wide range of potentials and current densities to minimize any potential effects of stepwise experimentation. This approach would provide a more comprehensive and accurate assessment of catalyst performance, closer to how electrochemical reactions would be operated commercially.

Furthermore, continuing studies should also include extended tests to assess the stability of the anodes for GOR production. Investigating the anode's long-term performance will shed light on its durability and potential degradation mechanisms, thereby guiding the development of robust and reliable electrocatalysts. Additionally, these extended tests can be utilized to investigate the susceptibility of the GOR products to be oxidized upon the depletion of other compounds that are more easily adsorbed onto the catalyst surface. For instance, Morales et al. [23] reported a decrease in the concentration of oxalate and glycolate after long electrolysis times. Such investigations regarding the sustainability of the product concentrations in the electrolyte would be very beneficial in optimizing this paired electrolysis system.

Additionally, a general scan of previous GOR studies (whether coupled to HER or CO_2RR) reveals that pure glycerol is the primarily used reactant. As opposed to its pure form, crude glycerol contains methanol and salt impurities that must be removed through vacuum distillation or an ion exchange process [21]. Given that these processes are costly, complex and crude glycerol is 20% cheaper than pure glycerol, the potential financial benefits of utilizing glycerol in its crude form should be pursued in future electrochemical systems [21].

Finally, in this thesis, the discussion regarding system activity and energy requirements relied on the total cell potential because a reference electrode was unavailable. However, future research can consider integrating a reference electrode into the MEA cell. This step would allow for the determination of individual electrode potentials, providing a more comprehensive understanding of the half-cell potentials needed in paired electrolysis systems, like GOR-CO_2RR.

6

Conclusions

This research aimed to explore and optimize the paired electrolysis of glycerol with CO_2 reduction to CO in zero-gap electrolyzers. The paired electrolysis of CO_2RR with GOR was pursued for its potential to address the challenges associated with the use of OER as the conventionally coupled anodic reaction in CO_2RR systems. These limitations include thermodynamic and kinetic unfavorability, the necessity for rare metals as catalysts, and the added need for a gas separation step due to the presence of O_2gas in the anodic outlet. Through experimentation, the performances of Pt (a PGM catalyst) and Ni (a PGM-free alternative) were investigated across multiple parameters, such as glycerol concentration, active surface area, and membrane types. These catalysts were evaluated under potential and current controls, focusing on their selectivity for GOR products and overall system activity. Products were analyzed using gas chromatography (GC) and proton nuclear magnetic resonance spectroscopy (H-NMR).

This study unveiled the viability of zero-gap electrolyzers for producing various GOR products in a paired electrolysis with CO_2RR. While formate and lactate emerged as the primary products, the presence of glycerate, DHA, and acetate in minor quantities for both Pt and Ni catalysts underscores the value-adding benefit of this coupling compared to one reliant on OER.

Intriguingly, while cyclic voltammetry measurements hinted at a more pronounced GOR activity with Pt, the paired electrolysis tests demonstrated Ni's superiority as a GOR catalyst in zero-gap electrolyzers at current densities below 200 mA/cm². It was hypothesized that the enhancement of CO poisoning due to the lack of electrolyte flow on the anode surface is the likely root cause for the worse performance of Pt in zero-gap electrolyzers. This outperformance of Ni challenges the convention that PGM catalysts reign supreme in GOR applications, prompting a call for future research to concentrate on these promising and cost-effective alternatives, especially for use in paired electrolysis with CO_2RR.

Furthermore, the influence of parameters on cell performance highlighted the adverse effect of increasing applied potentials on faradaic efficiencies (FEs), suggesting potential liquid-to-gas side reactions like OER or formate oxidation as part of total glycerol oxidation. Similarly, the impact of glycerol concentrations was demonstrated, and viscosity-related diffusivity issues were identified as a likely cause for reduced activities and FEs at higher glycerol concentrations. Notably, the utilization of Ni anodes revealed a significant reduction in total FEs at around 200 mA/cm², a phenomenon potentially tied to side reactions. However, it was determined that an increase in glycerol concentration or a reduction in the active surface area could somewhat alleviate this FE reduction, hinting at potential mitigation strategies in future investigations.

Having explored the parameters mentioned above in an AEMEA configuration and highlighted the superior performance of the Ni anode, attention was shifted towards investigating the effects of bipolar membranes on the paired electrolysis. This investigation was prompted by bipolar membranes' potential to address the widely acknowledged issue of long-term durability of Ni anodes in AEM utilizing

CO_2RR systems. Additionally, this investigation aimed to bridge the knowledge gap existing in current CO_2RR-GOR studies regarding the utilization of BPMs for this paired electrolysis. The Ni tests conducted on BPMEA cells unveiled a minor reduction in product selectivity, likely attributable to an elevated presence of OH^- ions near the anode. The absence of detectable O_2 in the anode outlet served as a pivotal clue, leading to the deduction that the reduction in faradaic efficiency stems from the oxidation of formate and complete glycerol oxidation. However, future tests are necessary to confirm these hypotheses and advance the performance of these electrochemical systems.

Regarding the anticipated reduction in the energy demand of the system with the incorporation of GOR as an alternative to OER, AEMEA tests did not yield any conclusive improvements in system activity (and thus energy needs) with glycerol presence. On the other hand, a slight improvement in effective cell potential (up to 0.3 V) was observed in the Ni anode using BPMEAs at 0.5 M glycerol content. Notably, the absence of a significant decrease in cell potential ($\sim$ 1.0 V) still contradicts prior studies in flow cell electrolyzers [12, 97, 103, 104], implying a potential correlation between the absence of a flowing electrolyte and the absence of a significant reduction in effective cell potential. Such conclusions underscore the need for modifications, particularly incorporating a reference electrode, to illuminate the reasons behind these disparities.

Although the paired electrolysis did not show any indication of a decrease in the energy demand in the system for AEMEAs and only a small one for the BPMEAs, this study investigating the paired electrolysis of GOR and CO_2RR in zero-gap electrolyzers still led to the production of value-added products, explored the intricate dynamics of various parameters on cell performance and underscored the potential of non-PGM catalysts to be utilized for GOR in CO_2RR electrolyzers. Collectively, these findings pave the way for future research within the MECS group and contribute to the evolution of electrochemical CO_2 reduction systems, inching them closer to commercial viability.

References

[1] Hannah Ritchie, Max Roser, and Pablo Rosado. “Energy”. In: *Our World in Data* (2022).

[2] *Fossil Fuels | EESI*. July 2021. URL: https://www.eesi.org/topics/fossil-fuels/description.

[3] Rebecca Lindsey. *Climate Change: Atmospheric Carbon Dioxide*. May 2023. URL: https://www.climate.gov/news-features/understanding-climate/climate-change-atmospheric-carbon-dioxide.

[4] Valérie Masson-Delmotte et al. *IPCC, 2021: Climate Change 2021 The Physical Science Basis. Contribution of Working Group I to the Sixth Assessment Report of the Intergovernmental Panel on Climate Change*. Tech. rep. New York: Intergovernmental Panel on Climate Change, 2021, pp. 1–2391. DOI: 10.1017/9781009157896.

[5] U.S. Energy Information Administration. *IEO 2021 Narrative*. Tech. rep. U.S. Department of Energy, 2021. URL: www.eia.gov.

[6] *Adoption of The Paris Agreement*. 2015.

[7] bp. *Statistical Review of World Energy 2022*. Tech. rep. 71. 2022.

[8] Vaclav Smil. *Energy Transitions: Global and National Perspectives*. 2nd ed. Praeger, Dec. 2017. ISBN: 144085324X.

[9] Hannah Ritchie. *How have the world’s energy sources changed over the last two centuries?* 2021. URL: https://ourworldindata.org/global-energy-200-years.

[10] Robert Gross et al. “The Costs and Impacts of Intermittency: An assessment of the evidence on the costs and impacts of intermittent generation on the British electricity network A report of the Technology and Policy Assessment Function of the UK Energy Research Centre, with financial support from the Carbon Trust”. In: (2006).

[11] E B Tchawou Tchuisseu, D Gomila, and P Colet. “Reduction of power grid fluctuations by communication between smart devices”. In: (2019). DOI: 10.1016/j.ijepes.2019.01.004. URL: https://doi.org/10.1016/j.ijepes.2019.01.004.

[12] Sumit Verma, Shawn Lu, and Paul J.A. Kenis. “Co-electrolysis of CO2 and glycerol as a pathway to carbon chemicals with improved technoeconomics due to low electricity consumption”. In: *Nature Energy* 4.6 (June 2019), pp. 466–474. ISSN: 20587546. DOI: 10.1038/s41560-019-0374-6.

[13] Huei Ru Molly Jhong, Sichao Ma, and Paul Ja Kenis. “Electrochemical conversion of CO2 to useful chemicals: current status, remaining challenges, and future opportunities”. In: *Current Opinion in Chemical Engineering* 2.2 (May 2013), pp. 191–199. ISSN: 2211-3398. DOI: 10.1016/J.COCHE.2013.03.005.

[14] Thomas Burdyny and Wilson A. Smith. “CO2 reduction on gas-diffusion electrodes and why catalytic performance must be assessed at commercially-relevant conditions”. In: *Energy and Environmental Science* 12.5 (May 2019), pp. 1442–1453. ISSN: 17545706. DOI: 10.1039/c8ee03134g.

[15] Mark Sassenburg et al. “Characterizing CO2Reduction Catalysts on Gas Diffusion Electrodes: Comparing Activity, Selectivity, and Stability of Transition Metal Catalysts”. In: *ACS Applied Energy Materials* (2022). ISSN: 25740962. DOI: 10.1021/acsaem.2c00160.

[16] A´ Dám Vass et al. “Anode Catalysts in CO 2 Electrolysis: Challenges and Untapped Opportunities”. In: *ACS Catalysis* (2022). DOI: 10.1021/acscatal.1c04978. URL: https://doi.org/10.1021/acscatal.1c04978.

[17] Zikai Xu, Chen Peng, and Gengfeng Zheng. *Coupling Value-Added Anodic Reactions with Electrocatalytic CO2 Reduction*. Feb. 2023. DOI: 10.1002/chem.202203147.

[18] Haeun Shin, Kentaro U. Hansen, and Feng Jiao. "Techno-economic assessment of low-temperature carbon dioxide electrolysis". In: *Nature Sustainability 2021 4:10* 4.10 (July 2021), pp. 911–919. ISSN: 2398-9629. DOI: 10.1038/s41893-021-00739-x. URL: https://www.nature.com/articles/s41893-021-00739-x.

[19] Carlo Santoro et al. "What is Next in Anion-Exchange Membrane Water Electrolyzers? Bottlenecks, Benefits, and Future". In: *ChemSusChem* 15.8 (Apr. 2022), e202200027. ISSN: 1864-564X. DOI: 10.1002/CSSC.202200027. URL: https://onlinelibrary.wiley.com/doi/full/10.1002/cssc.202200027%20https://onlinelibrary.wiley.com/doi/abs/10.1002/cssc.202200027%20https://chemistry-europe.onlinelibrary.wiley.com/doi/full/10.1002/cssc.202200027.

[20] Benjamin Katryniok et al. "Selective catalytic oxidation of glycerol: perspectives for high value chemicals". In: *Green Chemistry* (2011). DOI: 10.1039/c1gc15320j. URL: www.rsc.org/greenchem.

[21] Linfeng Fan et al. "Recent Progress in Electrocatalytic Glycerol Oxidation". In: *Energy Technology* 9.2 (Feb. 2021). ISSN: 21944296. DOI: 10.1002/ente.202000804.

[22] Ke Xie et al. "Eliminating the need for anodic gas separation in CO2 electroreduction systems via liquid-to-liquid anodic upgrading". In: *Nature Communications* 13.1 (Dec. 2022). ISSN: 20411723. DOI: 10.1038/s41467-022-30677-x.

[23] Dulce M. Morales et al. "Electrocatalytic Conversion of Glycerol to Oxalate on Ni Oxide Nanoparticles-Modified Oxidized Multiwalled Carbon Nanotubes". In: *ACS Catalysis* 12.2 (Jan. 2022), pp. 982–992. ISSN: 21555435. DOI: 10.1021/acscatal.1c04150.

[24] Kevin Fernández-Caso et al. "Continuous carbon dioxide electroreduction to formate coupled with the single-pass glycerol oxidation to high value-added products". In: *Journal of CO2 Utilization* 70 (Apr. 2023), p. 102431. ISSN: 22129820. DOI: 10.1016/j.jcou.2023.102431.

[25] Prashant Kamat and Phillip Christopher. "Gas Diffusion Electrodes for CO2and N2Reduction: A Virtual Issue". In: *ACS Energy Letters* 7.4 (Apr. 2022), pp. 1469–1472. ISSN: 23808195. DOI: 10.1021/acsenergylett.2c00606.

[26] Yuguang C. Li et al. "Bipolar Membranes Inhibit Product Crossover in CO2 Electrolysis Cells". In: *Advanced Sustainable Systems* 2.4 (Apr. 2018). ISSN: 23667486. DOI: 10.1002/adsu.201700187.

[27] Thomas Francis Fuller and John Naim Harb. *Electrochemical engineering*. 1st ed. Hoboken: Wiley, 2018.

[28] Joshua Halpern. *Chapter 19.1: Describing Electrochemical Cells - Chemistry LibreTexts*. 2023. URL: https://chem.libretexts.org/Courses/Howard_University/General_Chemistry%3A_An_Atoms_First_Approach/Unit_7%3A_Thermodynamics_and_Electrochemistry/Chapter_19%3A_Electrochemistry/Chapter_19.1%3A_Describing_Electrochemical_Cells.

[29] Allen J. Bard and Larry R. Faulkner. *Electrochemical methods : fundamentals and applications*, p. 833. ISBN: 0471043729.

[30] Jingfu He et al. "Design of pre-catalysts for heterogeneous CO2 electrochemical reduction". In: *Journal of Materials Chemistry A* 9.35 (Sept. 2021), pp. 19508–19533. ISSN: 2050-7496. DOI: 10.1039/D1TA03624F. URL: https://pubs.rsc.org/en/content/articlehtml/2021/ta/d1ta03624f%20https://pubs.rsc.org/en/content/articlelanding/2021/ta/d1ta03624f.

[31] Bowen Wu, Jian Chen, and Linping Qian. "Recent Advances in Heterogeneous Electroreduction of CO2 on Copper-Based Catalysts". In: *Catalysts 2022, Vol. 12, Page 860* 12.8 (Aug. 2022), p. 860. ISSN: 2073-4344. DOI: 10.3390/CATAL12080860. URL: https://www.mdpi.com/2073-4344/12/8/860/htm%20https://www.mdpi.com/2073-4344/12/8/860.

[32] Samah A. Mahyoub et al. “An overview on the recent developments of Ag-based electrodes in the electrochemical reduction of CO2 to CO”. In: *Sustainable Energy & Fuels* 4.1 (Dec. 2019), pp. 50–67. ISSN: 2398-4902. DOI: 10.1039/C9SE00594C. URL: https://pubs.rsc.org/en/content/articlehtml/2020/se/c9se00594c%20https://pubs.rsc.org/en/content/articlelanding/2020/se/c9se00594c.

[33] György Inzelt. “ Kinetics of Electrochemical Reactions”. In: *Electroanalytical methods : guide to experiments and applications*. First Online. Springer, 2009. Chap. 3, pp. 33–53.

[34] Maximilian Kö et al. “Solvents and Supporting Electrolytes in the Electrocatalytic Reduction of CO 2”. In: *iScience* (2019). DOI: 10.1016/j.isci. URL: https://doi.org/10.1016/j.isci..

[35] Eric W. Lees et al. *Gas diffusion electrodes and membranes for CO2 reduction electrolysers*. Jan. 2022. DOI: 10.1038/s41578-021-00356-2.

[36] Ádám Vass et al. “Local Chemical Environment Governs Anode Processes in CO2Electrolyzers”. In: *ACS Energy Letters* 6.11 (Nov. 2021), pp. 3801–3808. ISSN: 23808195. DOI: 10.1021/acsenergylett.1c01937.

[37] Stefan Ringe et al. “Understanding cation effects in electrochemical CO 2 reduction Understanding cation effects in electrochemical CO 2 reduction †”. In: *Energy Environ. Sci* 12 (2019), p. 3001. ISSN: 1754-5706. DOI: 10.1039/c9ee01341e.

[38] Marilia Moura de Salles Pupo and Ruud Kortlever. *Electrolyte Effects on the Electrochemical Reduction of CO2*. Nov. 2019. DOI: 10.1002/cphc.201900680.

[39] Kailun Yang et al. “Cation-driven increases of co2utilization in a bipolar membrane electrode assembly for co2electrolysis”. In: *ACS Energy Letters* 6.12 (Dec. 2021), pp. 4291–4298. ISSN: 23808195. DOI: 10.1021/acsenergylett.1c02058.

[40] Dunfeng Gao et al. “Designing Electrolyzers for Electrocatalytic CO2 Reduction”. In: *Acta Physico Chimica Sinica* 0.0 (2020), pp. 2009021–. ISSN: 1000-6818. DOI: 10.3866/PKU.WHXB202009021.

[41] David Raciti et al. “H-Cell Vs Gas Diffusion Electrolyzer for Evaluating Intrinsic Activity of Nanocatalysts for Electrochemical CO2 Reduction”. In: *ECS Meeting Abstracts* MA2019-02.22 (Sept. 2019), p. 1072. ISSN: 2151-2043. DOI: 10.1149/MA2019-02/22/1072. URL: https://iopscience.iop.org/article/10.1149/MA2019-02/22/1072%20https://iopscience.iop.org/article/10.1149/MA2019-02/22/1072/meta.

[42] Lien Chun Weng, Alexis T. Bell, and Adam Z. Weber. “Modeling gas-diffusion electrodes for CO2 reduction”. In: *Physical Chemistry Chemical Physics* 20.25 (June 2018), pp. 16973–16984. ISSN: 1463-9084. DOI: 10.1039/C8CP01319E. URL: https://pubs.rsc.org/en/content/articlehtml/2018/cp/c8cp01319e%20https://pubs.rsc.org/en/content/articlelanding/2018/cp/c8cp01319e.

[43] Kailun Yang et al. “Role of the Carbon-Based Gas Diffusion Layer on Flooding in a Gas Diffusion Electrode Cell for Electrochemical CO2Reduction”. In: *ACS Energy Letters* 6.1 (Jan. 2021), pp. 33–40. ISSN: 23808195. DOI: 10.1021/acsenergylett.0c02184.

[44] Asger B. Moss et al. “In operando investigations of oscillatory water and carbonate effects in MEA-based CO2 electrolysis devices”. In: *Joule* 7.2 (Feb. 2023), pp. 350–365. ISSN: 25424351. DOI: 10.1016/j.joule.2023.01.013.

[45] Emiliana R. Cofell et al. “Investigation of Electrolyte-Dependent Carbonate Formation on Gas Diffusion Electrodes for CO2Electrolysis”. In: *ACS Applied Materials and Interfaces* 13.13 (Apr. 2021), pp. 15132–15142. ISSN: 19448252. DOI: 10.1021/acsami.0c21997.

[46] McLain E. Leonard et al. “Investigating electrode flooding in a flowing electrolyte, gas□fed carbon dioxide electrolyzer”. In: *ChemSusChem* 13.2 (Jan. 2020), pp. 400–411. ISSN: 1864-5631. DOI: 10.1002/CSSC.201902547. URL: https://research.tue.nl/en/publications/investigating-electrode-flooding-in-a-flowing-electrolyte-gasfed-.

[47] Fei Yue Gao et al. *Electrochemical CO2-to-CO conversion: Electrocatalysts, electrolytes, and electrolyzers*. Aug. 2020. DOI: 10.1039/d0ta03525d.

[48] Marijn A. Blommaert et al. *Insights and Challenges for Applying Bipolar Membranes in Advanced Electrochemical Energy Systems*. 2021. DOI: 10.1021/acsenergylett.1c00618.

[49] M C. Porter. “Handbook of industrial membrane technology”. In: (Jan. 1989).

[50] Danielle Salvatore et al. “Designing anion exchange membranes for CO 2 electrolysers”. In: *Nature Energy* (2021). DOI: 10.1038/s41560-020-00761-x. URL: https://doi.org/10.1038/s41560-020-00761-x.

[51] Christopher McCallum et al. “Reducing the crossover of carbonate and liquid products during carbon dioxide electroreduction”. In: *Cell Reports Physical Science* 2.8 (Aug. 2021). ISSN: 26663864. DOI: 10.1016/j.xcrp.2021.100522.

[52] Gumaa A El-Nagar et al. “Unintended cation crossover influences CO2 reduction selectivity in Cu-based zero-gap electrolysers”. In: *Nature Communications* (2023). DOI: 10.1038/s41467-023-37520-x. URL: https://doi.org/10.1038/s41467-023-37520-x.

[53] R. Pärnamäe et al. *Bipolar membranes: A review on principles, latest developments, and applications*. Jan. 2021. DOI: 10.1016/j.memsci.2020.118538.

[54] Ke Xie et al. “Bipolar membrane electrolyzers enable high single-pass CO2 electroreduction to multicarbon products”. In: *Nature Communications* 13.1 (Dec. 2022). ISSN: 20411723. DOI: 10.1038/s41467-022-31295-3.

[55] Christine M Gabardo et al. “Continuous Carbon Dioxide Electroreduction to Concentrated Multicarbon Products Using a Membrane Electrode Assembly”. In: *Joule* (2019). DOI: 10.1016/j.joule.2019.07.021. URL: https://doi.org/10.1016/j.joule.2019.07.021.

[56] Joshua A Rabinowitz and Matthew W Kanan. “The future of low-temperature carbon dioxide electrolysis depends on solving one basic problem”. In: *Nature Communications* (2020). DOI: 10.1038/s41467-020-19135-8. URL: https://doi.org/10.1038/s41467-020-19135-8.

[57] Ming Ma et al. “Role of ion-selective membranes in the carbon balance for CO 2 electroreduction via gas diffusion electrode reactor designs †”. In: *Royal Society of Chemistry* (2020). DOI: 10.1039/d0sc03047c.

[58] Tengfei Li et al. “Electrolytic CO 2 Reduction in Tandem with Oxidative Organic Chemistry”. In: *ACS Central Science* 12 (2023), p. 13. DOI: 10.1021/acscentsci.7b00207. URL: http://pubs.acs.org/journal/acscii.

[59] Jonggeol Na et al. “General technoeconomic analysis for electrochemical coproduction coupling carbon dioxide reduction with organic oxidation”. In: *Nature Communications* (2019). DOI: 10.1038/s41467-019-12744-y. URL: https://doi.org/10.1038/s41467-019-12744-y.

[60] Rosaria Ciriminna et al. “Understanding the glycerol market”. In: *European Journal of Lipid Science and Technology* (2014). DOI: 10.1002/ejlt.201400229. URL: www.ejlst.com.

[61] Mário Simões, Stève Baranton, and Christophe Coutanceau. “Electrochemical Valorisation of Glycerol”. In: *ChemSusChem* 5.11 (Nov. 2012), pp. 2106–2124. ISSN: 1864-564X. DOI: 10.1002/CSSC.201200335. URL: https://onlinelibrary.wiley.com/doi/full/10.1002/cssc.201200335%20https://onlinelibrary.wiley.com/doi/abs/10.1002/cssc.201200335%20https://chemistry-europe.onlinelibrary.wiley.com/doi/10.1002/cssc.201200335.

[62] Xiaolan Luo et al. “Value-added processing of crude glycerol into chemicals and polymers”. In: *Bioresource technology* 215 (Sept. 2016), pp. 144–154. ISSN: 1873-2976. DOI: 10.1016/J.BIORTECH.2016.03.042. URL: https://pubmed.ncbi.nlm.nih.gov/27004448/.

[63] Weizhu Zeng et al. “Efficient 1,3-dihydroxyacetone biosynthesis in Gluconobacter oxydans using metabolic engineering and a fed-batch strategy”. In: *Bioresources and Bioprocessing* 9.1 (Dec. 2022), pp. 1–11. ISSN: 21974365. DOI: 10.1186/S40643-022-00610-7/TABLES/3. URL: https://bioresourcesbioprocessing.springeropen.com/articles/10.1186/s40643-022-00610-7.

[64] Rosaria Ciriminna et al. “Dihydroxyacetone:An Updated Insight into an Important Bioproduct”. In: *Chemistry Open* (2018). DOI: 10.1002/open.201700201. URL: https://doi.org/10.1002/open.201700201..

[65] Andreas Weilhard, Stephen P. Argent, and Victor Sans. “Efficient carbon dioxide hydrogenation to formic acid with buffering ionic liquids”. In: *Nature Communications* 12.1 (Jan. 2021), pp. 1–7. ISSN: 2041-1723. DOI: 10.1038/s41467-020-20291-0. URL: https://www.nature.com/articles/s41467-020-20291-0.

[66] Alexander Wotton et al. “Viologen Catalysts for a Direct Carbohydrate Fuel”. In: (2009). DOI: 10.1149/1.3183815.

[67] Wei Jiang et al. “Metabolic engineering strategies to enable microbial utilization of C1 feedstocks”. In: *Nature Chemical Biology* (2021). DOI: 10.1038/s41589-021-00836-0. URL: https://doi.org/10.1038/s41589-021-00836-0.

[68] Wei Wang et al. “ATP-free biosynthesis of a high-energy phosphate metabolite fructose 1,6-diphosphate by in vitro metabolic engineering”. In: *Metabolic engineering* 42 (July 2017), pp. 168–174. ISSN: 1096-7184. DOI: 10.1016/J.YMBEN.2017.06.006. URL: https://pubmed.ncbi.nlm.nih.gov/28624535/.

[69] Tawfik A. Khattab, Meram S. Abdelrahman, and Mohamed Rehan. “Textile dyeing industry: environmental impacts and remediation”. In: *Environmental Science and Pollution Research* 27.4 (Feb. 2020), pp. 3803–3818. ISSN: 16147499. DOI: 10.1007/S11356-019-07137-Z/FIGURES/12. URL: https://link.springer.com/article/10.1007/s11356-019-07137-z.

[70] Naef A.A. Qasem, Ramy H. Mohammed, and Dahiru U. Lawal. “Removal of heavy metal ions from wastewater: a comprehensive and critical review”. In: *npj Clean Water 2021 4:1* 4.1 (July 2021), pp. 1–15. ISSN: 2059-7037. DOI: 10.1038/s41545-021-00127-0. URL: https://www.nature.com/articles/s41545-021-00127-0.

[71] Waqar Ahmad et al. “Acetic acid and co-chemicals production from syngas”. In: *Advances in Synthesis Gas : Methods, Technologies and Applications* (Jan. 2023), pp. 199–223. DOI: 10.1016/B978-0-323-91878-7.00010-1.

[72] Yuye Chen et al. “An Overview of Chemical Additives on (Micro)Plastic Fibers: Occurrence, Release, and Health Risks”. In: *Reviews of Environmental Contamination and Toxicology 2022 260:1* 260.1 (Dec. 2022), pp. 1–25. ISSN: 2197-6554. DOI: 10.1007/S44169-022-00023-9. URL: https://link.springer.com/article/10.1007/s44169-022-00023-9.

[73] *CFR - Code of Federal Regulations Title 21*.

[74] *Lactic acids for leather and textile production | Corbion*. URL: https://www.corbion.com/en/Markets/Biochemical-specialties/Other-biochemicals/Leather-and-textiles.

[75] M. A. Pozdniakov et al. “Glyoxylic acid: synthesis, isolation, and crystallization”. In: *Russian Chemical Bulletin* 68.3 (Mar. 2019), pp. 472–479. ISSN: 15739171. DOI: 10.1007/S11172-019-2442-2/METRICS. URL: https://link.springer.com/article/10.1007/s11172-019-2442-2.

[76] Sandra Gerstenbruch et al. “Asymmetric synthesis of D-glyceric acid by an alditol oxidase and directed evolution for enhanced oxidative activity towards glycerol”. In: *Applied Microbiology and Biotechnology* 96.5 (Dec. 2012), pp. 1243–1252. ISSN: 01757598. DOI: 10.1007/S00253-012-3885-7/TABLES/5. URL: https://link.springer.com/article/10.1007/s00253-012-3885-7.

[77] Shun Sato, Dai Kitamoto, and Hiroshi Habe. “In vitro evaluation of glyceric acid and its glucosyl derivative, α-glucosylglyceric acid, as cell proliferation inducers and protective solutes”. In: *Bioscience, Biotechnology, and Biochemistry* 78.7 (July 2014), pp. 1183–1186. ISSN: 0916-8451. DOI: 10.1080/09168451.2014.885823. URL: https://dx.doi.org/10.1080/09168451.2014.885823.

[78] Kavindra Kumar Kesari et al. “Wastewater Treatment and Reuse: a Review of its Applications and Health Implications”. In: *Water, Air, and Soil Pollution* 232.5 (May 2021), pp. 1–28. ISSN: 15732932. DOI: 10.1007/S11270-021-05154-8/FIGURES/5. URL: https://link.springer.com/article/10.1007/s11270-021-05154-8.

[79] Aswatha Rabindranathnambi and Maaz Abid. “Topical treatments in dermatology”. In: *British journal of hospital medicine (London, England : 2005)* 82.8 (Aug. 2021). ISSN: 1750-8460. DOI: 10.12968/HMED.2020.0567. URL: https://pubmed.ncbi.nlm.nih.gov/34431347/.

[80] Adolf Zschunke. *Reference Materials in Analytical Chemistry*. Ed. by Adolf Zschunke. Vol. 40. Springer Series in Materials Science. Berlin, Heidelberg: Springer Berlin Heidelberg, 2000. ISBN: 978-3-642-63097-2. DOI: 10.1007/978-3-642-56986-9. URL: http://link.springer.com/10.1007/978-3-642-56986-9.

[81] Thomas P. Knepper. "Synthetic chelating agents and compounds exhibiting complexing properties in the aquatic environment". In: *TrAC Trends in Analytical Chemistry* 22.10 (Nov. 2003), pp. 708–724. ISSN: 0165-9936. DOI: 10.1016/S0165-9936(03)01008-2.

[82] Hui Luo et al. "Role of Ni in PtNi Bimetallic Electrocatalysts for Hydrogen and Value-Added Chemicals Coproduction via Glycerol Electrooxidation". In: *ACS Catalysis* 12.23 (Dec. 2022), pp. 14492–14506. ISSN: 21555435. DOI: 10.1021/ACSCATAL.2C03907/ASSET/IMAGES/LARGE/CS2C03907{_}0012.JPEG. URL: https://pubs.acs.org/doi/full/10.1021/acscatal.2c03907.

[83] Xing Zhang et al. "Highly selective and active CO2 reduction electrocatalysts based on cobalt phthalocyanine/carbon nanotube hybrid structures". In: *Nature Communications 2017 8:1* 8.1 (Mar. 2017), pp. 1–8. ISSN: 2041-1723. DOI: 10.1038/ncomms14675. URL: https://www.nature.com/articles/ncomms14675.

[84] Nivetha Jeyachandran, Wangchao Yuan, and Cristina Giordano. *Cutting-Edge Electrocatalysts for CO2RR*. Apr. 2023. DOI: 10.3390/molecules28083504.

[85] Qi Lu et al. "A selective and efficient electrocatalyst for carbon dioxide reduction". In: *Nature Communications* 5 (Jan. 2014). ISSN: 20411723. DOI: 10.1038/ncomms4242.

[86] A´ Dám Vass et al. "Anode Catalysts in CO 2 Electrolysis: Challenges and Untapped Opportunities". In: *ACS Catalysis* (2022). DOI: 10.1021/acscatal.1c04978. URL: https://doi.org/10.1021/acscatal.1c04978.

[87] Christine Minke et al. "Is iridium demand a potential bottleneck in the realization of large-scale PEM water electrolysis?" In: *International Journal of Hydrogen Energy* 46.46 (July 2021), pp. 23581–23590. ISSN: 0360-3199. DOI: 10.1016/J.IJHYDENE.2021.04.174.

[88] Janaina Fernandes Gomes et al. "The influence of the Pt crystalline surface orientation on the glycerol electro-oxidation in acidic media". In: *Electrochimica Acta* 76 (Aug. 2012), pp. 88–93. ISSN: 0013-4686. DOI: 10.1016/J.ELECTACTA.2012.04.144.

[89] Janaina Fernandes Gomes and Germano Tremiliosi-Filho. "Spectroscopic Studies of the Glycerol Electro-Oxidation on Polycrystalline Au and Pt Surfaces in Acidic and Alkaline Media". In: *Electrocatalysis* 2.2 (June 2011), pp. 96–105. ISSN: 18682529. DOI: 10.1007/S12678-011-0039-0/FIGURES/8. URL: https://link.springer.com/article/10.1007/s12678-011-0039-0.

[90] Yongfang Zhou et al. "Selective Electro-Oxidation of Glycerol to Dihydroxyacetone by PtAg Skeletons". In: *ACS Applied Materials and Interfaces* 11.32 (Aug. 2019), pp. 28953–28959. ISSN: 19448252. DOI: 10.1021/ACSAMI.9B09431/ASSET/IMAGES/LARGE/AM9B09431{_}0007.JPEG. URL: https://pubs.acs.org/doi/full/10.1021/acsami.9b09431.

[91] Fang Yang et al. "Ultrasmall Pd-Cu-Pt Trimetallic Twin Icosahedrons Boost the Electrocatalytic Performance of Glycerol Oxidation at the Operating Temperature of Fuel Cells". In: *Advanced Functional Materials* 30.11 (Mar. 2020), p. 1908235. ISSN: 1616-3028. DOI: 10.1002/ADFM.201908235. URL: https://onlinelibrary.wiley.com/doi/full/10.1002/adfm.201908235%20https://onlinelibrary.wiley.com/doi/abs/10.1002/adfm.201908235%20https://onlinelibrary.wiley.com/doi/10.1002/adfm.201908235.

[92] Qi Han et al. "Rational Design of Electrocatalytic Interfaces: Cd UPD Mediated Nitrate Reduction on Pd: Au Bimetallic Surfaces". In: *Journal of The Electrochemical Society* 166.13 (Aug. 2019), H640–H643. ISSN: 0013-4651. DOI: 10.1149/2.0921913JES/XML. URL: https://iopscience.iop.org/article/10.1149/2.0921913jes%20https://iopscience.iop.org/article/10.1149/2.0921913jes/meta.

[93] Rodrigo M. Castagna et al. "Electrooxidation of ethanol and glycerol on carbon supported PtCu nanoparticles". In: *International Journal of Hydrogen Energy* 44.12 (Mar. 2019), pp. 5970–5982. ISSN: 0360-3199. DOI: 10.1016/J.IJHYDENE.2019.01.090.

[94] Mohamed S. E. Houache et al. “Nanostructured Ni and Ni-Pd Catalysts for Glycerol Electro-Oxidation in Alkaline Media”. In: *ECS Meeting Abstracts* MA2018-02.25 (July 2018), p. 859. ISSN: 2151-2043. DOI: 10.1149/MA2018-02/25/859. URL: https://iopscience.iop.org/article/10.1149/MA2018-02/25/859%20https://iopscience.iop.org/article/10.1149/MA2018-02/25/859/meta.

[95] P. Sivasakthi and M. V. Sangaranarayanan. “Pulse electrodeposited nickel with structure directing agents as an electrocatalyst for oxidation of glycerol”. In: *New Journal of Chemistry* 43.21 (May 2019), pp. 8352–8362. ISSN: 1369-9261. DOI: 10.1039/C9NJ01351B. URL: https://pubs.rsc.org/en/content/articlehtml/2019/nj/c9nj01351b%20https://pubs.rsc.org/en/content/articlelanding/2019/nj/c9nj01351b.

[96] Yan Li et al. “Nickel-molybdenum nitride nanoplate electrocatalysts for concurrent electrolytic hydrogen and formate productions”. In: *Nature Communications 2019 10:1* 10.1 (Nov. 2019), pp. 1–12. ISSN: 2041-1723. DOI: 10.1038/s41467-019-13375-z. URL: https://www.nature.com/articles/s41467-019-13375-z.

[97] Yuhou Pei et al. “Glycerol oxidation-assisted electrochemical CO2 reduction for the dual production of formate”. In: *Journal of Materials Chemistry A* 10.3 (Jan. 2022), pp. 1309–1319. ISSN: 2050-7496. DOI: 10.1039/D1TA07119J. URL: https://pubs.rsc.org/en/content/articlehtml/2022/ta/d1ta07119j%20https://pubs.rsc.org/en/content/articlelanding/2022/ta/d1ta07119j.

[98] Jan Vehrenberg et al. “Paired electrochemical synthesis of formate via oxidation of glycerol and reduction of CO2 in a flow cell reactor”. In: *Electrochemistry Communications* 151 (June 2023), p. 107497. ISSN: 1388-2481. DOI: 10.1016/J.ELECOM.2023.107497.

[99] João R.C. Junqueira et al. “Simultaneous Anodic and Cathodic Formate Production in a Paired Electrolyzer by CO2 Reduction and Glycerol Oxidation”. In: *ChemSusChem* 16.11 (June 2023), e202202349. ISSN: 1864-564X. DOI: 10.1002/CSSC.202202349. URL: https://onlinelibrary.wiley.com/doi/full/10.1002/cssc.202202349%20https://onlinelibrary.wiley.com/doi/abs/10.1002/cssc.202202349%20https://chemistry-europe.onlinelibrary.wiley.com/doi/full/10.1002/cssc.202202349.

[100] Bart van den Bosch et al. “Formate Over-Oxidation Limits Industrialization of Glycerol Oxidation Paired with Carbon Dioxide Reduction to Formate”. In: *ChemPlusChem* 88.4 (Apr. 2023), e202300112. ISSN: 2192-6506. DOI: 10.1002/CPLU.202300112. URL: https://onlinelibrary.wiley.com/doi/full/10.1002/cplu.202300112%20https://onlinelibrary.wiley.com/doi/abs/10.1002/cplu.202300112%20https://chemistry-europe.onlinelibrary.wiley.com/doi/full/10.1002/cplu.202300112.

[101] Mark A. Bajada et al. “A Precious-Metal-Free Hybrid Electrolyzer for Alcohol Oxidation Coupled to CO2-to-Syngas Conversion”. In: *Angewandte Chemie* 132.36 (Sept. 2020), pp. 15763–15771. ISSN: 1521-3757. DOI: 10.1002/ANGE.202002680. URL: https://onlinelibrary.wiley.com/doi/full/10.1002/ange.202002680%20https://onlinelibrary.wiley.com/doi/abs/10.1002/ange.202002680%20https://onlinelibrary.wiley.com/doi/10.1002/ange.202002680.

[102] Xinyue Guo et al. “Engineering Hydrogen Generation Sites to Promote Electrocatalytic CO ₂ Reduction to Formate”. In: *ACS Catalysis* 12.17 (Sept. 2022), pp. 10551–10559. ISSN: 2155-5435. DOI: 10.1021/acscatal.2c02548.

[103] Genxiang Wang et al. “Cost-effective and durable electrocatalysts for Co-electrolysis of CO2 conversion and glycerol upgrading”. In: *Nano Energy* 92 (Feb. 2022), p. 106751. ISSN: 2211-2855. DOI: 10.1016/J.NANOEN.2021.106751.

[104] Mohamed S. E. Houache et al. “Selective Electrooxidation of Glycerol to Formic Acid over Carbon Supported Ni1- xMx(M = Bi, Pd, and Au) Nanocatalysts and Coelectrolysis of CO2”. In: *ACS Applied Energy Materials* 3.9 (Sept. 2020), pp. 8725–8738. ISSN: 2574-0962. DOI: 10.1021/acsaem.0c01282.

[105] Siddhartha Subramanian, Joost Middelkoop, and Thomas Burdyny. “Spatial reactant distribution in CO2 electrolysis: balancing CO2 utilization and faradaic efficiency”. In: *Sustainable Energy & Fuels* 5.23 (Nov. 2021), pp. 6040–6048. ISSN: 2398-4902. DOI: 10.1039/D1SE01534F. URL: https://pubs.rsc.org/en/content/articlehtml/2021/se/d1se01534f%20https://pubs.rsc.org/en/content/articlelanding/2021/se/d1se01534f.

[106] Hisan W Shafaque et al. “Boosting Membrane Hydration for High Current Densities in Membrane Electrode Assembly CO 2 Electrolysis”. In: *Cite This: ACS Appl. Mater. Interfaces* 12 (2020), p. 54595. DOI: 10.1021/acsami.0c14832. URL: https://dx.doi.org/10.1021/acsami.0c14832.

[107] *How Does Gas Chromatography Work? | PerkinElmer Blog*. URL: https://blog.perkinelmer.com/posts/gas-chromatography-explained-what-it-is-and-how-it-works/.

[108] *Human Metabolome Database*. URL: https://hmdb.ca/.

[109] *nmrshiftdb2 - open nmr database on the web*. URL: https://nmrshiftdb.nmr.uni-koeln.de/portal/media-type/html/user/anon/page/default.psml/js_pane/P-Home;jsessionid=9CE6B2F8971EA30C4859F0C18F78685F.

[110] Glenn Facey. *Tuning Problems for Samples of High Ionic Strength*. URL: http://u-of-o-nmr-facility.blogspot.com/2008/07/tuning-problems-for-samples-of-high.html.

[111] Yogesh Surendranath, Matthew W Kanan, and Daniel G Nocera. “Mechanistic Studies of the Oxygen Evolution Reaction by a Cobalt-Phosphate Catalyst at Neutral pH”. In: *JACS Articles* (2010). DOI: 10.1021/ja106102b. URL: https://pubs.acs.org/sharingguidelines.

[112] M. Favaro et al. “Elucidating the alkaline oxygen evolution reaction mechanism on platinum”. In: *Journal of Materials Chemistry A* 5.23 (June 2017), pp. 11634–11643. ISSN: 2050-7496. DOI: 10.1039/C7TA00409E. URL: https://pubs.rsc.org/en/content/articlehtml/2017/ta/c7ta00409e%20https://pubs.rsc.org/en/content/articlelanding/2017/ta/c7ta00409e.

[113] Marcelo M. Tusi et al. “The high activity of PtBi/C electrocatalysts for ethanol electro-oxidation in alkaline medium”. In: *Electrochemistry Communications* 13.2 (Feb. 2011), pp. 143–146. ISSN: 1388-2481. DOI: 10.1016/J.ELECOM.2010.11.035.

[114] Hossein Yadegari et al. “Glycerol Oxidation Pairs with Carbon Monoxide Reduction for Low-Voltage Generation of C2and C3Product Streams”. In: *ACS Energy Letters* 6.10 (Oct. 2021), pp. 3538–3544. ISSN: 23808195. DOI: 10.1021/acsenergylett.1c01639.

[115] Tianyu Li, David A Harrington, and Chemsuschem Reviews. “An Overview of Glycerol Electrooxidation Mechanisms on Pt, Pd and Au”. In: *ChemSusChem* 14 (2021), pp. 1472–1495. DOI: 10.1002/cssc.202002669. URL: https://chemistry-europe.onlinelibrary.wiley.com/doi/10.1002/cssc.202002669.

[116] M Fleischmann, K Korinek, and D Pletcher. *THE OXIDATION OF ORGANIC COMPOUNDS AT A NICKEL ANODE IN ALKALINE SOLUTION*. Tech. rep. 1970.

[117] Prashanth W. Menezes et al. “Facile Access to an Active γ-NiOOH Electrocatalyst for Durable Water Oxidation Derived From an Intermetallic Nickel Germanide Precursor”. In: *Angewandte Chemie International Edition* 60.9 (Feb. 2021), pp. 4640–4647. ISSN: 1521-3773. DOI: 10.1002/ANIE.202014331. URL: https://onlinelibrary.wiley.com/doi/full/10.1002/anie.202014331%20https://onlinelibrary.wiley.com/doi/abs/10.1002/anie.202014331%20https://onlinelibrary.wiley.com/doi/10.1002/anie.202014331.

[118] Arumugam Sivanantham et al. “Surface Activation and Reconstruction of Non-Oxide-Based Catalysts through in Situ Electrochemical Tuning for Oxygen Evolution Reactions in Alkaline Media”. In: *ACS Catalysis* 10.1 (Jan. 2020), pp. 463–493. ISSN: 21555435. DOI: 10.1021/ACSCATAL.9B04216/ASSET/IMAGES/LARGE/CS9B04216{_}0024.JPEG. URL: https://pubs.acs.org/doi/full/10.1021/acscatal.9b04216.

[119] Anubhav Jain et al. “Commentary: The materials project: A materials genome approach to accelerating materials innovation”. In: *APL Materials* 1.1 (July 2013), p. 11002. ISSN: 2166532X. DOI: 10.1063/1.4812323/119685/COMMENTARY-THE-MATERIALS-PROJECT-A-MATERIALS. URL: /aip/apm/article/1/1/011002/119685/Commentary-The-Materials-Project-A-materials.

[120] Tianyu Li and David A. Harrington. “An Overview of Glycerol Electrooxidation Mechanisms on Pt, Pd and Au”. In: *ChemSusChem* 14.6 (Mar. 2021), pp. 1472–1495. ISSN: 1864-564X. DOI: 10.1002/CSSC.202002669. URL: https://onlinelibrary.wiley.com/doi/full/10.1002/cssc.202002669%20https://onlinelibrary.wiley.com/doi/abs/10.1002/cssc.202002669%20https://chemistry-europe.onlinelibrary.wiley.com/doi/10.1002/cssc.202002669.

[121] V. L. Oliveira et al. “Kinetic Investigations of Glycerol Oxidation Reaction on Ni/C”. In: *Electrocatalysis* 6.5 (Sept. 2015), pp. 447–454. ISSN: 18685994. DOI: 10.1007/S12678-015-0261-2/FIGURES/8. URL: https://link.springer.com/article/10.1007/s12678-015-0261-2.

[122] Xiaoyi Hu et al. “Sustainable catalytic oxidation of glycerol: a review”. In: *Environmental Chemistry Letters 2023* 1 (June 2023), pp. 1–37. ISSN: 1610-3661. DOI: 10.1007/S10311-023-01608-Z. URL: https://link.springer.com/article/10.1007/s10311-023-01608-z.

[123] Jilei Liu et al. “Tackling CO Poisoning with Single-Atom Alloy Catalysts”. In: *Journal of the American Chemical Society* 138.20 (May 2016), pp. 6396–6399. ISSN: 15205126. DOI: 10.1021/JACS.6B03339/ASSET/IMAGES/LARGE/JA-2016-03339K{_}0004.JPEG. URL: https://pubs.acs.org/doi/full/10.1021/jacs.6b03339.

[124] Jimmy John et al. “Mechanistic studies of formate oxidation on platinum in alkaline medium”. In: *Journal of Physical Chemistry C* 116.9 (Mar. 2012), pp. 5810–5820. ISSN: 19327447. DOI: 10.1021/JP211887X/ASSET/IMAGES/MEDIUM/JP-2011-11887X{_}0015.GIF. URL: https://pubs.acs.org/doi/full/10.1021/jp211887x.

[125] Amanda C. Garcia et al. “Strong Impact of Platinum Surface Structure on Primary and Secondary Alcohol Oxidation during Electro-Oxidation of Glycerol”. In: *ACS Catalysis* 6.7 (July 2016), pp. 4491–4500. ISSN: 21555435. DOI: 10.1021/ACSCATAL.6B00709/ASSET/IMAGES/LARGE/CS-2016-00709H{_}0006.JPEG. URL: https://pubs.acs.org/doi/full/10.1021/acscatal.6b00709.

[126] S. Jiménez et al. “Assessment of the performance of a PEMFC in the presence of CO”. In: *Journal of Power Sources* 151.1-2 (Oct. 2005), pp. 69–73. ISSN: 0378-7753. DOI: 10.1016/J.JPOWSOUR.2005.02.049.

[127] P. N. Shankar and M. Kumar. “Experimental determination of the kinematic viscosity of glycerol-water mixtures”. In: *Proceedings - Royal Society of London, A* 444.1922 (1994), pp. 573–581. ISSN: 0962-8444. DOI: 10.1098/RSPA.1994.0039. URL: https://royalsocietypublishing.org/.

[128] Vincent S. Craig. “Gas Solubility of Electrolytes”. In: *Encyclopedia of Applied Electrochemistry* (2014), pp. 927–931. DOI: 10.1007/978-1-4419-6996-5{_}9. URL: https://link.springer.com/referenceworkentry/10.1007/978-1-4419-6996-5_9.

[129] Michael Guschakowski and Uwe Schröder. “Direct and Indirect Electrooxidation of Glycerol to Value-Added Products”. In: *ChemSusChem* 14.23 (Dec. 2021), pp. 5216–5225. ISSN: 1864564X. DOI: 10.1002/CSSC.202100556.

[130] Helmut Baltruschat. “Differential electrochemical mass spectrometry”. In: *Journal of the American Society for Mass Spectrometry* 15.12 (Dec. 2004), pp. 1693–1706. ISSN: 1044-0305. DOI: 10.1016/J.JASMS.2004.09.011.

[131] Déborah Z. Jeffery and Giuseppe A. Camara. “The formation of carbon dioxide during glycerol electrooxidation in alkaline media: First spectroscopic evidences”. In: *Electrochemistry Communications* 12.8 (Aug. 2010), pp. 1129–1132. ISSN: 1388-2481. DOI: 10.1016/J.ELECOM.2010.06.001.

[132] Jianshe Wang et al. “Antipoisoning Performance of Platinum Catalysts with Varying Carbon Nanotube Properties: Electrochemically Revealing the Importance of Defects”. In: *ChemElectroChem* 4.2 (Feb. 2017), pp. 296–303. ISSN: 2196-0216. DOI: 10.1002/CELC.201600589. URL: https://onlinelibrary.wiley.com/doi/full/10.1002/celc.201600589%20https://onlinelibrary.wiley.com/doi/abs/10.1002/celc.201600589%20https://chemistry-europe.onlinelibrary.wiley.com/doi/10.1002/celc.201600589.

A

Selectivity Calculations

A.1. Correction of the Outlet Flow Rate

As mentioned in Section 3.3.1, the MFM available in the lab is calibrated only for CO_2. In addition to the calibration, a previous flooding incident has also left the MFM indicating flow rates that are 87.5% of the actual flow rate. Thus, the first correction step is:

$$\dot{V}_{outlet} = \frac{\dot{V}_{mfm}}{0.875} \tag{A.1}$$

where:
$\dot{V}_{mfm}$ is the MFM reported outlet flow rate in mL/min,
$\dot{V}_{outlet}$ is the outlet flow rate where the flooding damage is accounted for in mL/min.

Once the flow rate is adjusted, a correction factor is calculated to account for each of the gasses present in the outlet gas flow. The gas mixture leaving the reactor is composed of CO_2, CO, H_2O, and H_2, and the relevant values for the calculation of the correction factor are listed in Table A.1 below.

Table A.1: Gas conversion factors of the cathodic outlet components

i	Species	Gas Conversion Factor
1	CO	1
2	H_2	1.01
3	H_2O	0.79
4	CO_2	0.74

Using the aforementioned correction factors, and the volume fraction measurements done by the GC, the correction factor for the gas mixture can be calculated as such:

$$\frac{1}{C_{mix}} = \frac{V_1}{C_1} + \frac{V_2}{C_2} + \frac{V_3}{C_3} + \frac{V_4}{C_4} \tag{A.2}$$

where:
C_{mix} is the correction factor for the gas mixture,
C_i is the gas conversion factor for gas species i,
V_i is the volume fraction of the gas species i in the outlet as reported by the GC.

Once C_{mix} is obtained Eq. A.3 can be used to find the real gas outlet flow now accounting for the mixed nature of the gas.

$$\dot{V}_{real} = \frac{\dot{V}_{outlet}}{C_4} \cdot C_{mix} \tag{A.3}$$

where:

V_{real} is the real outlet flow rate,

C_4 is the correction factor of CO_2.

The outlet flow rate obtained can now be used in selectivity calculations.

A.2. Sample Calculation for FE of Gas Products

To demonstrate a sample calculation of FE for gas products, several experimental values, such as the current and GC readings are necessary. For this purpose, the experimental parameters for one GC reading of experiment 4 are listed in Table A.2 below.

Table A.2: Corrected Experimental Data for Experiment 4, GC Reading 18

Applied Potential (V)	Current (A)	Corrected Mass Flow Rate (mL/min)	H_2 amount (ppm)	CO Amount (ppm)
2.61	0.5721	48.20	5874.8	70640.9

The calculation of FEs utilizing Eq. 3.2 and these values are as follows:

For H_2:

$$FE_{H2} = \frac{(5874.8\,ppm \cdot 10^{-6} \cdot \frac{101325\,Pa}{8.314\,Jmol^{-1}K^{-1} \cdot 273.15\,K} \cdot (48.20 \cdot 1.67E^{-8}\,m^3s^{-1})) \cdot 2 \cdot 96485\,Cmol^{-1}}{0.5721\,A} \cdot 100\% \tag{A.4}$$

$$FE_{H2} = 7.10\% \tag{A.5}$$

For CO:

$$FE_{CO} = \frac{(70640\,ppm \cdot 10^{-6} \cdot \frac{101325\,Pa}{8.314\,Jmol^{-1}K^{-1} \cdot 273.15\,K} \cdot (48.20 \cdot 1.67E^{-8}\,m^3s^{-1})) \cdot 2 \cdot 96485\,Cmol^{-1}}{0.5721\,A} \cdot 100\% \tag{A.6}$$

$$FE_{CO} = 85.40\% \tag{A.7}$$

The calculations showcased above were performed via a homemade Excel file for all experiments that utilized the GC.

A.3. Sample Calculation for FE of Liquid Products

The following sample calculation proceeds the analysis completed in the MestReNova software, which is the detection and integration of signals for the samples taken at 2.4V and 2.7V applied potential steps in Experiment 4. LA and its corresponding doublet at 1.1 ppm chemical shift is the compound and signal in question for the purposes of this sample calculation.

The experimental parameters considered and kept constant throughout all experiments are:

- I_{std} = 2
- N_{std} = 2
- C_{std} =0.0020833 M

- $V_{NMR\,tube}$ = 600 μL
- $V_{NMR\,sample}$ = 550 μL

The parameters obtained through the software or specific to this experiment/signal are:

- $N_{lactate}$ = 3
- n^e = 2
- $I_{lactate}$ in 2.4 V sample = 1.3
- $I_{lactate}$ in 2.7 V sample = 2.66
- Current, I, at the 2.7 V step = 0.572 A
- t = 20 min
- $V_{anolyte}$ = 250 mL

The parameters listed above can then be utilized in Eq. 3.3 as follows:

For the 2.4 V sample:

$$C_{LA,\,2.4\,V} = \frac{1.3}{2} \cdot \frac{2}{3} \cdot 0.0020833\,M \tag{A.8}$$

$$C_{LA,\,2.4\,V} = 0.0009028\,M \tag{A.9}$$

For the 2.7 V sample:

$$C_{LA,\,2.7\,V} = \frac{2.66}{2} \cdot \frac{2}{3} \cdot 0.0020833\,M \tag{A.10}$$

$$C_{LA,\,2.7\,V} = 0.00184\,M \tag{A.11}$$

Knowing the concentrations of lactate in samples taken at the end of 2.4 V applied potential and its consecutive step 2.7 V applied potential allows us to determine the concentration increase that happened specifically at the applied potential step of 2.7 V.

$$\Delta C_{LA,\,2.7\,V} = C_{LA,\,2.7\,V} - C_{LA,\,2.4\,V} = 0.0009372\,M \tag{A.12}$$

The above calculation is mainly necessary for experiments where a series of cell potentials or current densities were applied to the electrochemical cell. For experiments where only one electrical parameter is applied, the concentrations in the sample taken at the end of the experiment can be used directly for the FE calculation.

Having obtained the increase in the concentration of lactate, the FE of lactate from GOR is then calculated using equation 3.4.

$$FE_{LA,\,2.7\,V}(\%) = \frac{0.0009372\,M \cdot \dfrac{600\mu L \cdot 250mL}{550\mu L} \cdot 2 \cdot 96485\,Cmol^{-1}}{0.572A \cdot 20min} \cdot 100\% \tag{A.13}$$

$$FE_{LA,\,2.7\,V} = 7.24\% \tag{A.14}$$

The FEs of other compounds, such as acetate and glycerate, can also be calculated using the method showcased above; however, the calculation of faradaic efficiency of formate needs special considerations as described in 3.3.1 and can be found in A.4.

A.4. Formate FE Calculation

Since formate is a liquid product, and it can be produced through both the glycerol oxidation and CO_2 reduction, special considerations must be made for its FE calculations. Measuring its concentration via quantitative H-NMR like other liquid products of GOR is not enough to identify how much formate has been produced at the anode vs. the cathode. To achieve this distinction, it was assumed that the production of formate through the cathodic reaction can be deduced from the FEs of the measured gaseous products. This approach essentially entails the assumption that CO_2RR at the Ag GDE mainly produces CO and H_2, but for the cases where the total FEs of these two gaseous products do not add up to a 100%, formate is produced as well. This assumption allows the formate concentration increase via CO_2RR to be determined so that the formate concentration increase through the GOR only can be identified.

Another aspect to consider during this calculation is the sampling frequency for gaseous and liquid products. The faradaic efficiencies of gas-phase products were estimated from the GC volume fraction measurements of the gas output taken in 5-minute intervals. Whereas the faradaic efficiencies of liquids were measured through samples taken from the anolyte after each experimental condition had been completed. This means that for stepwise experiments, the sampling was done in 20-minute intervals, and for one-electrical-condition experiments, sampling was done at the end of the run.

Assuming that the calculation of the CO and H_2 FEs, as well as the concentration increase of liquid products, are completed, the following approach can be adopted to distinguish the FE of formate from GOR vs CO_2RR. First, the FEs of CO and H_2 of a GC reading were subtracted from 100%, resulting in the assumed FE of formate from CO_2RR in the previous five minutes that injection is representative of. Then this value was inputted into a rearranged version of the FE equation 3.2 as such:

$$n_{FA\ from\ CO_2RR} = \frac{(100 - FE_{CO} - FE_{H_2}) \cdot Q_{5\ mins}}{n^e \cdot F} \times \frac{1}{100\%} \tag{A.15}$$

where:

$n_{FAfromCO_2RR}$ is the moles of formate produced from CO_2RR during the GC injection interval of five minutes,

FE_{CO} is the faradaic efficiency of CO from CO_2RR,

FE_{H_2} is the faradaic efficiency of H_2 from CO_2RR,

$Q_{5\ mins}$ is the total amount of charge that has passed through the working electrode in the past five minutes.

Once the moles of formate contribution of CO_2RR for every 5 minutes have been calculated using Eq. A.15, its accumulation in the anolyte can be determined. For the step-wise experiments, the accumulated amount of formate was calculated for every 20 minutes when the same electrical conditions were applied to the cell.

$$n_{FA,\ step\ CO_2RR} = n_{FA,\ 5\ min} + n_{FA,\ 10\ min} + n_{FA,\ 15\ min} + n_{FA,\ 20\ min} \tag{A.16}$$

On the other hand, for the single current/potential experiments, the accumulated formate amount due to CO2RR was determined for the full duration of the experiment as shown in Equation A.17 below.

$$n_{FA,\ full\ CO_2RR} = n_{FA,\ 5\ min} + n_{FA,\ 10\ min} + n_{FA,\ 15\ min} + n_{FA,\ 20\ min} + n_{FA,\ 25\ min} + \ldots \tag{A.17}$$

where:

$n_{FA,\ step\ CO_2RR}$ is the accumulated formate amount from CO_2RR in each step,

$n_{FA,\ full\ CO_2RR}$ is the accumulated formate amount from CO_2RR in the full experiment,

$n_{FA,\ X\ min}$ is the amount of formate formed from CO_2RR in the 5 min interval preceding the X minute mark in which the GC injection was taken.

Later, these values were converted to concentration increases that can be attributed solely to CO_2RR via Eq. A.18.

$$\Delta C_{FA,\ CO_2RR} = \frac{n_{FA,\ CO_2RR}}{V_{anolyte}} \tag{A.18}$$

where:
$\Delta C_{FA,CO_2RR}$ is the concentration increase of formate in the anolyte caused by the CO_2RR in an experimental step or in the duration of a full experiment,
$n_{FA,\,CO_2RR}$ is the accumulated formate amount (either $n_{FA,\,step\,CO_2RR}$ or $n_{FA,\,full\,CO_2RR}$ depending on the type of experiment).

This concentration increase can be subtracted from the total concentration increase in the anolyte determined through H-NMR to distinguish the production of formate via GOR and CO_2RR. Finally, the faradaic efficiencies of formate from both reactions can be calculated as follows:

$$FE_{FA,\,CO_2RR} = \frac{\Delta C_{FA,\,CO_2RR} \cdot \frac{V_{nmr:tube} \cdot V_{anolyte}}{V_{nmr\ sample}} \cdot n^e \cdot F}{I \cdot t} \times 100\% \tag{A.19}$$

where:
$FE_{FA,\,CO_2RR}$ is the FE of formate from CO_2RR,
n^e is 2.

$$FE_{FA,\,GOR} = \frac{\Delta C_{FA,\,NMR} - \Delta C_{FA,\,CO_2RR}) \cdot \frac{V_{nmr\,tube} \cdot V_{anolyte}}{V_{nmr\ sample}} \cdot n^e \cdot F}{I \cdot t} \times 100\% \tag{A.20}$$

where:
$FE_{FA,\,GOR}$ is the FE of formate from GOR,
$\Delta C_{FA,\,NMR}$ is the concentration increase of formate calculated from consecutive NMR spectra,
n^e is $\frac{8}{3}$.

As a final note, it should be mentioned that for the GC measurements that indicate FEs for H_2 and CO that add up to 100%, it can be assumed that there is no formate production via the cathodic route.

B

List of Experiments

Below is the list of experiments performed for the duration of this thesis' experimental study. GDE stands for gas diffusion electrode, LSV for linear sweep voltammetry, CP for hydrophilic carbon paper, and CV for cyclic voltammetry throughout this table.

Table B.1: A list of the experiments performed during this thesis and the applied experimental parameters.

No	Anolyte	Anode	Cathode	Membrane	Gas inlet	Tests
1	KOH (0.5M)	Pt on Ti	Ag GDE	AEM	CO_2	LSV test, Chronoamperometry test with steps (1.8V to 3V)
2	KOH (0.5M)	Pt on Ti	Ag GDE	AEM	CO_2	Chronoamperometry test with steps (1.8V to 3V)
3	KOH (0.5M)	Ni foam	Ag GDE	AEM	CO_2	Impedance test, Chronoamperometry test with steps (1.8V to 3.6V)
4	KOH (0.5M)+ GLY (0.5 M)	Ni foam	Ag GDE	AEM	CO_2	Impedance test, Chronoamperometry test with steps (1.8V to 3.6V)
5	KOH (0.5M)+ GLY (1 M)	Ni foam	Ag GDE	AEM	CO_2	Impedance test, Chronoamperometry test with steps (1.8V to 3.6V)
6	KOH (0.5 M)+ GLY (0.1 M)	Ni foam	Ag GDE	AEM	CO_2	Impedance test, Chronoamperometry test with steps (1.8V to 3.6V)
7	KOH (0.5 M)+ GLY (0.5 M)	Pt on Ti	Ag GDE	AEM	CO_2	Impedance test, Chronoamperometry test with steps (1.8V to 3.6V)
8	KOH (0.5 M)+ GLY (0.5 M)	Ni foam	Ag GDE	AEM	CO_2	Impedance test, Chronoamperometry test with steps (1.8V to 3.6V)

Continuation of Table B.1

No	Anolyte	Anode	Cathode	Membrane	Gas inlet	Tests Performed
9	KOH (0.5 M)+ GLY (1 M)	Pt on Ti	Ag GDE	AEM	CO_2	Impedance test, Chronoamperometry test with steps (1.8V to 3.6V)
10	KOH (0.5 M)+ GLY (0.1 M)	Pt on Ti	Ag GDE	AEM	CO_2	Impedance test, Chronoamperometry test with steps (1.8V to 3.6V)
11	KOH (0.5 M)+ GLY (0.5 M)	Pt on Ti	Pt on CP	AEM	N_2	Impedance test, Chronoamperometry test with steps (1.8V to 3.6V)
12	KOH (0.5 M)+ GLY (1 M)	Pt on Ti	Pt on CP	AEM	N_2	Impedance test, Chronoamperometry test at 3V
13	KOH (1 M)	Ni foam	Ag GDE	BPM	CO_2	Impedance test, Chronoamperometry test with steps (1.8V to 3.6V)
14	KOH (0.5 M)+ GLY (0.5 M)	Ni foam	Pt on CP	AEM	N_2	Impedance test, Chronoamperometry test with steps (1.8V to 3.6V)
15	KOH (0.5 M)+ GLY (0.5 M)	Ni on Ti	Ag GDE	AEM	CO_2	Impedance test, Chronoamperometry test with steps (1.8V to 3.6V)
16	KOH (1 M)	Ni foam	Ag GDE	BPM	CO_2	Impedance test, Chronopotentiometry test with steps (25 to 200 mA·cm-2)
17	KOH (1 M)	Ni foam	Ag GDE	BPM	CO_2	Impedance test, Chronopotentiometry test with steps (25 to 200 mA·cm-2)
18	KOH (3 M)	Ni foam	Ag GDE	BPM	CO_2	Impedance test, Chronopotentiometry test with steps (25 to 200 mA·cm-2)
19	KOH (1 M)+ GLY (0.5 M)	Ni foam	Ag GDE	BPM	CO_2	Impedance test, Chronopotentiometry test with steps (25 to 200 mA·cm-2)
20	KOH (1 M)+ GLY (0.1 M)	Ni foam	Ag GDE	BPM	CO_2	Impedance test, Chronopotentiometry test with steps (25 to 200 mA·cm-2)
21	KOH (0.5 M)+ GLY (0.5 M)	Ni foam	Ag GDE	AEM	CO_2	Impedance test, Chronopotentiometry test at 50 mA·cm-2
22	KOH (0.5 M)+ GLY (0.5 M)	Ni foam	Ag GDE	AEM	CO_2	Impedance test, Chronoamperometry test at 3V
23	KOH (0.5 M)+ GLY (0.5 M)	Ni foam	Ag GDE	AEM	CO_2	Impedance test, Chronopotentiometry test at 100 mA·cm-2
24	KOH (0.5 M)+ GLY (0.5 M)	Pt on Ti	Ag GDE	AEM	CO_2	Impedance test, Chronopotentiometry test at 100 mA·cm-2

Continuation of Table B.1

No	Anolyte	Anode	Cathode	Membrane	Gas inlet	Tests Performed
25	KOH (0.5 M)+ GLY (0.5 M)	Ni foam	Ag GDE	AEM	N_2	Impedance test, Chronopotentiometry test at 100 mA·cm-2
26	KOH (0.5 M)+ GLY (0.5 M)	Pt on Ti	Ag GDE	AEM	N_2	Impedance test, Chronopotentiometry test at 100 mA·cm-2
27	KOH (1 M)+ GLY (0.1 M)	Pt on Ti	Ag GDE	BPM	CO_2	Impedance test, Chronopotentiometry test with steps (25 to 200 mA·cm-2)
28	KHCO3 (0.1 M)+ GLY (0.5 M)	Pt on Ti	Ag GDE	AEM	CO_2	Impedance test, Chronopotentiometry test at 100 mA·cm-2
29	KOH (0.5 M)+ GLY (0.5 M)	Pt on Ti	Ni foam	-	Ar	CV test
30	KOH (0.5 M)+ GLY (0.5 M)	Ni foam	Ni foam	-	Ar	CV test
31	KOH (1 M)+ GLY (0.5 M)	Ni foam	Ag GDE	BPM	CO_2	Chronopotentiometry test at 100 mA·cm-2
32	KOH (1 M)	Ni foam	Ag GDE	BPM	CO_2	Chronopotentiometry test at 100 mA·cm-2
33	KOH (1 M)+ GLY (0.5 M)	Ni foam	Ag GDE	BPM	CO_2	Chronopotentiometry test with steps (25 to 200 mA·cm-2)

C

FEs of CO_2RR Products

Below is a table containing the average CO_2RR faradaic efficiencies of gaseous products measured for each experiment. Experiments are referred to with their numbers as defined in Appendix B.1, and the entries labeled NaN are for experiments where the GC data was not available.

Table C.1: The average faradaic efficiencies of CO_2RR products in performed experiments.

No	FE_{H_2} (%)	FE_{CO} (%)
1	33.30	60.76
2	16.71	73.42
3	7.11	85.36
4	7.36	91.76
5	6.50	83.39
6	6.02	88.57
7	17.01	77.80
8	5.95	87.00
9	14.55	84.27
10	11.56	79.84
11	NaN	NaN
12	NaN	NaN
13	43.20	55.45
14	NaN	NaN
15	23.37	76.42
16	72.68	24.78
17	62.30	37.37
18	43.29	54.85
19	57.04	42.71
20	NaN	NaN
21	0.16	96.63

Table C.1 continued from previous page

No	FE_{H_2} (%)	FE_{CO} (%)
22	2.87	73.22
23	0.69	90.28
24	4.07	87.11
25	NaN	NaN
26	NaN	NaN
27	58.30	39.70
28	3.77	93.84
29	NaN	NaN
30	NaN	NaN
31	NaN	NaN
32	NaN	NaN
33	NaN	NaN

D

FEs of Minor GOR Products

Table D.1: The FEs of minor products for samples presented in Fig. 4.4

	FE (%)		
Sample	Acetate	Glycerate	DHA
2.4 V	0.63	0	0.71
2.7 V	0.75	0.28	0.12
3.0 V	0	1.8	0.18

Table D.2: The FEs of minor products for samples presented in Fig. 4.5

	FE (%)		
Sample	Acetate	Glycerate	DHA
2.4 V	0.18	0.23	0
2.7 V	0.06	0	0
3.0 V	0.16	0	0.22

Table D.3: The FEs of minor products for samples presented in Fig. 4.6a

			FE (%)		
		Sample	Acetate	Glycerate	DHA
GLY Concentration	0.5 M	2.4 V	0.63	0	0.71
		2.7 V	0.75	0.28	0.12
		3.0 V	0	1.8	0.18
	1.0 M	2.4 V	0.12	1.6	0
		2.7 V	0.17	0	0
		3.0 V	0.28	1.85	2.32

Table D.4: The FEs of minor products for samples presented in Fig. 4.6b

			FE (%)		
		Sample	Acetate	Glycerate	DHA
GLY Concentration	0.5 M	2.4 V	0.18	0.23	0
		2.7 V	0.06	0	0
		3.0 V	0.16	0	0.22
	1.0 M	2.4 V	0.57	2.89	0
		2.7 V	0.66	0	0.98
		3.0 V	0.94	0	0

Table D.5: The FEs of minor products for samples presented in Fig. 4.7

			FE (%)		
		Catalyst	Acetate	Glycerate	DHA
Potential	2.4 V	Ni Foam	0.18	0.23	0
		Pt on Ti	0.63	0	0.71
		Ni on Ti	0.1	2.9	0
	2.7 V	Ni Foam	0.06	0	0
		Pt on Ti	0.75	0.28	0.12
		Ni on Ti	0.25	0.9	0.68
	3.0 V	Ni Foam	0.16	0	0.22
		Pt on Ti	0	1.8	0.18
		Ni on Ti	0.17	0	0

Table D.6: The FEs of minor products for samples presented in Fig. 4.8

			FE (%)		
		Catalyst	Acetate	Glycerate	DHA
Cathodic Rxn	CO_2RR	Ni Foam	0.26	5.5	0.12
		Pt on Ti	0.13	8.1	0
	HER	Ni Foam	0.09	4.52	0.12
		Pt on Ti	0.4	0	0.02

Table D.7: The FEs of minor products for samples presented in Fig. 4.9

Current Density (mA/cm^2)			FE (%)		
		Catalyst	Acetate	Glycerate	DHA
50		AEM	0.18	0.23	0
		BPM	0	0.33	0.14
100		AEM	0.06	0	0
		BPM	0.38	0	0.07
200		AEM	0.16	0	0.22
		BPM	0.58	3.9	0.18

E

Results of Supplementary Tests

This section presents the results of the two investigations performed in this study that do not contribute to the main findings of this thesis.

E.1. Testing for Cation Concentration in BPMEA cells

Before testing the paired electrolysis of CO_2RR with GOR in a BPMEA cell, this investigation was performed to determine whether a 1M KOH or 3M KOH concentration for the electrolyte should be pursued. Two stepwise chronopotentiometry experiments were performed, both utilizing Ni foam as the anode. Ag-GDE as the cathode, a BPM as the membrane testing the cell's performance at applied current densities of 25, 50, 100, 150, and 200 mA/cm2.

The measurements aimed to understand the effect of cation concentration on the performance of the MEA cells as reported in previous studies [39]. The following results, displayed in Fig E.1, were obtained from these tests.

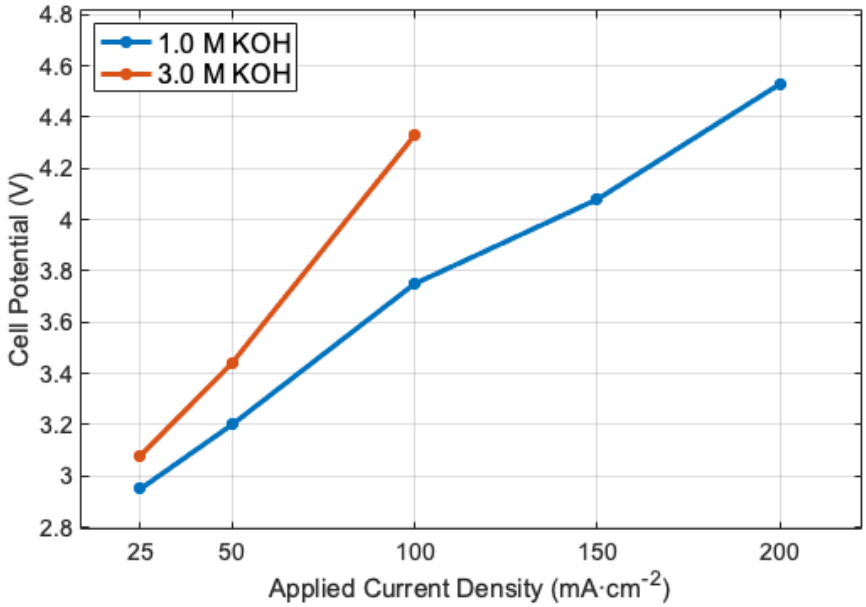

Figure E.1: Cell potential as a function of applied current density in 1.0 M or 3.0 M concentrations of KOH for the Ni anode utilizing BPMEA cell. The entire experimental range from 25 to 200 mA·cm^{-2} is shown.

The presented results reveal a lower effective cell potential for the 1.0 M case, indicating a reduced energy requirement. Notably, the 1.0 M KOH was examined throughout the experimental range, whereas cell potential data for the 3.0 M case at 150 and 200 mA/cm² is absent. This gap stems from an unexpected interruption during the 3.0 M KOH test, triggered by a potential overload detected by the potentiostat. Subsequent analysis of the cell revealed blistering on the bipolar membrane. An investigation to determine the cause for blistering is out of the scope of this thesis and was not pursued further; however, it is likely attributed to the elevated KOH concentration in the electrolyte.

Given the results of this study, a decision was made to keep the 1.0 M KOH concentration constant for the remaining BPMEA tests in this thesis.

E.2. Testing for Electrolyte Type

Due to the common occurrence of salt formation and blockages on the cathode side in AEMEA cells, this investigation was devised to test the performance of the paired electrolysis of CO_2RR and GOR in the use of KOH vs. $KHCO_3$ as the electrolyte. Two measurements were completed; both experiments utilized: Pt as the anode, Ag-GDE as the cathode, AEM as the membrane; they had 0.5 M glycerol content in the electrolyte and were tested for 30 minutes at 100 mA/cm². The KOH electrolyte had a concentration of 1.0 M, and the $KHCO_3$ electrolyte had a concentration of 0.1 M. $KHCO_3$ was selected due to its prevalence in conventional CO_2RR electrolyzers utilizing OER as the anodic reaction. Table E.1 below summarizes the results from their comparison.

Table E.1: The product selectivity and system activity performance of cells utilizing different types of electrolytes at 100 mA/cm² applied for 30 mins

Electrolyte Type	KOH	$KHCO_3$
Cell Potential (V)	2.62	4.0
FE_{CO} from CO_2RR (%)	85.54	98.54
$FE_{formate}$ from GOR (%)	34.90	5.39
$FE_{lactate}$ from GOR (%)	2.06	0.00

The results indicate a significant decline in GOR product selectivity, particularly concerning formate FE, when using $KHCO_3$ compared to KOH. This observation is coupled with $KHCO_3$ operating at a higher effective cell potential, indicative of increased energy demand for the system. Notably, the sole observed advantage of $KHCO_3$ electrolyte lies in the elevated FE for CO production. However, an in-depth analysis of cathodic product selectivities falls beyond the scope of this thesis. While the conducted measurements are not sufficient for definitive confirmation, it is hypothesized that the lower pH environment associated with $KHCO_3$ could be responsible for formate oxidation, a primary product of GOR in this study. Further investigation is required to understand the underlying mechanisms.

F

SEM Results

Below are the SEM images of the Ag-GDE cathode after experiment #7 was completed to ensure not Pt dissolution has happened in the system. The SEM images were taken by Siddhartha Subramanian and showed no presence of platinum.

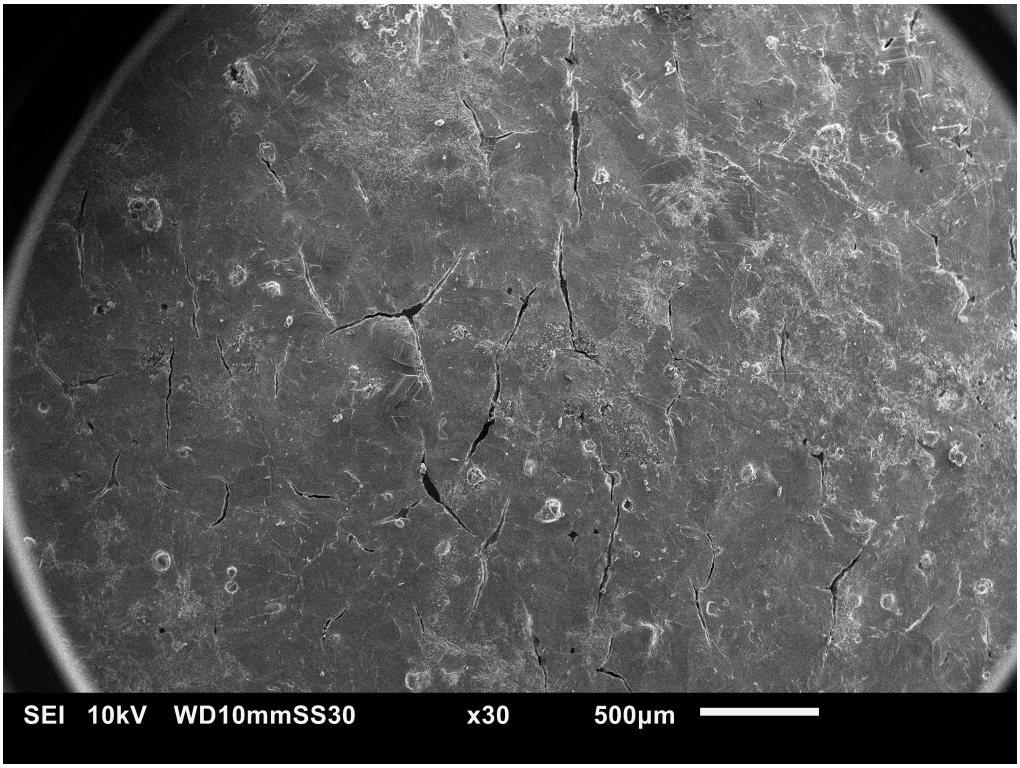

Figure F.1: SEI image of the Ag-GDE at 30x magnification

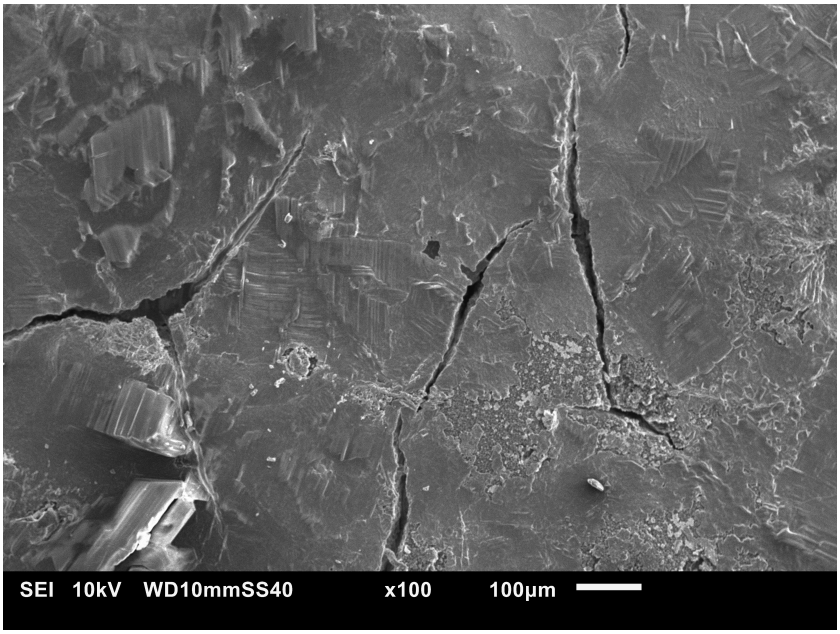

(a) SEI image of the Ag-GDE at 100x magnification

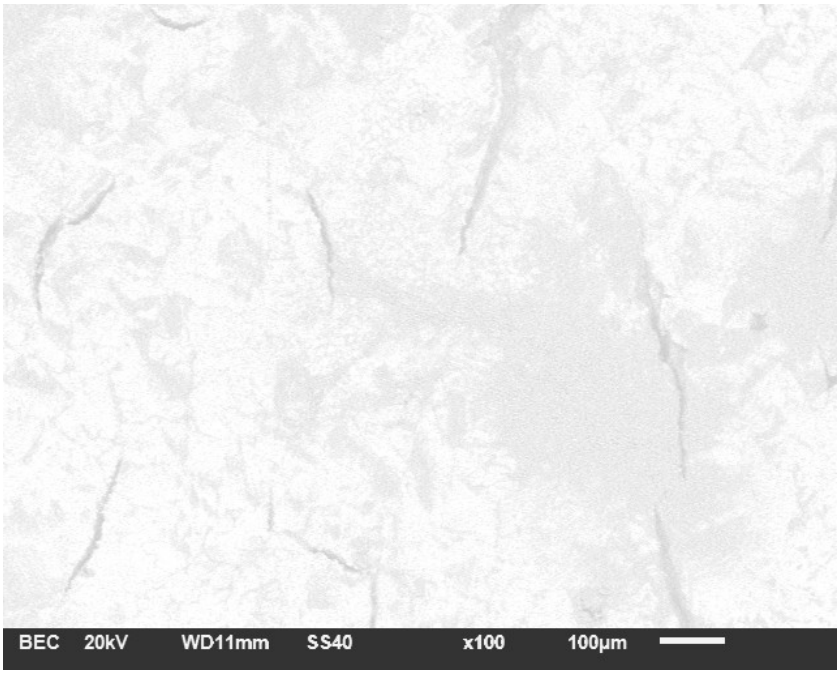

(b) BEC image of the Ag-GDE at 100x magnification (pt 1)

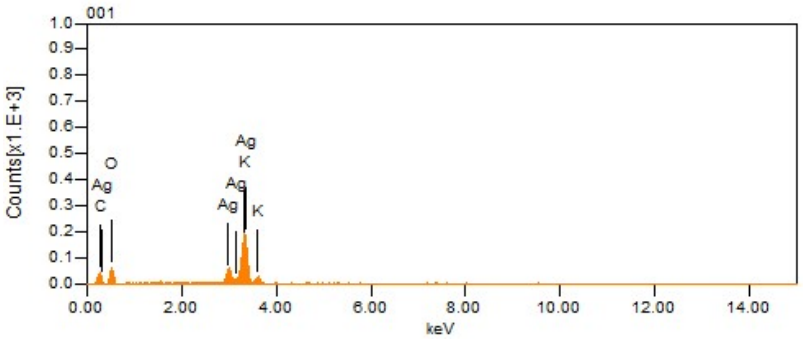

(c) EDS results for point 1

Figure F.2: SEM images for Ag-GDE sample that contains point 1

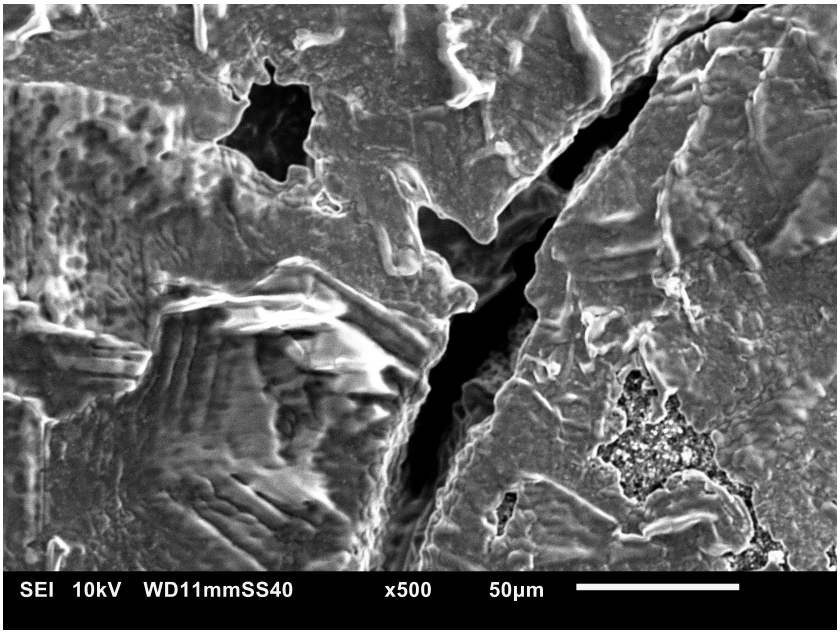

(a) SEI image of the Ag-GDE at 500x magnification

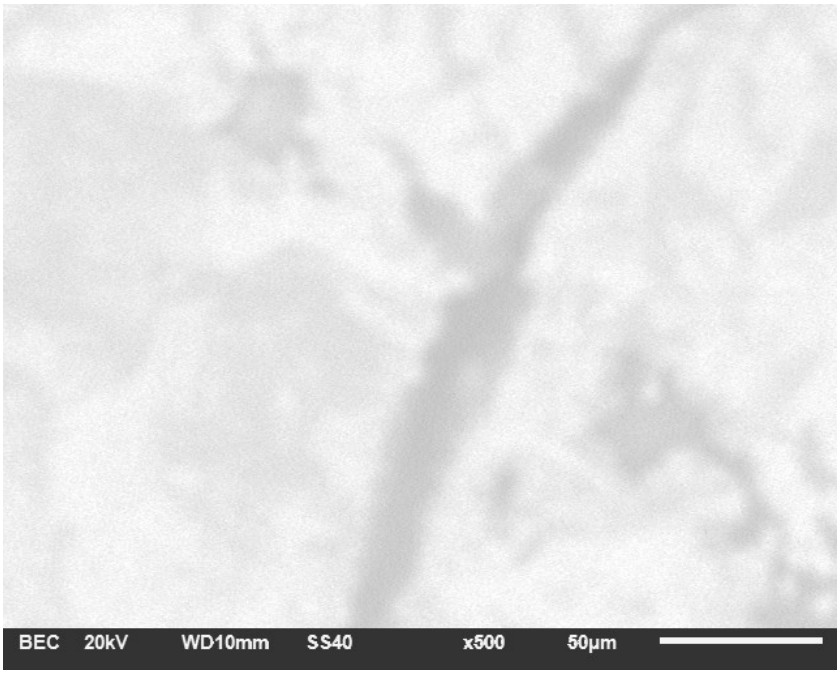

(b) BEC image of the Ag-GDE at 500x magnification (pt 2)

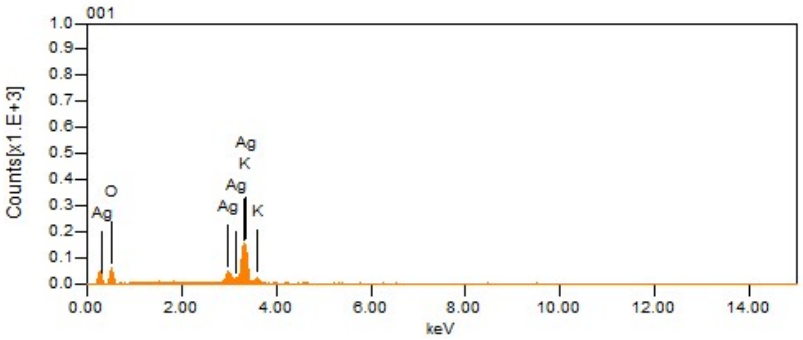

(c) EDS results for point 2

Figure F.3: SEM images for Ag-GDE sample that contains point 2